UTILIZING THE PHOTOTHERMAL EFFECT FOR RELEASING MOLECULES FROM THE SURFACES OF GOLD NANOPARTICLES

by

Amir Bahman Samsam Bakhtiari
Bachelor of Science, Simon Fraser University 2006

THESIS SUBMITTED IN PARTIAL FULFILLMENT OF
THE REQUIREMENTS FOR THE DEGREE OF

MASTER OF SCIENCE

In the
Department of Chemistry

© Amir Bahman Samsam Bakhtiari 2010

SIMON FRASER UNIVERSITY

Spring 2010

APPROVAL

Name:	**Amir Bahman Samsam Bakhtiari**
Degree:	**Master of Science**
Title of Thesis:	**Utilizing the photothermal effect for releasing molecules from the surfaces of gold nanoparticles**

Examining Committee:

        Chair: **Dr. Michael Eiklering**
Associate Professor

_____

Dr. Byron D. Gates
Senior Supervisor
Assistant Professor

_____

Dr. Neil R. Branda
Co-Supervisor
Professor

_____

Dr. Robert N. Young
Supervisor
Professor

_____

Dr. Robert A. Britton
Supervisor
Assistant Professor

_____

Dr. Hua-Zhong Yu
Internal Examiner
Professor

Date Defended/Approved: _____11 February, 2010_____

Declaration of
Partial Copyright Licence

The author, whose copyright is declared on the title page of this work, has granted to Simon Fraser University the right to lend this thesis, project or extended essay to users of the Simon Fraser University Library, and to make partial or single copies only for such users or in response to a request from the library of any other university, or other educational institution, on its own behalf or for one of its users.

The author has further granted permission to Simon Fraser University to keep or make a digital copy for use in its circulating collection (currently available to the public at the "Institutional Repository" link of the SFU Library website <www.lib.sfu.ca> at: <http://ir.lib.sfu.ca/handle/1892/112>) and, without changing the content, to translate the thesis/project or extended essays, if technically possible, to any medium or format for the purpose of preservation of the digital work.

The author has further agreed that permission for multiple copying of this work for scholarly purposes may be granted by either the author or the Dean of Graduate Studies.

It is understood that copying or publication of this work for financial gain shall not be allowed without the author's written permission.

Permission for public performance, or limited permission for private scholarly use, of any multimedia materials forming part of this work, may have been granted by the author. This information may be found on the separately catalogued multimedia material and in the signed Partial Copyright Licence.

While licensing SFU to permit the above uses, the author retains copyright in the thesis, project or extended essays, including the right to change the work for subsequent purposes, including editing and publishing the work in whole or in part, and licensing other parties, as the author may desire.

The original Partial Copyright Licence attesting to these terms, and signed by this author, may be found in the original bound copy of this work, retained in the Simon Fraser University Archive.

Simon Fraser University Library
Burnaby, BC, Canada

ABSTRACT

Nanomaterials, with unique physical and chemical properties, have the potential to help in the development of drug delivery systems. Some of these properties can be attributed to the nanoscale dimension of these materials. By masking, targeting, and release of a therapeutic agent, these nanomaterials can provide a delivery system that would reduce side effects.

Gold nanoparticles have been studied as a candidate for the drug delivery system. These materials can be decorated with molecules that have a thermally responsive reaction (i.e., Diels-Alder). In addition, gold nanoparticles when irradiated with a right wavelength of light produce heat. Consequently, the generated heat from nanoparticles causes a *retro*-Diels-Alder reaction, which release a segment of molecule (i.e., payload) from gold surfaces. This controlled release mechanism is a novel method to take advantage of the properties inherent in gold nanoparticles and have the potential to be used in drug delivery system.

DEDICATION

To my parents and family who supported me throughout these years.

ACKNOWLEDGEMENTS

TABLE OF CONTENTS

LIST OF FIGURES

LIST OF SCHEMES

GLOSSARY

°C	degree Celsius
arb. units	arbitrary units
CH_2Cl_2	dichloromethane
d	doublet
DCC	dicyclohexylcarbodiimide
EA	elemental analysis
EOF	electroosmotic flow
Eq.	equation
EtOH	ethanol
Et_2O	diethyl ether
EtOAc	ethyl acetate
fs	femtosecond
g	gram
GC	gas chromatography
h	hour
ICP-MS	inductively coupled plasma mass spectrometry
m.p.	melting point

H	proton
hv	photon energy
Hz	hertz
ICP-MS	inductively coupled plasma mass spectrometry
J	coupling constant
K	kelvin
k	kilo
m/z	mass-to-charge ratio
MeOH	methanol
MEKC	micellar electrokinetic chromatography
mmHg	millimetres of mercury
min	minutes
mL	millilitre
mol	mole
M	mole/litre
n	nano
ng	nanogram
nm	nanometer
nM	nanomolar
NPs	nanoparticles
Nd:YAG	neodymium-doped yttrium aluminium garnet
Nd:YLF	neodymium-doped yttrium lithium fluoride

NMR	nuclear magnetic resonance
psi	pound per square inch
ppm	parts per million
rpm	revolutions per minutes
s	second
s	singlet (in NMR spectroscopy)
SDS	sodium dodecylsulfate
SPR	surface plasmon resonance
NaOH	sodium hydroxide
T	temperature
t	triplet
TEM	transmission electron microscopy
TLC	thin layer chromatography
UV	ultraviolet
Vis	visible
V	voltage
W	watt
λ	wavelength

CHAPTER 1: INTRODUCTION TO NANOMATERIALS

1.1 A General Introduction to Nanomaterials in Medical Applications

In recent years, nanotechnology has been expanding rapidly due to the support from researchers in the academic, industrial and government sectors.[1] According to the U.S. National Nanotechnology Initiative, nanotechnology is defined as: "the understanding and control of matter at dimensions of roughly 1 to 100 nanometer (nm), where unique phenomena enable novel applications."[2] Nanotechnology for medical applications is one area of interest that has attracted the attention of many researchers.[3]

One of the areas of nanotechnology is drug delivery. The goal is to utilize nanomaterials in drug delivery systems in order to deliver a non-toxic and inactive form of a drug to specific organs or tissues and then release the activated drug only at designated sites of interest. If nanomaterials can facilitate the masking, targeting and release of therapeutic agents then they can be considered as drug delivery systems.[3]

1.2 Nanomaterials as Drug Delivery Systems

Currently, some specific nanomaterials, such as liposomes,[4] polymeric micelles,[5] dendrimers[6,7] and gold nanoparticles[8] (NPs) have been utilized in drug delivery systems to mask drugs by incorporating them either onto the surfaces or

within these nanostructures. These nanomaterials have been demonstrated to be useful as vehicles to facilitate controlled drug delivery.

The use of nanomaterials as delivery vehicles can also solve the problem of drug solubility by incorporating the drug inside or onto these nanomaterials while also masking the drug. The transport of drug molecules by nanomaterials can also increase the efficiency of the drug by targeted delivery as well as reducing side effects.[9] However, there are limitations to the aforementioned specific to each type of nanomaterials. These limitations help to define a list of criteria that must be considered when designing nanosystems for drug delivery. One of the concerns about these nanomaterials is their biocompatibility.[10] For example, dendrimers, which are starburst polymeric complexes that contain a series of well defined branches in their inner core, can encapsulate a drug in void spaces within their interiors.[7,10] However, in some cases, the positively charged surfaces of dendrimers may lead to increased toxicity and immunogenicity. These limitations have raised some concerns about the use of dendrimers in drug delivery systems. Therefore, the first criterion is: *the nanomaterial used in drug delivery systems must be biocompatible.*

Another issue is the ability to consistently reproduce these nanomaterials with reliable sizes. For example, liposomes,[4] which are defined as vesicles in which an aqueous volume is surrounded by a phospholipid bilayer, mask the drug by entrapping it within their aqueous core. The efficiency of trapping the drug within the liposome and the reproducibility of the size of the vesicle can be difficult.[10] The non-reproducibility of results for encapsulating drugs in liposomes

make them less attractive as drug delivery systems. The second criterion is: *the synthesis of the nanomaterial and the loading of the drug molecules must be reliable, reproducible, and scalable for production.*

One more issue of concern is the stability of some nanomaterials. For example, polymeric micelles are self-assemblies of amphiphiles that form core-shell structures in aqueous environments when the concentration of amphiphile exceeds the critical micelle concentration.[10] Similar to liposomes, micelles also encapsulate the drug in their core. These nanomaterials have limited stability for transport in biological systems, which is caused by degradation of the polymer due to hydrolysis. Consequently, limited stability leads to undesirable drug leakage during the transportation.[10] The third criterion is: *nanomaterials used in drug delivery systems should be able to deliver their package with minimal leakages as they travel to their final destinations.*

In summary, three major issues have to be addressed when designing nanostructures as drug delivery systems:

1. the nanomaterial must be biocompatible,

2. the synthesis of the nanomaterials and loading of the drug molecules must be reliable, reproducible, and scalable, and

3. the nanomaterial should be able to deliver a package with minimal leakage *en route* to its target.

These issues are some of the most common challenges that are faced by researchers, which have been discussed in the introductory section. Even with

their limitations, some of these nanomaterials are currently in clinical trials and on-going studies in an effort to overcome these limitations and eventually develop more suitable drug delivery systems.[10]

1.3 Nanomaterials and Targeted Drug Delivery in the Human Body

Once the nanomaterials mask the drug, they can be targeted to specific sites in the body by *passive* or *active* targeting.[10] Passive targeting happens due to the accumulation of nanomaterials at the diseased site. The cause of accumulation is the leaky microvasculature of the diseased site such as tumor and inflamed tissues. The leakiness of the tumor vascular is caused by irregular diameters and branching of capillaries and venulature due to a faster rate of cellular growth in those areas.[10] On the other hand, active targeting is achieved by conjugating the nanomaterial to biorecognition molecules. For example, NPs can be decorated with antibodies and peptides to recognize proteins that are over-expressed on the surface of tumor cells such as the epidermal growth factor receptor (EGFR).[11] The result is the targeting of nanomaterials, which contain the drug, to a designated location in the body. A combination of both types of targeting methods can provide ideal targeted delivery for drug delivery systems.

1.4 Nanomaterials and Mechanism to Release Their Payloads

Once the delivery vehicle reaches it final destination, there are two common methods that have been used to release the therapeutic agent which results in an unmasking of the drug molecule.[12,9] One method uses nanomaterials that are responsive to an internal stimulus (within the body or a

specific tissue) such as pH[13] or the presence of enzymes[14] to release the drug molecules.[13] The former works in the case of cancer cells because the pH value of the interstitial space of solid is more acidic (about 5−6.4) compared to the rest of the body (i.e., pH about 7.4).[15,16] A second method uses an external stimulus, such as light or localized heating[15] to trigger the release of drug molecules from the nanomaterial. The use of an external trigger has an advantage over internally triggered release because it provides more control. This control comes from the fact that externally applied light or heat provides both temporal and spatial control, an advantage to be discussed in more detail later on in this chapter. On the other hand, the external method has its own limitations. The major limitation is the accessibility of the stimulus to different organs due to low tissue penetration, and the damage that can be caused to healthy tissue in the local area of exposure.

Numerous examples of a release mechanism for nanomaterials have been reported.[9,10] However, the release of payload in a controlled manner presents a challenge. As a result, a controlled release mechanism needs to be developed. The purpose of this thesis is to present a novel controlled release mechanism. To demonstrate this mechanism, gold NPs are chosen as a platform for developing this new drug delivery system.

1.5   The Advantages of Using Gold NPs for Drug Delivery Systems

Gold NPs have not been given as much attention for drug delivery system in comparison to liposomes, micelles, and dendrimers.[9] Gold NPs have unique properties from both a chemical[17] (i.e., surface functionalization) and physical[18]

(i.e., interaction of light with gold NPs) point of view. Although their chemical and physical properties have been studied extensively for many years,[18] these properties could be utilized in drug delivery systems to a greater extent than has been reported in the literature.

Gold NPs possess distinctive advantages that make them promising candidates for drug delivery systems. A few of these are outlined below.

1. *They have high level of chemical inertness* and they can be oxidized only under harsh conditions, such as aqua regia.[19]

2. *They do not cause acute cytotoxicity to human cells* when their surfaces are coated with capping groups, such as citrate.[20]

3. *They have the ability to be surface-functionalized through Au−S linkages*.[17] These functional groups have directed the use of gold in many applications in the area of diagnostics[21] and biosensing[22]. In addition, there are numerous examples of bio-conjugated of protein to gold NPs, to target specific cells.[23,9] Bio-conjugation of protein to gold NPs can be applied in drug delivery systems to target a specific site within a biological system before unloading the drug from the surface of the NPs.

4. *They are easy to synthesize*. Their synthesis results in structures with monodisperse sizes and shapes, such as solid spherical gold NPs.[24] A variety of published synthetic routes can be used to prepare gold NPs of different shapes and sizes.[25] Shape and size

are the two major factors that control the physical properties of gold NPs.

1.6   Harnessing the Properties of Gold NPs in Medical Applications

Gold NPs are attractive for drug delivery system due to their chemical and physical properties. The specific physical property relevant to this thesis is the interaction of light with gold NPs. Light of specific wavelengths are either scattered or absorbed by the gold NPs. The absorption of specific wavelength leads to excitation of electrons in the gold NPs.[18] This process is known as surface plasmon resonance (SPR). Chapter 2 explains SPR in more detail. In addition, the absorption of light at the SPR frequency causes the gold NPs to generate heat, a phenomena known as the photothermal effect.[26] It is this effect that will be used to trigger the release mechanism described in this thesis.

Photothermal effect can increase the temperature of a bulk solution which contains the NPs.[27] There are, however, very few publications that have reported harnessing the photothermal effect for medical applications.[28] El-Sayed *et al.*, who are the pioneers in studying the photothermal effect, have demonstrated the ability to kill cells using both gold NPs and the photothermal effect.[29] They were able to kill cells (epithelial cell line, human keratinocytes) containing the gold NPs by thermal denaturation of proteins resulting from the photothermal effect.[30] In another approach, it was shown that a polymeric capsule doped with gold NPs can be used to deliver a payload which has been contained within the polymer. The release mechanism uses near-infrared (NIR) light to initiate the photothermal

effect, resulting in the production of heat to melt the polymer layer and consequently releases the payload from the polymer (Figure 1.1).
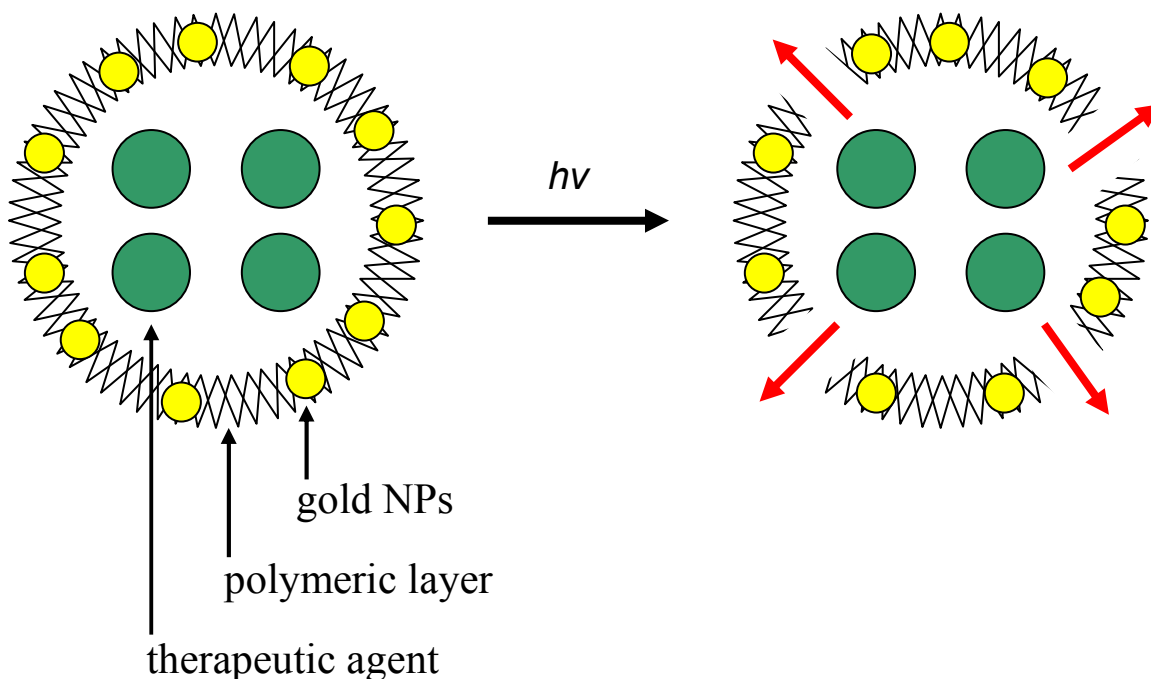
Figure 1.1 Releasing an encapsulated material from within a polymer capsule by using the photothermal effect from gold NPs doped into the polymer to melt the polymer upon irradiation with light.

Although the photothermal effect has proven to be an effective way to directly kill cells and melt materials containing the NPs, in all the previously published studies, the photothermal effect has not been used to release molecules directly from the surface of gold NPs while keeping the cells alive. The goal of the research described in this thesis is to harness the photothermal effect in order to trigger a controlled release of molecules directly from the surface of

gold NPs without heating the environment around the cell, thus keeping the cell alive.

1.7   The Project Goals

The long-term goals of this research project are to utilize gold NPs to deliver therapeutic agents to specific cells and release the drug molecules using the photothermal effect. Numerous tasks must be achieved in order to reach this goal, many of which are beyond the scope of this thesis. The short-term goal of this project, which is the main purpose of this thesis, is to demonstrate that the photothermal effect can be used as a trigger to release molecules from the surface of gold NPs. This hypothesis can be tested by attaching molecules with three specific components to the surface of gold NPs (Figure 1.2). These three components are listed below.

1. *A thiol or disulfide functional group*. This group can be used to anchor the molecule through a covalent Au−S bond to the gold surface.

2. *A thermally responsive bond*. This is the bond that is cleavable in the presence of heat.

3. *A dye reporter molecule*. The role of this molecule is to illustrate molecular release from the gold surface after the photothermal effect is initiated as shown in Figure 1.2.

A hybrid organic-NP system such as the one shown in Figure 1.2 will absorb specific wavelengths of light (by the gold NPs), resulting in localized

heating at the gold surfaces through the photothermal effect. The heat generated will be harnessed to drive a chemical reaction, which breaks the bonds between the payload and the group anchoring it to the gold NPs. Consequently, the payload is released from the gold NPs into the aqueous environment surrounding the NPs.
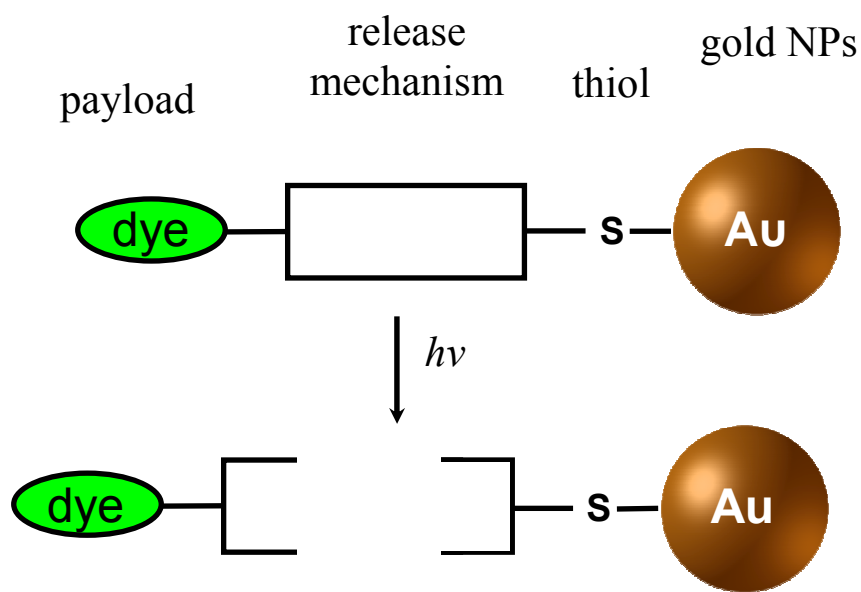
Figure 1.2 Schematic of decorated gold NPs with a thermally responsive linker before and after the photothermal effect.

Factors that influence the amount of heat generated from the photothermal effect (other than the size and shape of the NP as has been briefly mentioned and will be discussed in more detail in Chapter 2) are the intensity and the wavelength of the absorbed light. The intensity of light is defined by the amount of energy in joule (J) per unit of area (cm^2) per time (s).[31] The intensity and wavelength of light can be tuned depending on the light source (e.g., laser). By tuning the intensity, the heat generated through the photothermal effect can

be used to trigger the thermally responsive bond as this heat dissipates from gold surfaces. As a result, the payload (i.e., a dye molecule) will be released from the surfaces of gold NPs.

1.8   Triggering the Release of Molecules from the Surface of Gold NPs

1.8.1   Release Mechanism from Gold NPs

Until recently, using light as a stimulus to trigger the release from gold NPs had not been studied. Rotello and co-workers[32] have demonstrated the release of molecules from gold NP surfaces using light (Scheme 1.1). However, in this experiment ultraviolet (UV) light was used to trigger the cleavage of an ester bond. The disadvantage of this technique in medical applications is the use of ultraviolet light (λ = 350 nm) as a stimulus to trigger a release, which penetrates poorly into biological tissues and is harmful to biological tissues. UV light is harmful to biological tissues due to the fact that it damages DNA bases.[33] In addition, Rotello and co-worker did not take advantage of the photothermal effect in this experiment.
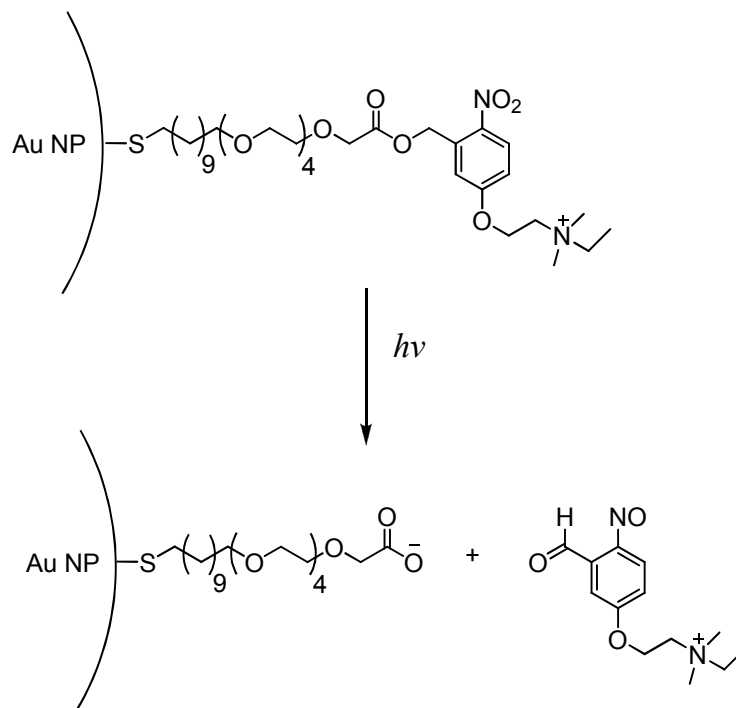
Scheme 1.1 Schematic of decorated gold NPs with a UV responsive linker before and after light treatment.

The results presented in this thesis have shown the release of molecules from gold NPs using the photothermal effect. Lee and co-workers[34] also illustrated the use of the photothermal effect with gold NPs as an optical switch for gene release. In their experiment, Lee and co-workers, have attached double stranded oligonucleotides to the gold nanorods (through a thiol linkage), and then used low energy light (λ = 800 nm) to induce the photothermal effect in the gold nanorods (Figure 1.3). When the heat from the gold surfaces reaches the melting temperature of the short DNA duplex, the double stranded oligonucleotides denatures. This process releases the antisense oligonucleotides into living cells.
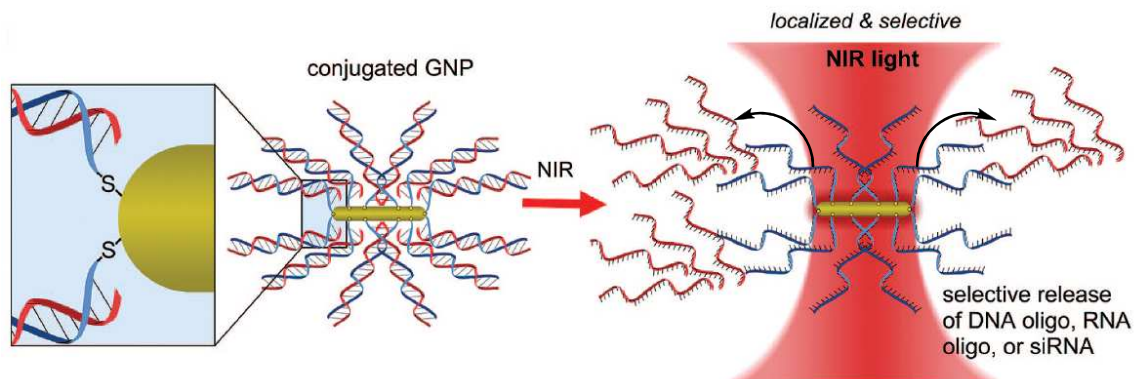
Figure 1.3 Thiol-modified sense oligonucleotides (shown in blue) are attached to gold NPs. Antisense oligonucleotides (shown in red) are then hybridized to the sense oligonucleotides. Using 800 nm wavelength cause the photothermal effect to heat the gold NPs and cause the double-stranded oligonucleotides to denature at their melting temperature and the antisense oligonucleotides to be released from the gold NPs. Reprinted with permission from Lee, S. E.; Liu, G. L.; Kim, F.; Lee, L. P. *Nano Letters* **2009**, *9*, 562. Copyright 2009 American Chemical Society.[34]

1.8.2 The *retro*-Diels-Alder Reaction and the Release Mechanism

In order to use the heat generated at the surface of the gold NPs during the photothermal effect, a thermally responsive bond is required to enable the release mechanism. In the presence of heat, this linkage, which is between the gold NPs and the payload, can break and cause the release of the payload. A well-studied thermally responsive reaction is the Diels-Alder reaction. The Diels-Alder reaction presented in Scheme 1.2 involves the cycloaddition of a diene and dienophile to form a cyclohexene ring. One benefit of the Diels-Alder reactions is reversibility. The reverse reaction is known as a *retro*-Diels-Alder reaction. This process produces the two products (Scheme 1.2).[35] An advantage of using a *retro*-Diels-Alder reaction as a release mechanism is that, depending on the choice of substituent groups on the cyclohexene (Scheme 1.2 R and R', respectively), the equilibrium rate can be controlled.[35,36] In particular, a Diels-

13

Alder adduct with substituent groups that allow the reverse process with a minimal increase in the local temperature is highly desirable. This Diels-Alder adduct can be incorporated between the gold NPs and the payload which can act as the thermally activated switch. By increasing the local temperature the Diels-Alder adduct can be dissociated into diene and dienophile. As a result the payload attached to the surfaces of gold NPs can be released from these surfaces.
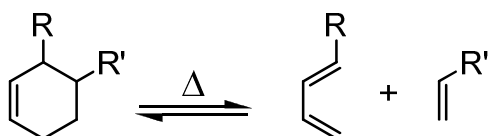
Scheme 1.2 Thermal dissociation of Diels-Alder adduct to form diene and dienophile.

1.8.3 Using the Photothermal Effect to Trigger the *retro*-Diels-Alder on Gold NPs

Many chemical reactions require heat as an activator. In most reactions the heat is provided externally to the bulk solution. However, for chemical reactions to take place it is not necessary to heat up the bulk material, but only to heat the local environment where the reaction is taking place. Using low energy light such as NIR as the stimulus to initiate the photothermal effect, gold NPs could potentially provide enough heat to cause the reaction to take place on the gold surfaces. The advantages of using light as a stimulus for triggering molecular release are spatial and temporal control. For example, comparing light to heat as a stimulus magnifies these advantages. Diffusion of heat within a solution is by propagation and spreads throughout the volume of material in

which it travels. This effect reduces the precision of heat delivered to the targeted area as well as the intensity of heat. On the other hand, coherent light travels in a narrow beam and can target, with high precision, a specific area. Targeted drug delivery using light as a stimulus provides spatial control with higher accuracy than externally applying heat for the release at the designated site. In addition, the time that a stimulus takes to reach its target differs depending on the stimuli. For example, the rate of heat flow is proportional to the thermal conductivity of materials, which is low (i.e., 0.5-1 W/m.K)[37] in biological tissues. The advantage of applying light as a stimulus is that light reaches the target almost instantaneously, which provides temporal control.

By harnessing the properties of gold NPs, such as the photothermal effect and the ease of surface decoration, gold NPs can be used as a platform for initiating thermally driven chemical reactions. In addition, by attaching molecules onto surfaces of gold NPs that contain a thermally responsive (i.e., cyclohexene) adduct, an on demand molecular release system can be achieved for drug delivery systems.

CHAPTER 2: THE PROPERTIES AND SYNTHESIS OF GOLD NANOPARTICLES

In this chapter, the properties of gold NPs relevant to the research in this thesis are discussed in more detail. These properties are SPR and photothermal effect. In addition, the modified synthesis of two different types of gold NPs are presented in this chapter. One type is a solid spherical gold NP with an average diameter of 18 nm and the other is a silica/gold core-shell NP with an average diameter of 204 nm. These two NPs were chosen because each has different SPR absorption peaks. The silica/gold core-shell NPs were synthesized by Dennis Hsiao from Dr. Byron D. Gates' laboratory. These particles will be discussed in Chapter 4, where they are used as a platform to show the release of molecules from their surfaces using the photothermal effect.

2.1   Electron Confinement and Properties of Gold NPs

Electron movement plays a key role in the physical properties (i.e., SPR and photothermal effect) of gold NPs.[38] These properties arise from the confinement of electrons in space. When electrons are bound to nuclei their motions become highly quantized and restricted to discrete energy levels. The quantization of gold NPs takes place when the size of gold particles falls into the nanometer scale.[38] Quantization of gold NPs produce unique physical properties, which is one of the reasons that their properties have been studied extensively.[18,9]

Physical properties of gold NPs are influenced by their size, shape and composition.[18] From a chemical point of view, the size, shape and composition of gold NPs can be controlled by the environment in which they are synthesized.[39] The concentration of the starting materials, reducing agents and capping groups each play a significant role in determining the final dimensions of these particles.[24] Synthesis of these NPs can require one or more steps, depending on the desired dimensions and composition of the final product.[40] For example, solid spherical gold NPs can be prepared in a one step synthesis but silica/gold core-shell NPs require a multi-step synthesis. Gold NPs can be designed to be uniform in shape and size, which make their physical properties more consistent.[39,41]

2.2   Surface Plasmon Resonance of Gold NPs

One of the properties of interest of gold NPs is their susceptibility to SPR.[30] The SPR phenomenon happens when the frequency of an oscillating electric field of incident electromagnetic waves (i.e., light) overlap with the oscillating frequency of electrons in the gold NPs.[18] The overlapping frequencies results in the absorption of an electromagnetic wave by electrons in gold NPs. The absorbed electromagnetic wave causes the displacement of electrons from the nuclei while coulombic attractions act to restore the electrons with respect to the nuclei (Figure 2.1). The alternating displacement/restoration process results in the collective oscillation of the electrons. This collective oscillation of electrons in the presence of light is known as SPR. The SPR frequency is determined by the electron density, shape and size of the electron cloud.[18]
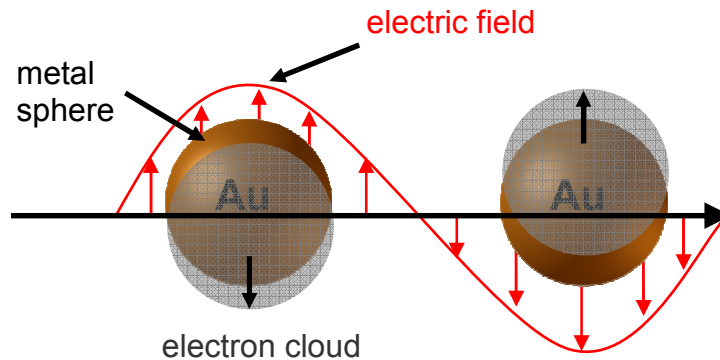
Figure 2.1 Schematic of surface oscillation for gold NPs indicating the displacement of electron cloud relative to the gold nuclei.

The SPR absorption of gold NPs (a representative SPR absorption spectrum shown in Figure 2.2) is a phenomenon that can be observed only for NPs with nanoscale dimensions (1 to 100 nm).[2] The SPR phenomenon disappears in the bulk form of gold. The SPR absorption for gold NPs follows Beer's law, which states that the absorption is dependent on concentration, extinction coefficient and path length of a sample.[42] The extinction coefficient of gold NPs consists of two components: i) absorption and ii) scattering.[41] The ratio of these two components depend on the size, shape and composition of the nanostructures.[41] Changing any one of these factors (e.g., size), will alter the SPR absorption peak. For example, changing the size of the NPs could results in three changes. They are: i) a change in the ratio of absorption to scattering for the SPR absorption peak, ii) a shift in the peak maximum, or iii) a combination of former and the latter. Therefore, to have a specific SPR absorption peak for NPs, each factor (i.e., size, shape, and composition) must be selected to produce the desirable SPR properties.
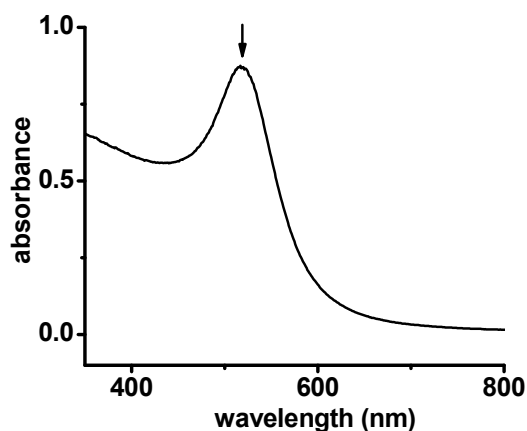
Figure 2.2 UV/Vis absorption spectrum for an aqueous dispersion of solid spherical gold NPs with diameter of ~18 nm. The SPR absorption peak maxima is at 520 nm.

2.3 Some Medical Applications of Surface Plasmon Resonance of Gold NPs

In the field of nanobiotechnology, gold NPs offer an effective method for the development of sensitive diagnostics and tumor targeting.[43] Gold NPs provide a useful method to enhance tumor imaging for several reasons:[44]

1. gold NPs can be conjugated to antibodies and used to collectively target a specific tumor,

2. the SPR signals of gold NPs are more intense than any common dye on the market (about 100,000 times),[23] which makes gold NPs detectable in low concentrations (femtomolar), and

3. compared to most organic dyes, which lose their fluorescence properties due to photo-bleaching, gold NPs are robust upon repeated exposure to high intensity light.[23]

An example of using NPs for cell targeting and imaging has been shown by El-Sayed *et al.*,[30] in which two kinds of gold NPs (solid spherical and rods) were functionalized with anti-EGFR and incubated with healthy cells (HaCat) and cancer cells (HSC). The images shown in Figure 2.3 are produced by dark field microscopy, which is a microscopy method that uses scattered light to image the sample. Dark field microscopy is a useful method when imaging cells containing NPs because the light scattering properties of NPs easily differentiate them from cells due to the fact that cells have a low optical scattering component. Figure 2.3 (left column) indicates that in the case of healthy cells, due to the lack of the EGFR in those cells, aggregation of solid nanospheres and nanorods are not observed around the cell. However, Figure 2.3 (right column), indicates the aggregation of solid gold nanospheres and nanorods in the presence of cancer cells, which express the EGFR. Hence, this result shows that functionalized NPs can be used for both cell targeting as well as enhanced cell imaging.
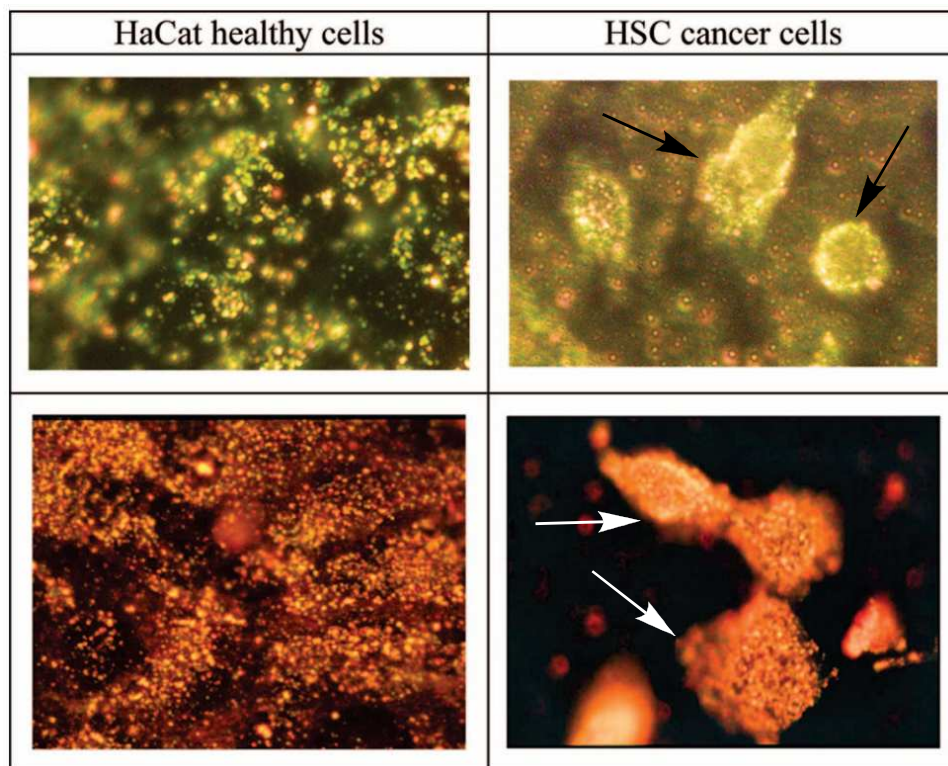
Figure 2.3 Molecular-specific imaging of cancer cells using solid spherical gold NPs with and without anti-EGFR conjugates. Dark-field microscopy shows (left column) HaCat healthy cells have (top) gold nanospheres and (bottom) gold nanorods randomly dispersed without specific binding, whereas (right column) HSC cancer cells clearly defined by the strong localized optical scattering from (top) gold nanospheres and (bottom) gold nanorods bound specifically to the surfaces of cancer cells. The scattering color of the nanospheres and nanorods can be clearly distinguished in these images. Reprinted with permission from Jain, P. K.; Huang, X.; El-Sayed, I. H.; El-Sayed, M. A. *Accounts of Chemical Research* **2008**, *41*, 1578. Copyright 2008 American Chemical Society.[30]

2.4 Photothermal Effect of Gold NPs

When gold NPs are irradiated with light corresponding to their SPR frequencies, the NPs absorb light and transform that energy to heat through a series of cascading events.[45] There are two pathways for oscillating electrons to lose the absorbed energy, one is through electron-electron collisions, which is negligible and takes place on a short time scale (~500 fs).[46] Another pathway is

through electron-phonon couplings. Phonons are quantized modes of vibrations that are allowed in a crystal lattice to transport vibrational motions in the solid structure (i.e., metals and semiconductors).[45] Electron-phonon coupling transfers the energy to the phonon. Electron-phonon coupling happens in a very short time interval, which has been measured to be on the order of 1 to 8 ps.[47] Electron-phonon coupling triggers phonon-phonon coupling, which takes place on a time scale of 100 to 400 ps.[47] The time scale of coupling is dependent on the composition and size of the nanoscale material as well as its surrounding environment.[26] The phonon-phonon interaction causes quantized vibrations in the crystal lattice and the generation of heat at the surface of gold NPs.[48]

In summary, absorption of light at the SPR frequency of the gold NPs causes a collective oscillation of electrons. As the electrons go through a relaxation process, the energy of the electron is transferred to the crystal lattice causing vibrations. Heat is generated as a result of this vibration.

2.5 Uses of the Photothermal Effect of Gold NPs in Medical Applications

The heat generated by the photothermal effect of gold NPs has been applied in medical applications. West and co-workers[49] have demonstrated the irreversible photothermal abolition of human breast epithelial carcinoma cells *in vitro*. In their study, they showed that cells maintained their viability when exposed to a NIR laser (7 min, coherent, 820 nm, 35 W), in the absence of silica/gold core-shell NPs. They also showed that cells incubated with core-shell NPs maintained their viability in the absence of a laser. However, when cells were incubated with core-shell NPs; the subsequent laser irradiation produced

localized cell death which was confined to the laser irradiation region. Furthermore, similar experiments to that of West *et al.* have been published with different NPs, such as solid spherical gold NPs.[30] These studies have had similar results to that of West and co-workers. The technique described by West and co-workers has the potential to be used as a non-invasive treatment of tumors.

The aforementioned examples that have been discussed from the literature on the optical properties of gold NPs was used for imaging purposes. In addition, the photothermal effect of gold NPs was used to kill cells or melt a polymeric layer. No previous experiment has ever taken advantage of using the heat generated from gold NPs, following the photothermal effect, to release a molecule from the gold surfaces. The photothermal release mechanism could deliver a beneficial payload decorated on the NPs surfaces.

2.6   Synthesis and Characterization of Solid Spherical Gold and Silica/Gold Core-Shell NPs

We used two different types of gold NPs as a platform to demonstrate the photothermal release of a molecule from the surface of NPs. One type was a solid spherical gold NP[24] and the other type was silica/gold core-shell NP[40]. These types of particles are specifically chosen because each type of particle, relative to each other, has a unique SPR absorption peak. Using these two types of NPs can, hypothetically, enable the release of payloads at two different wavelengths.

2.6.1   Synthesis of Solid Spherical Gold NPs

Solid spherical gold NPs are one of the most commonly used particles because of their ease of synthesis.[24] In addition, the synthesis of solid gold NPs produces particles of a uniform size and shape.[24]   The synthesis of solid spherical gold NPs starts by adding an aqueous solution of trisodium citrate to a boiling/stirring aqueous solution of tetrachloroauric (III) acid. The trisodium citrate acts as a reducing agent and reduces Au (III) to Au (0) (Scheme 2.1).[50]

$$2\ HAuCl_4 + 3 \quad\text{[citrate]} \quad \xrightarrow[\text{H}_2\text{O}]{100\ ^\circ\text{C}} \quad 2\ Au^\circ + 3 \quad\text{[product]}\quad + 8\ Cl^- + 5\ H^+ + 3\ CO_2$$
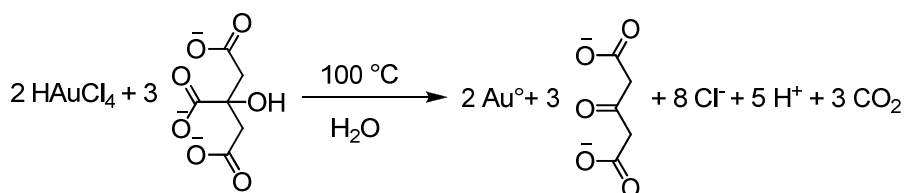
Scheme 2.1 Synthesis scheme of reduction of Au (III) to Au (0) in the presence of citrate.

Once the solution is saturated with Au (0), the gold atoms start to form seeds. More gold atoms are added to these seeds as the reduction reaction proceeds and the seeds start to form larger solid spheres of gold in the solution. The growth process of these NPs is regulated by attachment of a citrate capping group to the exposed surfaces of gold. The capping group also stabilizes the particles in the aqueous solution due to the solvated negative charges of the citrate group.[50] Since each particle is decorated with negative charges, the repulsion between each particle prevents aggregation and precipitation of the NPs. The aqueous solution of solid spherical gold NPs has a burgundy color (Figure 2.4) and is suspended in water for months without precipitation.

Figure 2.4 Aqueous solution of solid spherical gold NPs with white light illumination from behind the sample.

2.6.2   Characterization of Solid Spherical Gold NPs

To characterize the solid spherical gold NPs, two common techniques are used: i) transmission electron microscopy (TEM),[51] and ii) UV/Vis absorption spectroscopy.

Transmission electron microscopy techniques can image the gold NPs to characterize their dimensions and crystallinity. In a typical TEM analysis a beam of electrons pass through a sample holder that contains dried NPs. The electrons interact with the specimen by scattering and as a result of these interactions an image is formed. The image can be recorded on phosphorescent screen or a camera containing a charge-couple device.[51] The TEM images show the size and shape of NPs (Figure 2.5A). The preparation of TEM samples was done by placing a droplet of an aqueous solution of synthesized NPs onto formvar/carbon coated copper grids at room temperature (~22 °C) and the grid was left on the bench over night to air dry. (Note: the copper grid was covered with a watch glass to protect the sample from collecting dust.) This copper grid was then placed under vacuum to further dry at 20 mmHg for 2 h. Samples for the TEM

analysis have to be as dry as possible because the electron microscope is under high vacuum (~10^{-7} mbar). The high vacuum is necessary for TEM imaging because the air molecules will scatter the electrons. If the copper grid that enters the TEM instrument is wet or contains volatile molecules, it would prevent the instrument from achieving the high vacuum necessary for high resolution imaging. As a result, the instrument would require a few hours of pumping to create the necessary vacuum. In addition, a vacuum failure could damage the instrument. Once the copper grid is dry, the specimen is inserted into the TEM instrument. Then TEM images can be recorded for the solid spherical gold NPs. A representation of such an image is shown in Figure 2.5A.

(A)   **(B)**
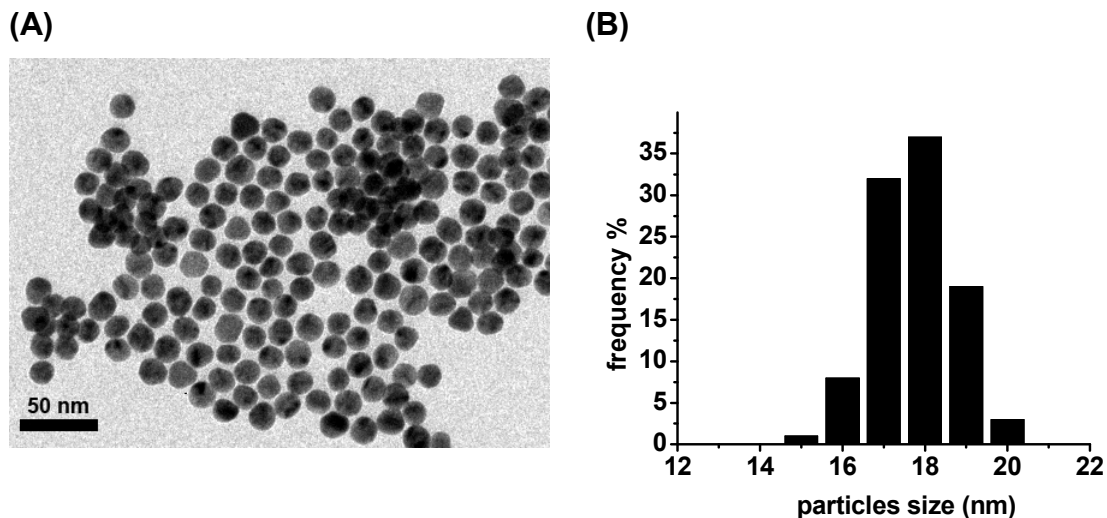
Figure 2.5 (A) TEM images of 18 nm diameter solid spherical gold NPs, and (B) a histogram corresponding to the size distribution of gold NPs counted for a sample of 100 NPs.

The electron microscopy analysis indicates a uniform shape and size distribution of spherical gold NPs (Figure 2.5A). To find the average diameter of the solid spherical gold NPs, the diameter of 100 randomly chosen particles were measured for comparison. To measure the size of each NPs, digital TEM images

of the NPs were imported into Adobe Photoshop® and the measuring tool therein was calibrated and used to measure the diameter of each particle. A histogram for solid spherical gold NPs was constructed based on this analysis of TEM image as shown in Figure 2.5B. The average diameter of the solid spherical gold NPs was found to be 17.8 ± 0.9 nm (one standard deviation, which includes ~68% of the data values). The average diameter is a good estimate of the NPs dimensions and will be used in Chapter 4 to estimate the concentration of solid spherical gold NPs in the aqueous solution.

A UV/Vis absorption spectroscopy was used as a second technique to characterize the SPR of gold NPs. This technique provides a UV/Vis absorption spectrum of an aqueous suspension of solid spherical gold NPs as shown in Figure 2.6. The SPR peak for these particles is centred at 520 nm.
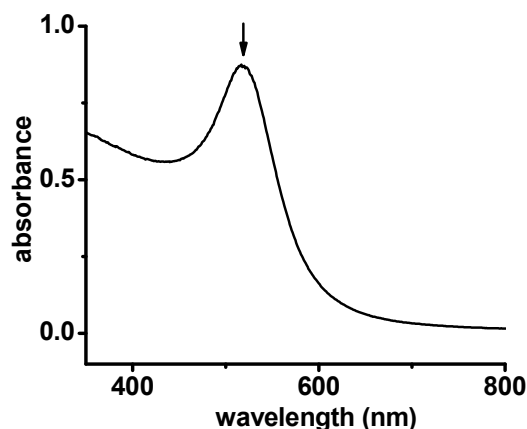
Figure 2.6 UV/Vis absorption spectrum of an aqueous dispersion of solid spherical gold NPs with diameter of 18 nm. The SPR absorption peak maxima is at 520 nm.

Based on theoretical calculations performed by El-Sayed and co-workers,[41] the SPR peak at 520 nm for solid spherical gold NPs is mainly due to

absorption rather than scattering of light. Therefore, most of the light absorbed at 520 nm is converted to heat due to the photothermal effect.

The uniformity in shape and size of the NPs provide consistency in their SPR absorption frequency. As a result of a decrease in the size uniformity, the shape of absorption peak would broaden,[52] which would lower the efficiency for absorption of light at a specific frequency. Therefore, the efficiency of heat generation from the NPs through the photothermal effect decreases as the uniformity in the size of the NPs also decreases. Factors such as higher SPR absorption for solid spherical gold NPs and uniformity in the size of NPs should be considered in detail when it comes to photothermal effect because these factors contribute greatly to higher efficiency of converting light into heat through the use of these NPs.

2.6.3 Some Challenges for the Synthesis of Solid Spherical Gold NPs

It is important to mention some of the difficulties and challenges that were encountered during the preparation of solid spherical gold NPs. The synthetic procedures for the preparation of these particles was reproduced from the current literature,[24,40] but uniform solid spherical gold NPs that were stable in solution could not be achieved without some modification to the procedure. The synthesis of solid spherical gold NPs initially followed a procedure obtained from Plech and co-workers.[24] In the synthesis of gold NPs, the size and shape of the flask and the size of the stir bar can play an important role in the uniformity of the synthesized NPs[24] as these factors have a direct effect on the dynamics of stirring. Therefore, one needs to repeat and tune the procedures and select ideal

apparatus to find the optimal conditions for the synthesis of NPs. Other factors can be important as well, such as the molar ratio of the starting materials. Following the exact concentration of starting material and reducing agent reported in the literature had to be modified to produce the described uniformity in the size of solid spherical gold NPs. To obtain uniformity, the ratio of reducing agent with respect to starting material was modified (i.e., concentrations of trisodium citrate to tetrachloroauric (III) acid were used from: 10:1, 5:1, 4:1, 3:1, 2:1 to 1:1 molar ratio, respectively). Some images of NPs from failed syntheses are shown in Figures 2.7A and B, which indicate the polydispersity (broad range of sizes) of size and aggregation of gold NPs due to a lack of stability, respectively. Even after tuning the procedure to produce uniform solid spherical gold NPs, the reproducibility is not 100%. Experience has shown that using glassware that has not been properly cleaned (i.e., with aqua regia and piranha) before use, results in NPs that are not stable and precipitate from the solution as black aggregates a few hours after synthesis. The instability could be due to the presence of impurities, such as organic residue from soap, inadvertently introduced before or after synthesis, which results in the aggregation of the gold NPs in the aqueous solution. In summary, the synthesis of gold NPs requires fine attention to details in order to produce reproducible results of uniform structures.

(A)

(B)
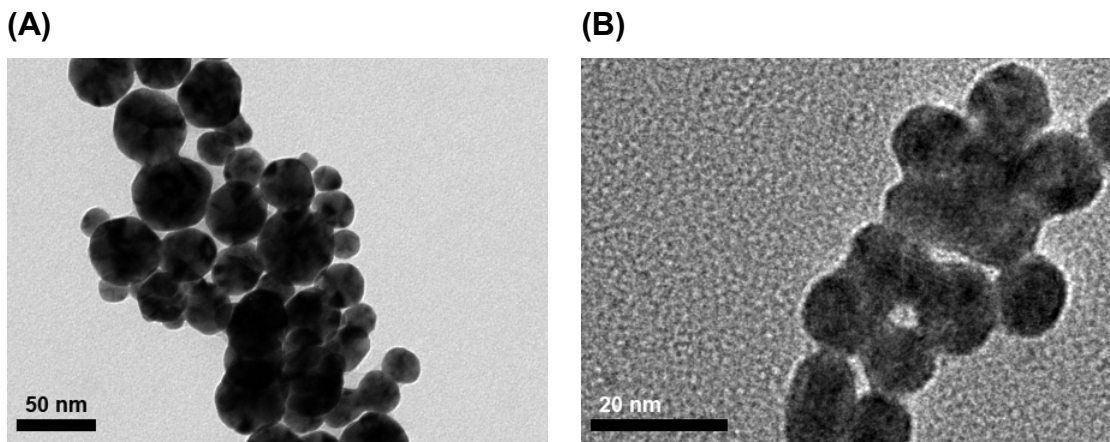
Figure 2.7 TEM images of samples from the failed synthesis of stabilized solid spherical gold NPs: (A) polydisperse gold NPs, and (B) aggregated gold NPs.

2.7 Synthesis of Silica/Gold Core-Shell NPs

Silica/gold core-shell NPs consist of a silica core (180 nm diameter) and a layer of gold with a thickness of ~10 nm over the silica particle. Their synthesis requires four steps:

1. *Formation of solid silica particles* by addition of tetraethyl orthosilicate to aqueous ammonia in ethanol, which starts the nucleation and growth of silica particles (Scheme 2.2A). The reaction is followed by the addition of (3-aminopropyl) triethoxysilane, which caps the silica particles through a condensation reaction and functionalizes the particles with amine groups (Scheme 2.2B).

(A)

$$Si(OCH_2CH_3)_4 \xrightarrow{\text{NH}_3, \text{H}_2\text{O}} (CH_3CH_2O)_3Si\text{-}OH + CH_3CH_2OH$$

$$2\,(CH_3CH_2O)_3Si\text{-}OH \xrightarrow{\text{Condensation}} (CH_3CH_2O)_3Si\text{-}O\text{-}Si(OCH_2CH_3)_3 + H_2O$$

(B)

$$\text{SiO}_2\text{ NPs}\!\!\begin{Bmatrix}\text{-OH}\\\text{-OH}\\\text{-OH}\end{Bmatrix} + 3\,(CH_3CH_2O)_3Si\text{-}CH_2CH_2CH_2NH_2 \xrightarrow{\Delta} \text{SiO}_2\text{ NPs}\!\!\begin{Bmatrix}\text{-O-Si-}CH_2CH_2CH_2NH_2\\\text{-O-Si-}CH_2CH_2CH_2NH_2\\\text{-O-Si-}CH_2CH_2CH_2NH_2\end{Bmatrix}$$

$$+ \, n\, CH_3CH_2OH$$
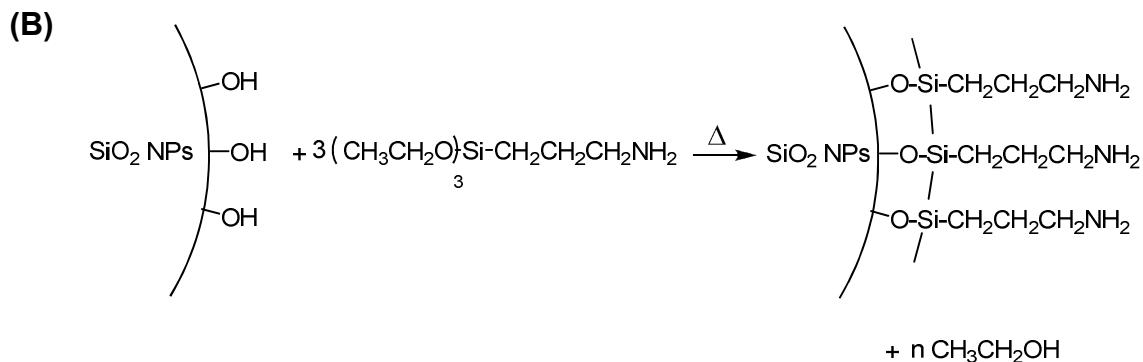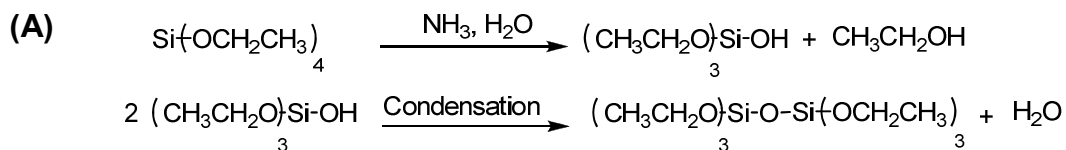
Scheme 2.2 (A) Synthesis of silica particles through multiple hydrolysis and condensation of tetraethyl orthosilicate, and (B) Functionalization of the surface of the silica particles with amine groups.

2. *Preparation of gold seeds* by reduction of tetrachloroauric (III) acid to Au (0) in presence of tetrakis (hydroxymethyl) phosphonium chloride as a reducing agent in water. When the solution is saturated with gold atoms, the solid spherical gold seeds grow to a diameter of 3-6 nm (Scheme 2.3).

$$2\,HAuCl_4 + 3\,(HOCH_2)_4PCl \xrightarrow[\text{H}_2\text{O}]{\text{NaOH}} 2\,Au^\circ + 3\,(HOCH_2)_3P$$

$$+ \, 5\,H^+ + 11\,Cl^- + 3\,HCHO$$
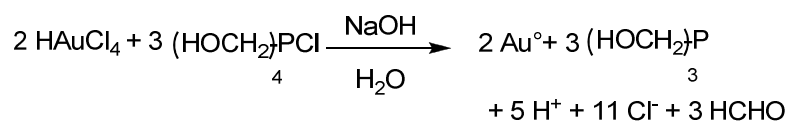
Scheme 2.3 Synthesis for the reduction of Au (III) to Au (0) in the presence of tetrakis (hydroxymethyl) phosphonium chloride.[53]

3. *Attachment of the gold seeds onto the surface of silica particles* by adding a solution containing the seeds to the solution of silica particles. Since the surface of silica particles are decorated with amines, the amine group

forms a covalent bond with the gold seeds. As a result, the surface of silica particles is partially decorated by gold seeds. Any un-attached gold seeds are removed from the solution by centrifugation of the decorated silica particles followed by re-suspension of these silica spheres in high purity water.

4. *Growth of a gold layer over the decorated silica particles* by reduction of more gold onto the surface of decorated silica particles. In a solution of seeded silica NPs, tetrachloroauric (III) acid was reduced to Au (0) by formaldehyde as shown in Scheme 2.4. The reduced gold atoms were added to the seeded silica to form a layer of gold around the silica particles.

$$HCHO + H_2O \xrightleftharpoons[H_2O]{Keq = 2280} H_2C(OH)_2$$

$$2\ HAuCl_4 + 3/2\ H_2C(OH)_2 \longrightarrow 2\ Au^\circ + 3/2\ CO_2 + 8\ Cl^- + 8\ H^+$$
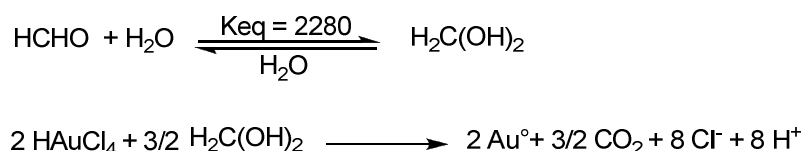
Scheme 2.4 Synthesis scheme for the reduction of Au (III) to Au (0) in the presence of formaldehyde. [54]

A solution of silica/gold core-shell NPs has a blue colour as shown in Figure 2.8. Silica/gold core-shells has blue colour because they absorb and scatter low energy light (600-1000 nm) and transmit higher energy light (400-500 nm). These NPs can be dispersed into solution for ~2 h and after that they start to visibly settle to the bottom of the container. These particles can be easily re-suspended by shaking the glass vial.

Figure 2.8 Aqueous solution of silica/gold core-shell NPs with white light illumination from behind the sample.

2.7.1 Characterization of Silica/Gold Core-Shell NPs

To characterize the synthesized silica/gold core-shell NPs, TEM images were taken of the sample. The preparation of TEM samples of aqueous dispersions of silica/gold core-shell NPs was identical to that for solid spherical gold NPs. A representative TEM image of silica/gold core-seeds, which was produced in the third step of the synthesis of the silica/gold core-shell NPs, is shown in Figure 2.9A. The image shows a uniform shape and size of silica particles that are decorated with seeds of solid spherical gold NPs. Further reduction of tetrachloroauric (III) acid in the fourth step of the silica/gold core-shell NPs synthesis, adds more gold atoms to the gold seeds to form a layer of gold over the silica particles. A complete shell of gold on the silica particles can be seen in Figure 2.9B.

To find the average diameter of the silica/gold core-shell NPs, the diameter of 100 randomly chosen particles were measured from the TEM images. A histogram for silica/gold core-shell NPs was constructed based on

these measurements as a representation of size distribution, as shown in Figure 2.9C. The average diameter of NPs was found to be 204 ± 9 nm (reported error of one standard deviation).

(A)

(B)

(C)
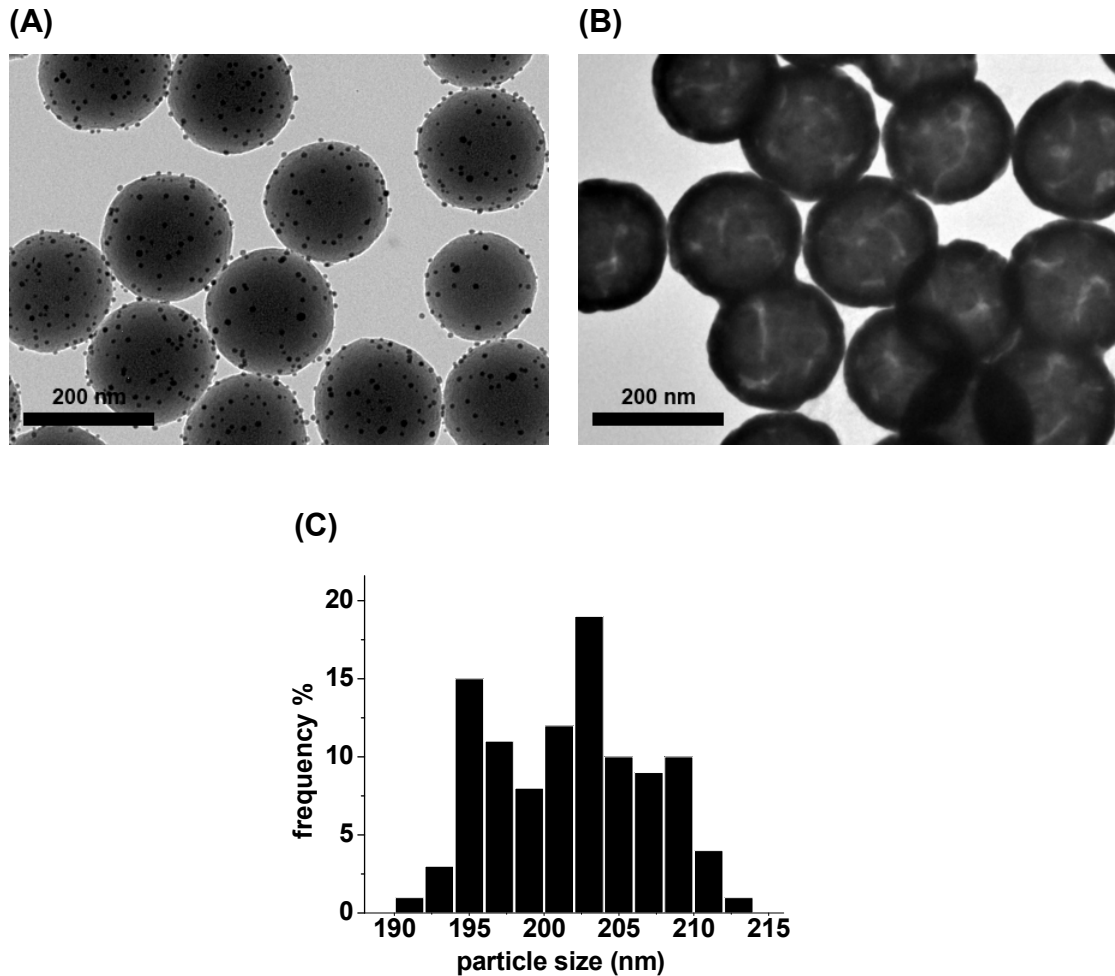
Figure 2.9 TEM images of (A) silica/gold core-seeds with a diameter of ~180 nm silica particles, and (B) silica/gold core-shell NPs with a ~204 nm diameter. (C) Histogram corresponding to the size distribution of silica/gold core-shell NPs, measured from a sample of 100 NPs.

The absorption properties of silica/gold core-shell NPs, were determined by acquiring a UV/Vis absorption spectrum of aqueous dispersions of these NPs.

The spectrum (Figure 2.10) shows that NPs have two primary absorption bands at 650 and 900 nm. The thickness of the gold shell plays a major role in the observed SPR absorption band. The SPR absorption is tunable depending on the thickness of the gold shell.[55] An advantage of using these larger particles in comparison to solid spherical gold NPs (e.g., 18 nm diameter) is the tunability of its SPR to the NIR region of the electromagnetic spectrum. These particles seem to be a better candidate for delivery of a payload in biological systems because the NIR region of the electromagnetic spectrum has better tissue penetration than the visible region of the electromagnetic spectrum.[56] In addition, NIR light has a lower energy that than visible light, which makes it less harmful to biological tissues.
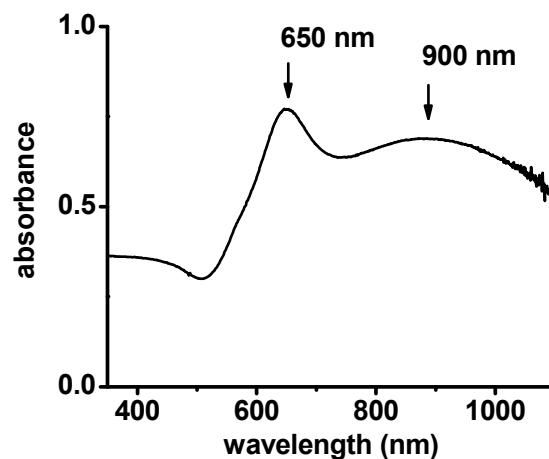
Figure 2.10 UV/Vis absorption spectra for aqueous dispersions of silica/gold core-shell NPs with a diameter of ~204 nm. The SPR absorption peak maxima are at 650 and 900 nm.

Other structures such as gold nanorods could be great candidates as well due to the tunability of the SPR absorption in the visible and NIR regions of the

electromagnetic spectrum.[57] The SPR of gold nanorods can be tuned by changing the aspect ratio of the rods.[57] This thesis, however, only focuses on the use of solid gold NPs and core/shells for the photothermal effect.

2.8   Decoration of the Surfaces of Gold NPs

After synthesizing the gold NPs, the surface chemistry of these NPs can be modified by the introduction of molecules containing thiol or disulfide into a solution of gold NPs.[58] Due to the strong affinity between the gold and the sulfur, a covalent bond forms between gold and sulfur.[59] The exact nature of the Au−S bond has not been understood completely, most likely because of the formation of multiple bonds between sulfur and surface of gold clusters.[60] Due to Au−S interactions, a variety of functional groups containing thiol can be added to the surface of gold NPs to make the surface charged, hydrophilic or hydrophobic (Scheme 2.5).[58] The ease of changing the surface chemistry enables these particles to be dispersed in a variety of solvents, from water to hexane.[58]
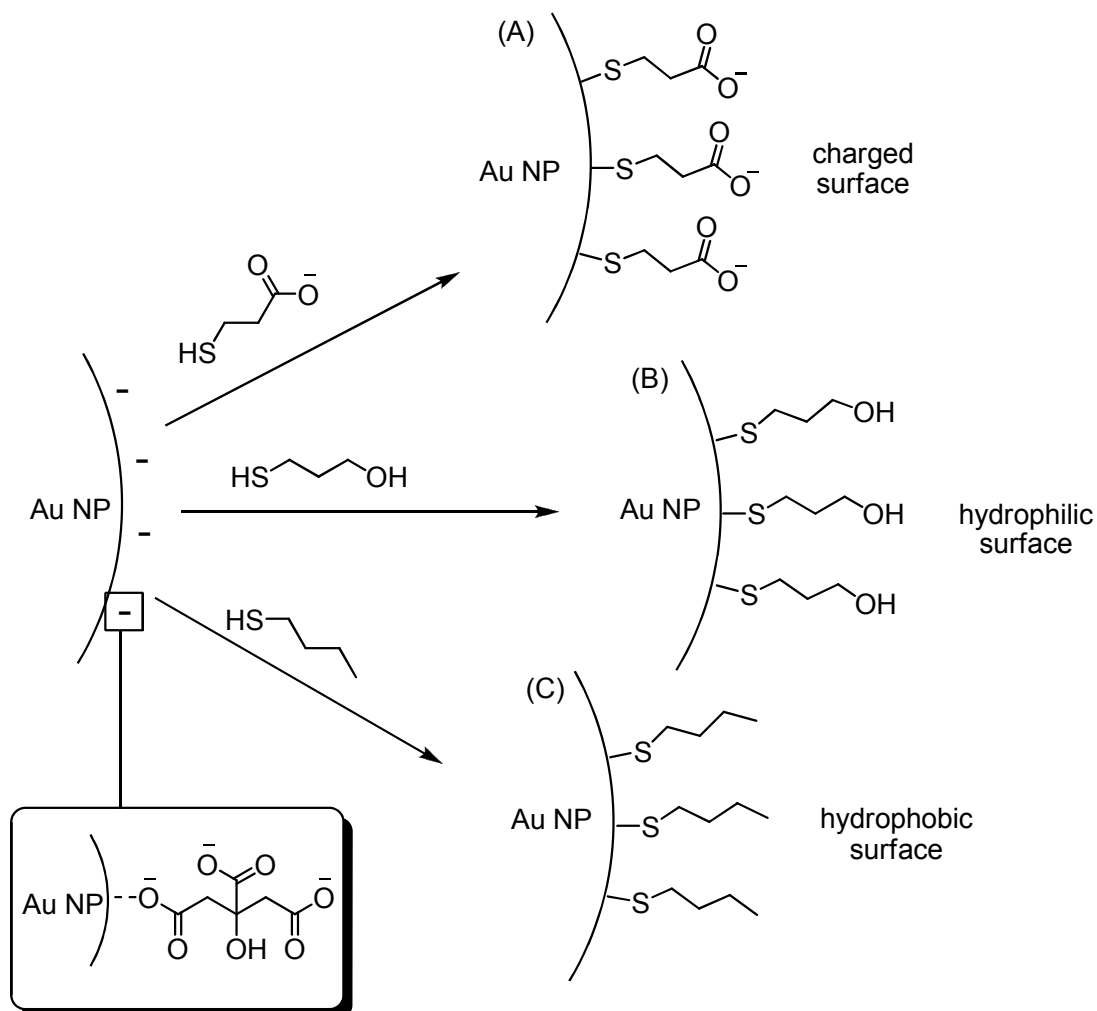
Scheme 2.5 Surface modification of negatively charged solid spherical gold NPs by introduction of (A) 3-mercaptopropionic acid, (B) 3-mercaptopropanol, and (C) 1-mercaptobutane.

In addition, macro-molecules can be attached onto gold NP surfaces, such as proteins[61] or DNA.[14,8] The coupling of macro-molecules to gold can also be due to the presence of a thiol or disulfide moiety in the structure of macro-molecules. The coupling of proteins to gold NPs enables the particles to be targeted to specific cells, or coupling of DNA to gold NPs enables the particles to be used for gene and drug delivery.[14]

In this thesis, to attach the molecules to the gold NPs surfaces, a disulfide moiety was incorporated in the proposed molecules to link the molecules of interest to the gold surfaces. Further discussion about the proposed molecules is in Chapter 3.

2.9   Conclusions

Gold NPs can be used as a delivery vehicle by conjugation of a payload to the gold surfaces. Furthermore, harnessing the unique properties of gold NPs, such as the photothermal effect, as stimuli to trigger the release of payloads, opens a new direction of research into the use of these materials. Using two different gold nanostructures provides flexibility of choosing between the different wavelengths for their SPR properties as well as the different sizes of these structures. Besides the spatial and temporal control, using both structures simultaneously can provide sequential release of different payloads.[62]

2.10   Experimental Section

2.10.1 General Information

Unless otherwise stated, all the chemicals were purchased from Sigma Aldrich and used without further purification. Water used in the synthesis and purification of NPs was from a Barnstead NANOpure Diamond water purification system (18 MΩ). The UV/Vis absorption spectra were obtained using Varian Cary 300-Bio and fluorescence spectra were recorded using a Photon Technology International QuantaMaster spectrometer with a photomultiplier tube as the detector. TEM images were taken on an FEI Tecnai G2 STEM. TEM grids were prepared by spotting a 10 μL droplet of solution containing gold NPs onto a copper grid (300 mesh) coated with a carbon/formvar layer. The TEM sample was dried at room temperature over night followed by 2 h under vacuum (-975 mbar). All the glassware were washed with *aqua regia* [(3:1 (v/v) hydrochloric acid (37%):nitric acid (70%)], with high purity water (x3), and *piranha* [7:2 (v/v) sulfuric acid (98%):hydrogen peroxide (30%)] each for ~10 min. (*Caution: Piranha solution is highly reactive toward organic material and aqua regia is also a strong oxidizer. Handle these solutions with extreme care.*) Solvent allocations were measured using VWR Signature single-channel pipettors with variable volume adjustment (volumes: 0.5-10, 10-100 and 100-1000 μL). The stir bar used in the synthesis of solid gold NPs was a VWR magnetic stirring bar coated with Teflon (7/8"x5/16" Catalogue number: 58947-106) and stirring hotplates was a IKA$^®$ RET Basic.

2.10.2 Synthesis of Solid Spherical Gold NPs

Solid Spherical gold NPs were synthesized according to the Turkevich method with some modifications.[24] A solution of tetrachloroauric (III) acid 99.9% (0.15 mM) was prepared in water (18 MΩ), (50 mL, in a 250 mL round bottom flask) and heated to boiling. The stirring (VWR magnetic stirring bar coated with Teflon 7/8"x5/16" Catalogue number: 58947-106, at 1500 rpm) solution of tetrachloroauric acid was treated with a preheated 5 mL aqueous solution of trisodium citrate 99% (4.5 mM). During this thermal reduction process, the appearance of the solution changed from a transparent yellow to a transparent red coloration. After 20 min of boiling and stirring, the reaction was removed from the heat and left at room temperature to cool down. To characterize the size and shape of the synthesized NPs, the TEM images of the sample were recorded using different magnifications (Figure 2.11A and B). Based on the TEM analysis of 100 NPs, the average particle size was found to be 17.8 ± 0.9 nm.

(A)   **(B)**
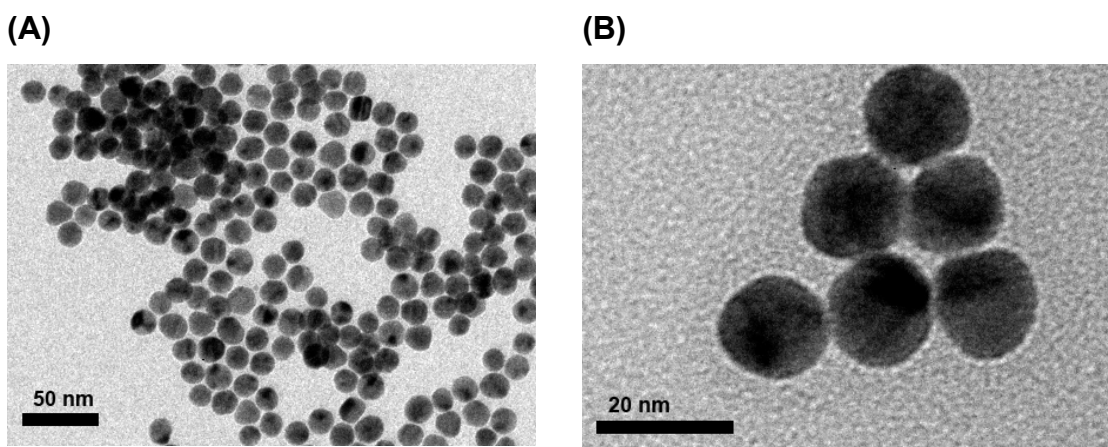
Figure 2.11 TEM images of 18 nm diameter solid spherical gold NPs at two different magnifications.

2.10.3 Synthesis of Silica/Gold Core-Shell NPs

Silica particles were synthesized according to the Stöber method.[63] The silica NPs were prepared by the addition of tetraethyl orthosilicate 98% (3.6 mL) to a stirred solution of aqueous ammonia (7.1 mL, 30%) in EtOH (99.9 %, 50 mL) and the reaction stirred at room temperature overnight. The suspension was treated with (3-aminopropyl) triethoxysilane 98% (100 μL) and the mixture was allowed to stir for 2 h at room temperature followed by 1 h of heating at reflux using a heating mantle.[64] Gold NP seeds were prepared according to the method published by Duff.[64] Sodium hydroxide 97% (0.2 M, 1.5 mL) was added to high purity water (45.5 mL) followed by addition of tetrakis (hydroxymethyl) phosphonium chloride 80% (84 mM, 1 mL) and tetrachloroauric (III) acid 99.9% (25 mM, 2 mL). After adding each compound, the solution was stirred for 2 min before adding the next reagent. Gold NPs seeds (100 µM) were mixed with the

functionalized silica NPs (1 mL) and the solution left for 8 h to attach the seeds onto the surface of the silica.[65] Gold seeds that are not attached to the silica NPs were removed by centrifugation at 13,500 rpm for 4 min followed by decantation of supernatant liquid and re-suspension of the collected solids in water. This purification process was repeated 5 times. The gold shell was grown from the layer of gold seeds in a solution containing a tetrachloroauric (III) acid (0.384 mM, 4 mL), gold seeded silica (20 µL) and formaldehyde (10 µL) as a reducing agent.[66] Excess gold salt was removed by a procedure of centrifugation at 4,000 rpm for 15 min followed by decanting and re-suspension in water. This purification process was repeated 3 times. Particles were characterized by TEM

and the average size of the core-shell particle was determined to be 204 ± 9 nm (Figure 2.12).
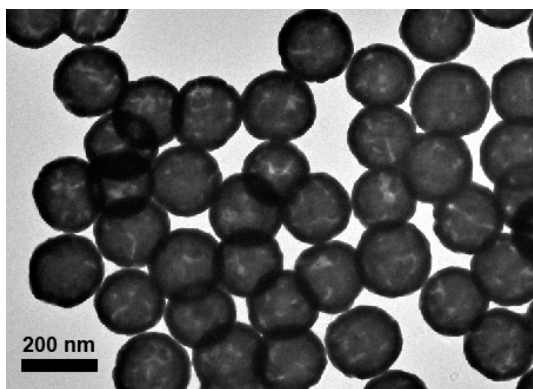
(A)   **(B)**
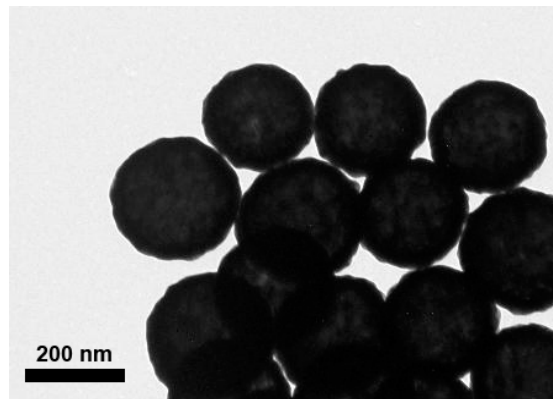
Figure 2.12 TEM image of 204 ± 9 nm diameter silica/gold core-shell NPs at two different magnifications.

CHAPTER 3: DESIGN AND SYNTHESIS OF A THERMALLY RESPONSIVE MOLECULE

3.1   Requirements for the Thermally Responsive Molecule

As mentioned in Chapter 1, the goal of this thesis is to demonstrate the release of molecules from the surface of gold NPs using low energy light. This release can be demonstrated in two steps: i) by the attachment of a molecule to the gold NPs surfaces, and then ii) by the detachment of a segment of this molecule initiated using the photothermal effect. The aim of this chapter is to describe the design and synthesis of a molecule that can demonstrate such a release. From a design perspective, three major features should be included in the molecule:

1. The molecule must include a functional group that enables anchoring to the surface of gold NPs. Since gold reacts spontaneously with sulphur to form a covalent Au-S bond, a thiol or disulfide moiety should be included in the molecule.[17]

2. To confirm molecular release after the photothermal effect, a monitoring technique is required that can differentiate between the bound and unbound molecules. This monitoring can be achieved by integrating a fluorescent dye into the molecule, which allows the release to be detected by fluorescence spectroscopy.

3. A thermal labile bond relative to the rest of the linker, should be incorporated between the thiol or disulfide and the dye moiety of the targeted molecule. The purpose of this labile bond is to break only when adequate heat is released from the gold NPs, thereby allowing the dye to separate from the surface of the gold NPs.

In this chapter, the discussion will focus on the design and synthesis of a molecule that includes all the features listed above.

3.2   Requirements for the Thermally Labile Linker

A thermally labile component, which in the presence of heat can act as the release mechanism, is an essential part of the molecular linker. Selecting an appropriate reaction with a suitable molecule is the requirement of a successful release mechanism.

In terms of the long-term goals of this project (which is to use gold NPs as a drug delivery vehicle in biological systems) the temperature that would activate the reaction should be above 37 °C (i.e., average body temperature of a human). In addition, the activation temperature should not be too high (e.g., a few hundred degrees) to require minimal photothermal energy to activate the reaction and thus, minimize localized damage due to an increase in the temperature of the surrounding environment.

Additionally, stability in aqueous solution is crucial because any side reaction could have detrimental consequences. It is also essential to use a

compound that is biocompatible and nontoxic to a biological organism in its un-activated or activated form.

3.3   Exploiting the *retro*-Diels-Alder Reaction for a Release Application

Most fragmentation reactions require catalysts, high temperature, specific reagents, or a combination of these factors.[67] However, one fragmentation reaction has been extensively applied to produce thermally reversible polymers,[68] thermally remendable cross-linked polymers[69] and thermally removable epoxy adhesives[70] at low temperatures. In all the above examples, a *retro*-Diels-Alder reaction was used as a thermal trigger. More specifically a *retro*-Diels-Alder reaction of bicyclic compound **3.1** (Scheme 3.1) to form furan **3.2** and maleimide **3.3**, was used as the release mechanism.

| **3.1** | **3.2** | **3.3** |
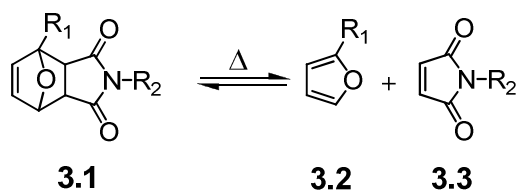
Scheme 3.1 Furan-maleimide Diels-Alder adduct dissociation and formation.

The Diels-Alder reaction[35] is a cycloaddition between a diene **3.2** and dienophile **3.3** to form a cyclohexene **3.1**. Often times, in the presence of heat, Diels-Alder adducts dissociate to reform the diene and dienophile. This process is called a *retro*-Diels-Alder reaction. Although the number of reports on Diels-Alder reactions is much greater than that on *retro*-Diels-Alder reactions, this does not reduce the potential applications of *retro*-Diels-Alder reactions. The Diels-Alder reaction and, particularly, the bicyclic compound **3.1** is ideal for the

demonstration of a release mechanism because it does not require a catalyst, additional reagents, or high temperature for reversibility.

Among all the reported *retro*-Diels-Alder reactions, there are many that proceed at relatively low temperatures (i.e., ~50 °C).[71-73] A Diels-Alder reaction shows appreciable reversibility when the free energy of the products is similar to that of the starting materials (Figure 3.1). Another factor that influences the reactivity of the Diels-Alder reaction is the activation energy. For a Diels-Alder reaction to be reversible at low temperature both the activation energy and reaction free energy should be minimal to permit reversibility.
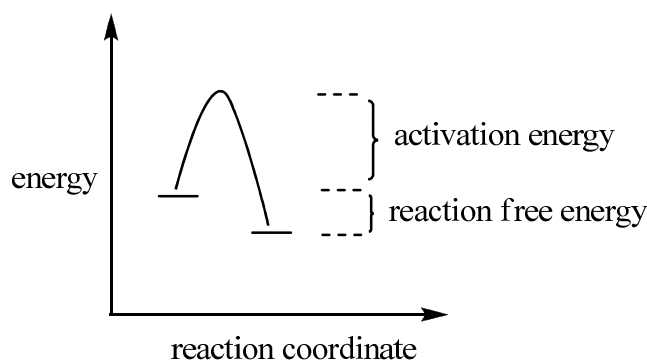
Figure 3.1 Energy profile of a reaction.

3.4   Kinetics versus Thermodynamics of Diels-Alder Reactions

The reaction between furan **3.4** and maleimide **3.5** (Scheme 3.2) results in the formation of two diastereomers, *endo* **3.6** and *exo* **3.7**. In this case, the *endo* Diels-Alder adduct is the kinetic product and the *exo* Diels-Alder adduct is the thermodynamic product.[74]
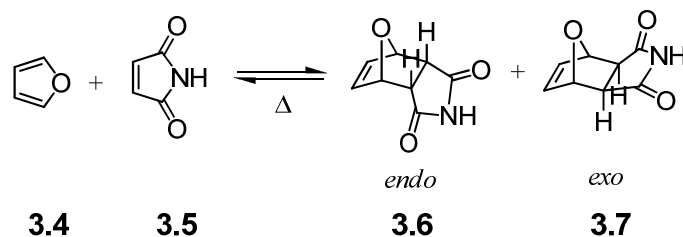
Scheme 3.2 Stereoselectivity of the Diels-Alder adduct synthesized from furan and maleimide.

The awareness of thermodynamic versus kinetic selectivity was observed during the 1940's in different laboratories.[75] In 1944, Woodward and Baer shed more light on the principle of kinetics versus thermodynamics of Diels-Alder reactions. They summarized their proposal in terms of relative activation energies as illustrated in Figure 3.2.[76] Based on relative activation energy in Figure 3.2, formation of the *endo* adduct **3.6** involves a lower energy transition state and thus this compound forms faster than the *exo* **3.7** adduct. However, the *endo* product is less stable.
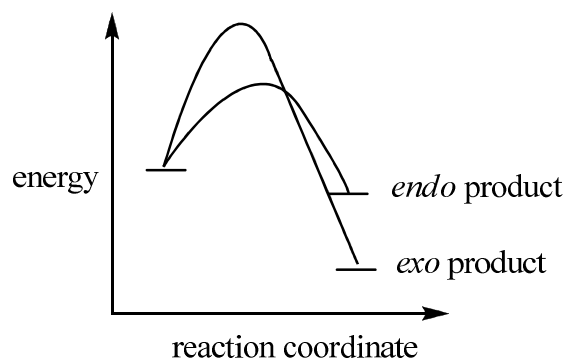
Figure 3.2 Diagram of energy versus reaction coordinate for the Diels-Alder reaction.

The important difference between the *endo* and *exo* adducts is in their respective activation energies for the *retro*-Diels-Alder reaction. The energy that

is required to cause the reverse process is lower for the *endo* adduct compared to the *exo* adduct. Therefore, the *endo* adduct **3.6** is preferred to the *exo* adduct **3.7** for our release application. Another criterion for selecting one adduct over the other, is the rate of reactivity of each adduct at room temperature. For example, if the *retro*-Diels-Alder reaction for the *endo* adduct proceeds at room temperature, the substrate would be undesirable for our release application because the measurement for the photothermal release of molecules from NPs depends on two factors: i) the *retro*-Diels-Alder reaction due to room temperature, and ii) *retro*-Diels-Alder reaction due to the photothermal effect. Therefore, to find a better understanding about compounds **3.6** and **3.7**, an experiment was performed to determine which one would be a better candidate to be incorporated in the molecular linker.

3.5   *endo* versus *exo* *retro*-Diels-Alder Adduct

An experiment comparing the rates of the *retro*-Diels-Alder reaction on *endo* and *exo* Diels-Alder adducts (Figure 3.3A) was conducted by Dr. Guoxia Jin from Dr. Neil R. Branda's laboratory. In this experiment, substrates were specifically chosen to have similar substituent groups to that in the proposed linker. This similarity in the structure should minimize any substituent effect on the rate of the *retro*-Diels-Alder reactions as compared to the target molecule.

The goal of this study was to determine which isomer (Figure 3.3A, **3.8** and **3.9**) is best suited to undergo *retro*-Diels-Alder reaction triggered by a photothermal effect. The criteria for this evaluation are the stability and reactivity at both ambient temperatures (~22 °C) and ~60 °C for each isomer. Any *retro*-

Diels-Alder reaction at room temperature would be undesirable due to an unwanted release of dye from the surfaces of the gold NPs when preparing for the photothermal study. In addition, a study at ~60 °C provides a qualitative rate of the *retro*-Diels-Alder reaction for each isomer.

The experiments were conducted by preparing pure samples of **3.8** and **3.9** in deuterated acetonitrile. To determine the stability of these adducts, both were left at room temperature for a period of 24 h. ^{1}H NMR spectroscopy confirmed that there was no measurable change in the ^{1}H NMR spectrum of either isomer after this period.

The samples were then heated in a water bath at 60 °C. During this study ^{1}H NMR spectra of each sample were recorded 5 times at 1 h intervals (except for the last measurement of *exo* adduct, which had a 2 h interval). Both **3.8** and **3.9** underwent a *retro*-Diels-Alder reaction as indicated in Figure 3.3 A, however, the conversion was different for each isomer. Based on analysis of the ^{1}H NMR spectra and integration of appropriate peaks, the percentage change of **3.8** was found to be 63% (Figure 3.3 B, based on molar ratio), compared to only 33% for **3.9** after 5 h. As a result of this experiment the *endo* Diels-Alder adduct was chosen to be a better candidate since its reverse process requires less heat. Therefore, minimizing the thermal impact on the surrounding caused by the photothermal effect during and after irradiation.

(A)

endo
3.8

60°C
CD₃CN

3.10   **3.11**

exo
3.9

60°C
CD₃CN

3.10   **3.11**

(B)
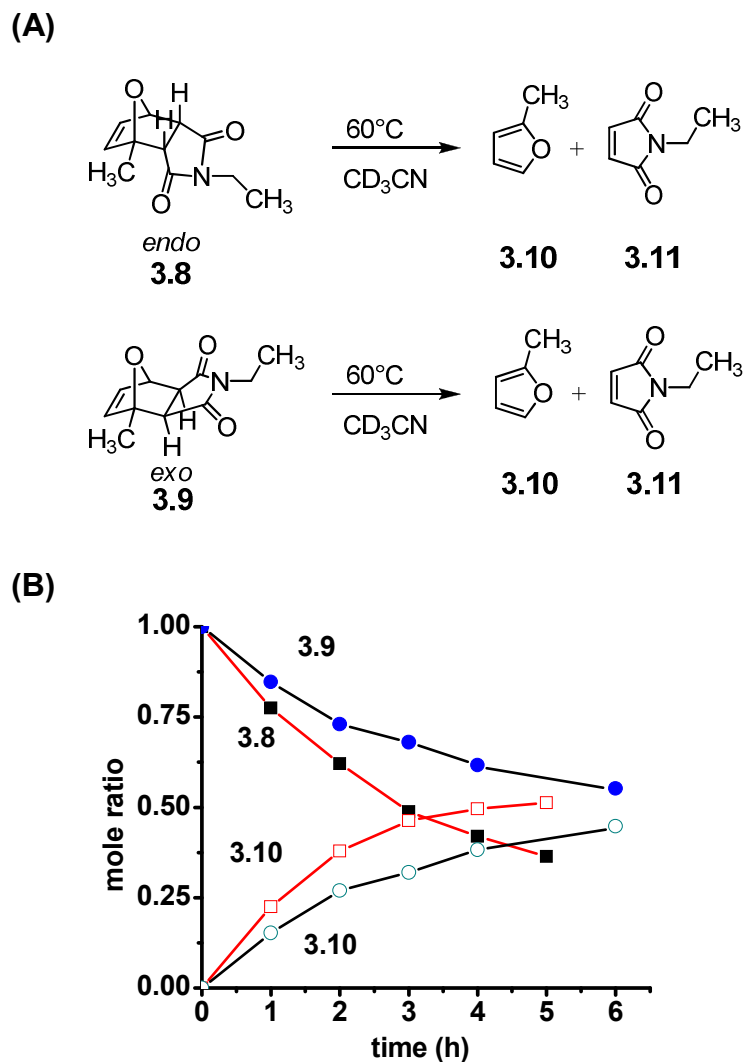
Figure 3.3 (A) Schematic of the *retro*-Diels-Alder reaction for the *endo* **3.8** and *exo* **3.9** adducts. (B) Change in the molar ratio of the two Diels-Alder isomers (*endo* **3.8** and *exo* **3.9**) and 2-methylfuran **3.10** when CD₃CN solutions of *endo* **3.8** and *exo* **3.9** adducts are heated in a water bath at 60 °C. The relative amount of each component was determined by integration of the area under the appropriate peaks in the ¹H NMR spectra.

3.6   Proposed Linker for Demonstration of the Photothermal Release

The linker **3.12** (Scheme 3.3) was proposed to demonstrate the release mechanism from gold NPs. The design incorporates a disulfide moiety, a

fluorescent dye, and *endo* Diels-Alder adduct, which should together allow the photothermal release and monitoring of the fluorescein moiety from gold NPs. The long alkyl chain in the proposed structure is expected to increase the stability over the surface of gold NPs compared to shorter alkyl chains.[77] This increase in stability is due to the increasing van der Waals interactions as the chain length increases.

3.12
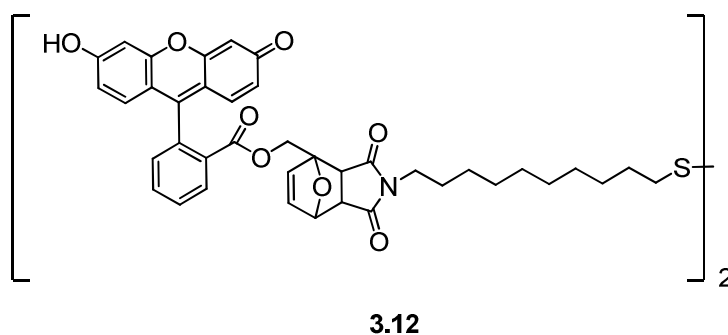
Scheme 3.3 Structure of proposed molecular linker for the photothermal release studies using gold NPs.

3.7   Synthesis of the Proposed Molecular Linker

The synthesis and characterization of compound **3.12** (Scheme 3.3) was conducted in collaboration with Dr. Guoxia Jin from Dr. Neil Branda's laboratory. Molecules that are presented in Scheme 3.4 were synthesized and charaterized by the author of this thesis. According to Scheme 3.4, maleimide **3.13** undergoes a [4+2] cycloaddition with furan to generate the 3,6-*exo*-tetrahydrophthalhide **3.14**. The sequence of reactions was designed to protect the maleimide from thiol nucleophilic attack in a later step. Addition of 1,10-dibromodecane to compound **3.14** under basic conditions afforded 10-(3,6-*exo*-tetrahydrophthalhide)bromodecane **3.15**. Further, nucleophilic substitution of

3.15 by thiourea and subsequent treatment with sodium metabisulfite afforded 10-(3,6-*exo*-tetrahydrophthalhide)mercaptodecane **3.16**. Oxidation of compound **3.16** with iodine effected an oxidative dimerization and the crude product was heated to 130 °C, resulting in deprotection of the maleimide through a *retro*-Diels-Alder reaction. Column chromatography on silica afforded a 22 % yield of **3.17**.
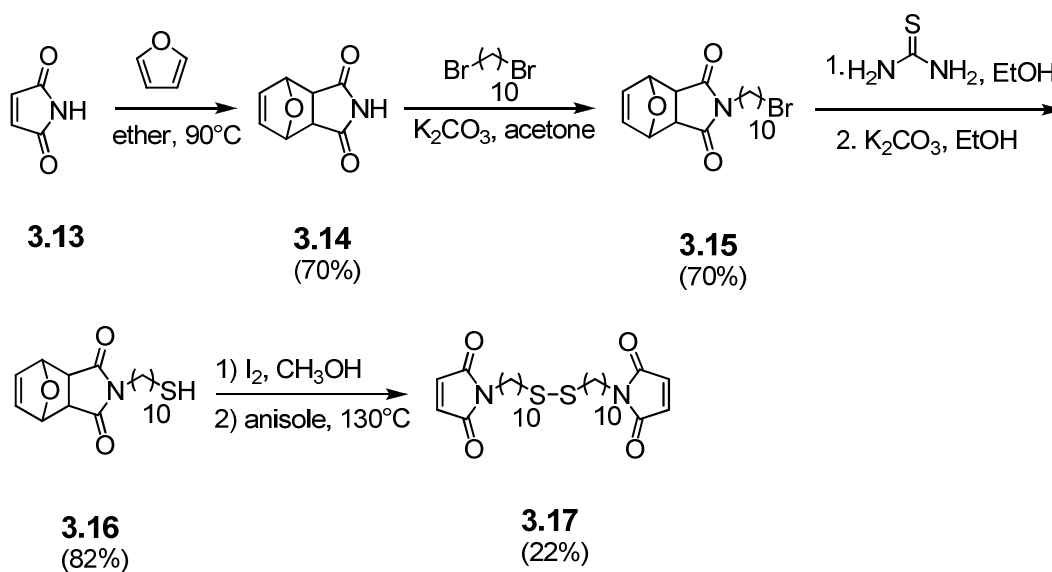
Scheme 3.4 Synthesis scheme for the preparation of **3.17**.

Fluorescein furfuryl ester **3.20** was prepared according to Scheme 3.5. Fluorescein **3.18** was dissolved in dichloromethane and the carboxylate was activated by treatment with *N,N'*-dicyclohexylcarbodiimide. The addition of furfuryl alcohol **3.19** produced compound **3.20**. Compound **3.20** was purified by column chromatography on silica gel.
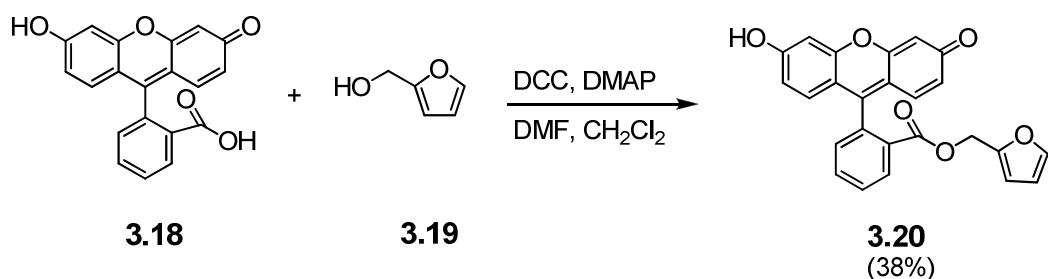
Scheme 3.5 Synthesis of fluorescein furfuryl ester **3.20** through DDC coupling.

The last step is the cycloaddition of maleimide **3.17** and furan **3.20** to form a fluorescein Diels-Alder linker **3.21** (Scheme 3.6). The reaction proceeded over 7 days in methanol at room temperature.
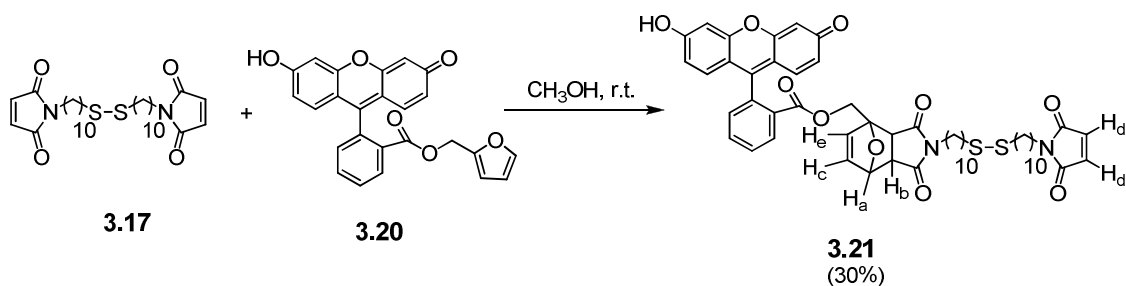
Scheme 3.6 Diels-Alder reaction of maleimide **3.17** with furan **3.20** to form the fluorescein Diels-Alder linker **3.21**.

A crude ^{1}H NMR spectrum of the reaction is shown in Figure 3.4A, which contains a mixture of *endo* and *exo* adduct of compound **3.21**. In the crude spectrum, two signals are specified at 4.98 ppm for the $H_{a\text{-}exo}$ adduct and 5.05 for the $H_{a\text{-}endo}$ adduct of compound **3.21** (peak integration 1:1.8, respectively). The *endo* and *exo* adduct can be distinguished by the torsion angle between proton H_a and H_b of compound **3.21** (Scheme 3.6). Geometry optimization of both isomers at the MM2 shows that the torsion angle between H_a and H_b for the *endo* product is 37° whereas the angle between the same protons for the *exo* adduct is

76°. Therefore, based on Karplus curve a larger coupling is expected for the *endo* product. It was concluded that the peak at 5.05 ppm was the $H_{a\text{-}endo}$ adduct since the product show a larger coupling. [78]
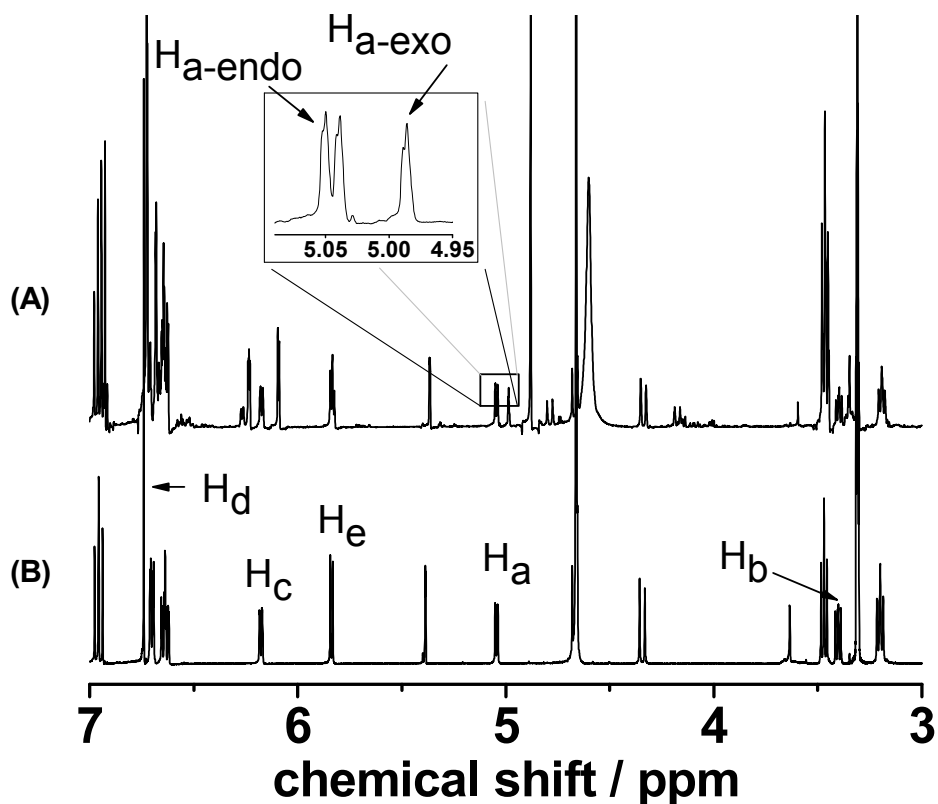
Figure 3.4 (A) ^{1}H NMR spectra (600 MHz) of the crude reaction product of compounds **3.17** and **3.20**, the presence of both isomers are indicated at around 5 ppm, and (B) ^{1}H NMR spectra of *endo* fluorescein Diels-Alder linker **3.21**. The peak integration of H_d to H_c indicates a 2:1 ratio, respectively.

Furthermore, the ^{1}H NMR spectrum of isolated *endo* adduct is shown in Figure 3.4 B. The ^{1}H NMR confirms that the peak integration of H_d and H_c have a ratio of 2:1, respectively (Scheme 3.6). The presence of H_d indicates that there is a maleimide moiety in the compound **3.21**. Since H_c and H_e have different chemical shift, the peak integration of 2:1 ratio of H_d compared to H_c (Scheme 3.6) indicates that for every maleimide moiety in compound **3.21** there is a single Diels-Alder adduct. Hence, the final structure differs from the proposed molecule in that it has only one fluorescein attached to compound **3.21**

3.8   Conclusions

The isolated molecule **3.21** has only one fluorescein in its structure, in contrast with the proposed target structure which was a double Diels-Alder adduct. It nevertheless fulfills all the requirements for our short-term goal, which is a dye linked through a Diels-Alder adduct to a disulfide. The disadvantage of the obtained structure is that for every fluorescein linker attached to gold NPs, one maleimide linker would also be attached to the NPs, thus reducing the potential amount of fluorescein moiety released from each NP by half.

It should be noted that for the short-term project goal, compound **3.21** can be used with no concern. However, for the long-term goals of this project any presence of maleimide could cause complications due to its reactivity in a biological environment.[78] As a result, the release mechanism requires further modification to incorporate a biocompatible structure. Another method to improve biocompatibility and systemic circulation of gold NPs is the addition of a polymeric layer on the surface of the NPs. Thiol-polyethyleneglycol, which is a non-toxic and hydrophilic polymer, is commonly used as an additional coating on the gold NPs surfaces *in vivo*.[79-82] By adding this coating on the decorated gold NPs, the interaction of maleimide with its environment should reduce. For either route, further follow-up studies are required to determine the biocompatibility of the gold NPs *in vivo* before and after photothermal release.

3.9　Experimental Section

3.9.1　General Information

Unless otherwise stated, all the chemicals were purchased from Sigma Aldrich and were used without further purification. Thin-layer chromatography (TLC) was performed on a glass plate pre-coated with 0.25 mm of silica gel with fluorescent indicator UV254. TLC plates were visualized by exposure to ultraviolet light. Column chromatography was performed with silica gel 60 (40–63 μm, 230–400 mesh). ^{1}H NMR were performed on a Bruker Avance 600 TCI cryoprobe instrument working at 600.334 MHz or a Varian Inova 500 instrument working at 499.767 MHz . ^{13}C NMR spectra were recorded on a Bruker Avance 600 TCI cryoprobe instrument working at 150.968 MHz or a Varian Inova 500 instrument working at 125.679 MHz with solvents used as the internal reference. Data for ^{1}H NMR characterizations are reported as follows: Chemical shift (δ, ppm), multiplicities: s=singlet, d=doublet, t=triplet, q=quartet, m=multiplet. Infrared (IR) spectra were acquired on a Bomem (Hartmann & Braun, MB-Series) spectrometer. High resolution mass spectra for the compounds were obtained using an Agilent 6210 TOF LC/MS (ESI+), and in addition elemental analysis was obtained using an EA 1110 from CE Instruments.

3.9.2 Syntheses
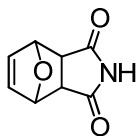
3.14

Synthesis of 3,6-exo-tetrahydrophthalhide (3.14)

Maleimide **3.13** (1.0 g, 10.3 mmol) and furan (1.05 g, 15.5 mmol) were dissolved in Et_2O (15 mL) in a sealed tube and heated at 90 °C for 12 h. After cooling the mixture to room temperature a white solid precipitated out of the solution. The product was filtered and then washed with cold Et_2O (3x10 mL) to remove the un-reacted maleimide and dried by rotary evaporation under reduced pressure to afford 62% of the product as a white crystalline, m.p. 147-150 °C.

^{1}H NMR (600 MHz, $CDCl_3$) δ = 8.10 (broad s, 1H), 6.52 (d, J=0.8 Hz, 2H), 5.31 (d, J=0.8 Hz, 2H), 2.89 (s, 2H); ^{13}C NMR (600 MHz, $CDCl_3$) δ = 175.91, 136.55, 80.95, 48.68; IR (dropcast on NaCl plate, cm^{-1}): v 3185, 3089, 3029, 2995, 1705, 1356, 1258, 1189, 856, 822; HRMS (ESI+) *m/z* Calculated for $[M+Na]^+$ 188.0323, found 188.0318.
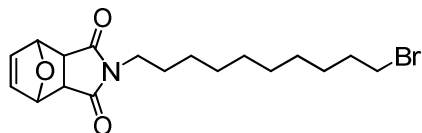
3.15

Synthesis of 10-(3,6-exo-tetrahydrophthalhide)bromodecane (3.15)

A mixture of 3,6-*exo*-tetrahydrophthalhide **3.14** (1.25 g, 7.57 mmol) and 1,10-dibromodecane (6.81 g, 22.7 mmol) dissolved in spectral grade acetone (55 mL) was treated with potassium carbonate (3.14 g, 22.7 mmol). The resulting mixture was stirred at room temperature for 12 h, at which time the solvent was removed by rotary evaporation under reduced pressure and the residue partitioned between CH_2Cl_2 and water. The aqueous layer was removed, extracted with CH_2Cl_2 (2 × 40 mL), the combined organic layers were dried over $MgSO_4$, filtered and the solvent was removed by rotary evaporation under reduced pressure. Purification by column chromatography using silica gel (first with hexane to remove the excess 1,10-dibromodecane,) followed by column chromatography on silica gel (95:5 v/v CH_2Cl_2:CH_3OH) afforded 2.0 g (70 %) of the product as a white crystalline solid, m.p. 62-65 °C .

^{1}H NMR (500 MHz, $CDCl_3$): δ = 6.52 (s, 2H), 5.27 (s, 2H), 3.46 (t, J = 7.5 Hz, 2H), 3.41 (t, J = 7.0, 2H), 2.84 (s, 2H), 1.85 (quintet, J = 7.0 Hz, 2H), 1.55 (quintet, J = 7.7 Hz, 2H), 1.42 (quintet, J = 7.0 Hz, 2H), 1.27 (m, 10H); ^{13}C NMR (500 MHz, $CDCl_3$): δ = 176.25, 136.49, 80.84, 47.34, 38.95, 34.05, 32.77, 29.25, 29.24, 28.98, 28.65, 28.10, 27.52, 26.57; IR (KBr, cm^{-1}): v 3000, 2912, 2848,

1708, 1407; HRMS (ESI+) *m/z* calculated for [M+H]$^+$ 384.1175, found 384.1187.
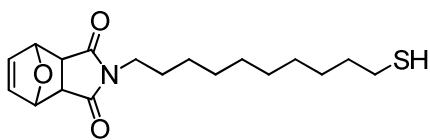
3.16

Synthesis of 10-(3,6-exo-tetrahydrophthalhide)mercaptodecane (3.16)

A solution of 10-(3,6-*exo*-tetrahydrophthalhide)bromodecane **3.15** (0.5 g, 1.30 mmol) and thiourea (198 mg, 76.1 mmol) in EtOH (15 mL) was heated at 60 °C for 24 h. The solvent was removed under vacuum, the solid residue (the thiouronium adduct) was dissolved in water (15 mL) and treated with sodium metabisulfite (0.49 g, 2.57 mmol) followed by CH_2Cl_2 (20 mL). The reaction mixture was heated at reflux for 4 h until the thiourea derivative had completely reacted as indicated by TLC. The reaction was cooled to room temperature and the organic layer was separated from the aqueous layer. The aqueous layer was further extracted with CH_2Cl_2 (2 × 40 mL), the combined organic phases were dried over $MgSO_4$, filtered and evaporated under reduced pressure. Purification by column chromatography on silica gel (95:5 v/v CH_2Cl_2:CH_3OH) afforded 0.36 g (82%) of the product as a white solid.

^{1}H NMR (500 MHz, CDCl$_3$): *δ* = 6.49 (s, 2H), 5.23 (s, 2H), 3.43 (t, *J* = 7.5 Hz, 2H), 2.80 (s, 2H), 2.48 (q, 7.5 Hz, 2H), 1.56 (quintet, *J* = 7.0 Hz, 2H), 1.52 (quintet, *J* = 7.5 Hz, 2H), 1.31 (m, 13H); ^{13}C NMR (500 MHz, CDCl$_3$): *δ* = 176.63, 136.77, 81.11, 47.61, 39.22, 34.27,29.56, 29.27, 29.22, 28.57, 27.79, 26.85, 24.89; IR (KBr, cm^{-1}): *v* 3054, 2930, 2856, 2305, 1773, 1700, 1402, 1265; LRMS (ESI+) *m/z* calculated for $C_{18}H_{27}NO_3S$ [M+H]$^+$ 338.1791, found 338.2.
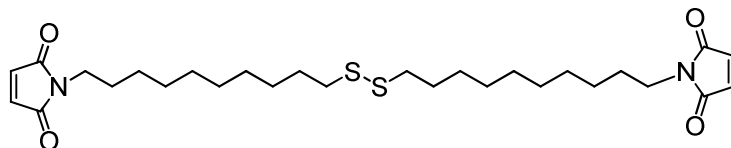
3.17

Synthesis of 1,1'-(10,10'-disulfanediylbis(decane-10,1-diyl))bis(1H-pyrrole-2,5-dione) (3.17)

A solution of 10-(3,6-*exo*-tetrahydrophthalhide)mercaptodecane **3.16** (0.44 g, 1.30 mmol) in CH_3OH (20 mL) was treated with iodine (165 mg, 0.65 mmol) and stirred for 1 h at room temperature. The resulting mixture was washed with concentrated aqueous sodium metabisulfite until the colour of the solution disappeared. The resulting solution was extracted with CH_2Cl_2, dried over $MgSO_4$ and filtered. The solvent was removed by rotary evaporation and the residue was dissolved in anisole (5 mL). The resulting solution was heated at 130–140 °C for 1 h. After cooling the mixture to room temperature, purification by column chromatography on silica gel (2:1 v/v hexane:EtOAc) afforded 153 mg (22 %) of the product as a white solid, m.p. 64-67 °C.

^{1}H NMR (500 MHz, $CDCl_3$): δ = 6.66 (s, 4H), 3.47 (t, J = 7.0 Hz, 4H), 2.63 (t, J = 7.0 Hz, 4H), 1.65–1.50 (m, 8H), 1.34 (m, 24H); ^{13}C NMR (500 MHz, $CDCl_3$): δ = 171.14, 134.27, 39.39, 38.16, 29.64, 29.63, 29.45, 29.43, 29.33, 28.78, 28.74, 26.97; IR (KBr, cm^{-1}): v 2919, 2850, 1699; HRMS (ESI+) *m/z* calculated for $C_{28}H_{44}N_2O_4S_2$ [M+H]$^+$ 537.2820, found 537.2819.
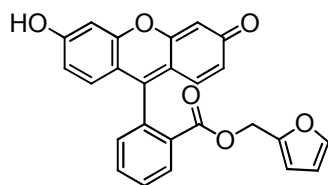
3.20

Synthesis of the fluorescein furfuryl ester (3.20)

A solution of fluorescein **3.18** (332 mg, 1 mmol) in CH_2Cl_2 (3 mL) and dimethylformamide (2 mL) was treated with *N,N'*-dicyclohexylcarbodiimide (0.227 g, 1.1 mmol) and then furfuryl alcohol **3.19** (0.259 mL, 2.98 mmol). The reaction mixture was stirred for 3 days at room temperature at which time the solvent was removed under vacuum. Purification by column chromatography on silica gel (10:1 v/v EtOAc:CH_3OH) afforded 157 mg (38%) of the ester as a yellow solid, m.p. 210-215 °C.

^{1}H NMR (600 MHz, CD_3OD/CD_2Cl_2): δ = 8.22 (d, *J* = 7.8 Hz, 1H), 7.79 (t, *J* = 7.5 Hz, 1H), 7.72 (t, *J* = 7.2 Hz, 1H), 7.35 (d, *J* = 7.5 Hz, 1H), 7.29 (s, 1H), 6.81 (d, *J* = 9.3 Hz, 2H), 6.48 (m, 4H), 6.23 (dd, *J* = 1.9, 3.2 Hz, 1H), 6.05 (d, *J* = 3.2 Hz, 1H), 4.84 (s, 2H); ^{13}C NMR (600 MHz, (CD_3COD, CD_2Cl_2)): δ = 182.11, 166.80, 159.98, 156.89, 149.45, 144.82, 136.04, 133.70, 131.95, 131.66, 131.62, 131.31, 130.70, 124.19, 113.18, 111.59, 111.33, 104.67, 59.71; IR (KBr, cm^{-1}): v 2459, 1726, 1640, 1584, 1459; Fluorescence: $\lambda_{ex.}$ = 490 nm, $\lambda_{em.}$ = 514 nm; HRMS (ESI+) *m/z* calculated for $C_{25}H_{16}O_6$ [M+H]$^+$ 413.1025, found 413.1027.
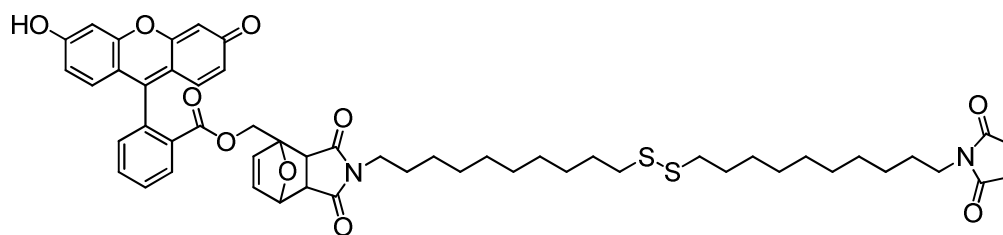
3.21

Synthesis of fluorescein Diels-Alder linker (3.21)

A solution of 1,1'-(10,10'-disulfanediylbis(decane-10,1-diyl))bis(1H-pyrrole-2,5-dione) **3.17** (14 mg, 0.03 mmol) and the fluorescein furfuryl ester **3.20** (20 mg, 0.021 mmol) in CD$_3$OD (0.3 mL) and CD$_2$Cl$_2$ (0.3 mL) was stirred at room temperature for 7 days. At this time, ^{1}H NMR spectroscopy indicated a 50% formation of *endo* and *exo* Diels-Alder products. Purification by column chromatography on silica gel (12:1 v/v EtOAc:CH$_3$OH) afforded 6 mg (30%) of the desired *endo*-isomer.

^{1}H NMR (600 MHz, CD$_3$OD/CD$_2$Cl$_2$): *δ* = 8.32 (d, *J* = 7.0 Hz, 1H), 7.82 (t, *J* = 7.5 Hz, 1H), 7.77 (t, *J* = 7.8 Hz, 1H), 7.35 (d, *J* = 7.5 Hz, 1H), 6.97 (dd, *J* = 9.3, 10.6 Hz , 2H), 6.77 (s, 1H), 6.71 (dd, *J* = 1.8, 7.0 Hz , 2H), 6.65 (t, *J* = , 9.0 Hz, 1H), 6.16 (d, *J* = 5.6 Hz, 1H), 5.82 (d, *J* = 5.7 Hz, 1H), 5.02 (dd, *J* = 1.4, 5.5 Hz, 1H), 4.66 (d, *J* =12.7 Hz, 1H), 4.47 (broad, 1H), 4.30 (d, *J* =12.7 Hz, 1H), 3.47 (t, *J* =7.1 Hz, 2H), 3.41 (dd, *J* = 5.6, 7.5 Hz, 1H), 3.21 (d, *J* = 7.3 Hz, 2H), 2.98 (d, *J* = 7.6 Hz, 1H), 2.66 (d, *J* = 7.2 Hz, 4H), 1.65 (quintet, *J* = 7.4 Hz, 4H), 1.55 (quintet, *J* = 7.4 Hz, 2H), 1.28 (m, 26H), 1.16 (m, 2H); ^{13}C NMR (600 MHz, CD$_3$OD/CD$_2$Cl$_2$): *δ* = 175.00, 174.80, 171.25, 165.42, 158.15, 154.83, 135.42, 133.97, 132.78, 131.28, 130.59, 130.49, 130.44, 129.97, 129.82, 114.87, 103.08, 88.59, 79.26, 62.92, 46.49, 38.61, 38.11, 37.32, 29.11, 29.07, 28.87, 28.80,

28.69, 28.17, 28.08, 27.06, 26.47, 26.42; IR (KBr, cm^{-1}): v 3054, 2987, 2686, 2305, 1422, 1265; Fluorescence: $\lambda_{ex.}$ = 490 nm, $\lambda_{em.}$ = 514 nm; HRMS (ESI+) *m/z* calculated for $C_{53}H_{60}N_2O_{10}S_2$ [M+H]$^+$ 949.3768, found 949.3757.

.

CHAPTER 4: RELEASE OF MOLECULES FROM GOLD NPS

This chapter demonstrates a photothermal release of molecules from the surfaces of gold NPs. In addition, characterization and quantification of the released molecules per NP are presented. The research in this chapter was published in-part in: A. B. Samsam Bakhtiari, D. Hsiao, G. Jin, B. D. Gates and N. R. Branda, "An Efficient Method Based on the Photothermal Effect for the Release of Molecules from Metal Nanoparticle Surfaces" *Angew. Chem. Int. Ed.* **2009**, *48*, 4166. The silica/gold core-shells particles were provided by Dennis Hsiao from Dr. Gates' laboratory and the fluorescein Diels-Alder linker was synthesized in collaboration with Guoxia Jin from Dr. Branda's laboratory

4.1 Monitoring the Release Process from Gold NPs

Fluorescent molecules are good candidates for monitoring when it comes to analytical measurements because they are detectable at very low concentrations (e.g., picomolar).[83]

In this thesis, fluorescent molecules were used to monitor the release process from gold NPs surfaces. More specifically, the fluorescein moiety was chosen because:

1. fluorescein has a high quantum yield of 95%, which is higher than most dyes,[84]

2. fluorescein has functional groups such as carboxylate and phenol that can be used to couple fluorescein to other molecules,

3. fluorescein is cheap, and

4. gold NPs quench fluorescein's fluorescence when the fluorescein is less than 10 nm away from the NPs.[85]

Quenching is due to Föster resonance energy transfer, which transfers the energy from the excited state of the fluorophore to gold NPs through nonradiative coupling. However, the quenching effects disappear when the fluorescein adducts are detached from the surface of the gold NPs. The quenching effect reduces the experiment time drastically since the release of the fluorescein adduct can now be directly monitored with respect to the low background fluorescence of the solution containing decorated gold NPs. Without the quenching process, the solution would need to be pelleted by centrifugation after each release of fluorescein adduct in order to remove the decorated gold NPs. Following this, the fluorescence of the supernatant without the decorated gold NPs would need to be measured and the decorated gold NPs would have to be re-suspended back into the solution. Thus, the centrifugation and re-suspension steps would have added an extra level of inconvenience to the measurement of each data point. For these reasons, fluorescein was used in the photothermal release experiment.

4.2 Decoration of Gold NPs with Fluorescein Diels-Alder Linkers

Fluorescein Diels-Alder linkers, dissolved in methanol, were added in excess to the aqueous solution of gold NPs (Scheme 4.1). The amount was confirmed to be in excess through analysis of the supernatant by fluorescence spectroscopy after removing the decorated gold NPs by centrifugation in order to detect the presence of unbounded linkers. The fluorescein adducts attached to the gold surface via Au−S interactions.

fluorescein Diels-Alder linker
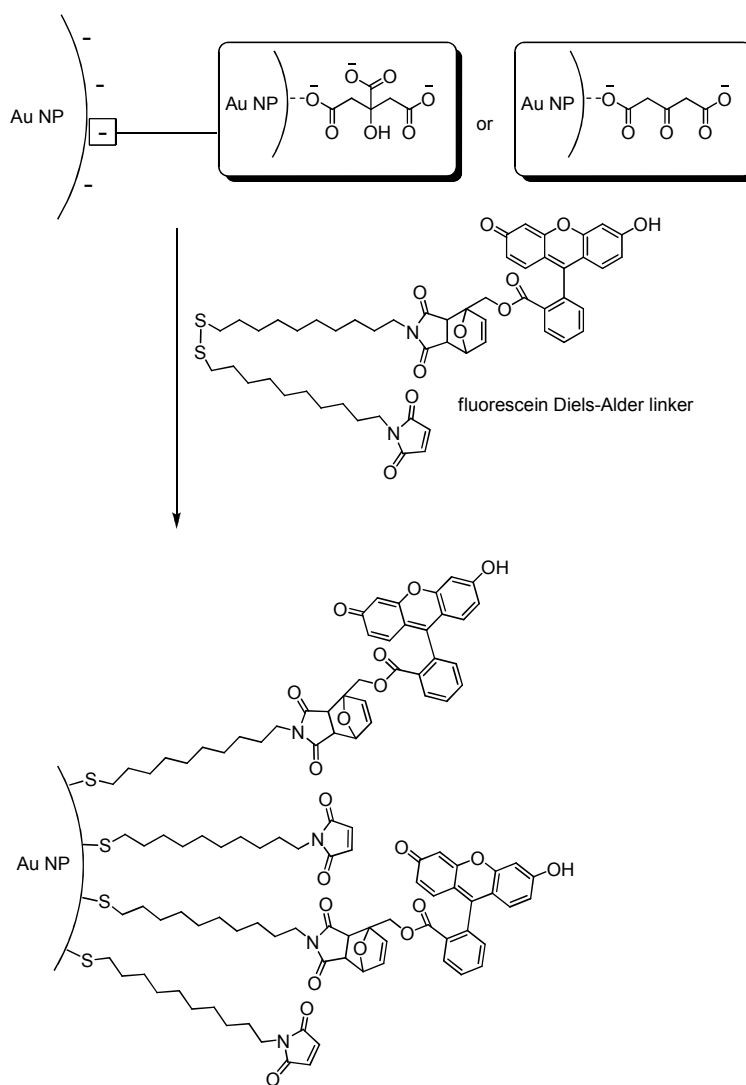
Scheme 4.1 Decoration of gold NP with fluorescein Diels-Alder linker.[86]

Both the concentration of the fluorescein Diels-Alder linkers and the length of reaction time play significant roles in the rate of decoration.[87] The coverage is maximized by having an excess amount of the fluorescein Diels-Alder linkers and a longer incubation time (>8 h). To prepare the sample for further experiments, unbound fluorescein Diels-Alder linkers (Scheme 4.1) must be removed to reduce the background fluorescence signal from the solution.

4.3   Purification Method for the Decorated Gold NPs

In order to remove the excess unbound fluorescein Diels-Alder linkers, centrifugation was used to separate decorated gold NPs from excess fluorescein Diels-Alder linkers. Due to the higher density of gold NPs compared to aqueous solution, centrifugation causes the gold NPs to form a pellet at the bottom of a microcentrifuge tube (1.5 mL). The decorated NPs were purified by centrifugation and the subsequent removal of supernatant followed by re-suspension in high purity (18 MΩ) water. Solid spherical gold NPs (18 nm diameter) required 8 min at 10,000 rpm and silica/gold core-shell NPs (204 nm diameter) required 8 min at 3,000 rpm. After three washes, no difference was observed in the fluorescence emission between samples that had been purified 3 times and 4 times. This result indicates that the background noise can no longer be significantly reduced by further purification. Therefore, the sample was ready for the release experiment.

4.4 Thermal and Photothermal Release from Solid Spherical Gold NPs (18 nm diameter)

4.4.1 Thermal Release of Molecules from Decorated Solid Spherical Gold NPs

A sample of decorated solid spherical gold NPs was purified as previously explained in section 4.3. A fluorescence spectrum of the sample was taken to determine the background fluorescence emission. The background spectrum is the lowest fluorescence spectrum between 500−600 nm in Figure 4.1A. This background would later be used to normalize the rest of the data from the same set of experiments. To examine the release of the thermally induced *retro*-Diels-Alder reaction, the sample was placed in a water bath at 80 °C and a fluorescence spectrum was taken after 20 min. The water bath treatment and fluorescence measurement were repeated until the fluorescence intensity reached a maximum as shown in Figure 4.1A. An increase in the fluorescence intensity of the sample was observed over time. It is important to mention that gold NPs do not have fluorescent properties.[88] Therefore, the increase in the fluorescence intensity can only come from the molecules released from the gold NPs, which are no longer quenched by the gold surface.
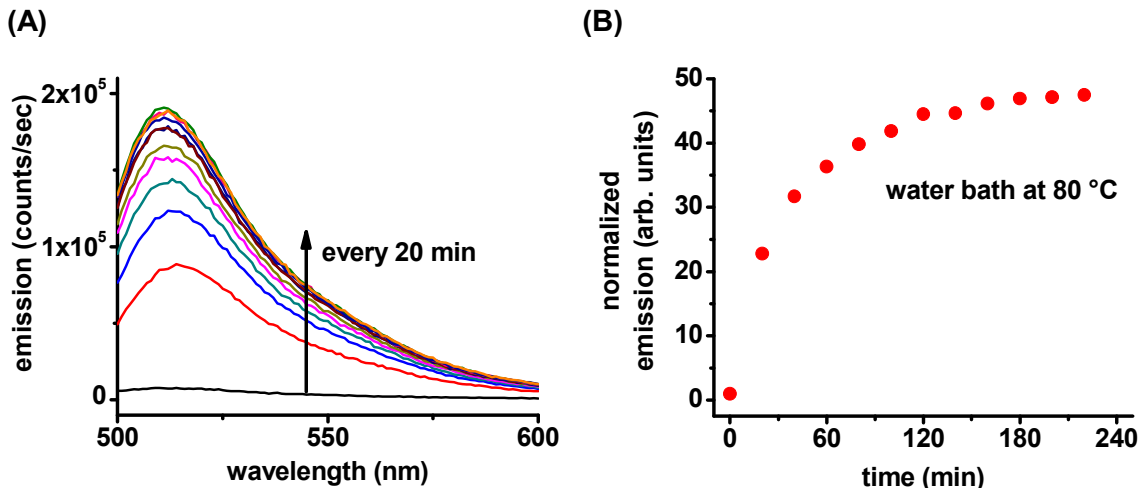
Figure 4.1 (A) Representative spectra showing changes in the fluorescence intensity (excitation at 490 nm) when an aqueous dispersion of decorated solid spherical gold NPs with the fluorescein Diels-Alder linker is heated in a water bath at 80 °C. (B) Each fluorescence spectrum (excitation 490 nm) was normalized by dividing the area of each spectrum by area of background spectrum (area between 500-600 nm).

Fluorescence emission is also plotted with respect to time (Figure 4.1B). Data presented in Figure 4.1B are normalized by dividing the area under each spectrum in Figure 4.1A (between 500−600 nm) at each point in time, by the area under the background spectrum. The area was calculated by integrating each spectrum between 500−600 nm using OriginPro 8. Figure 4.1B indicates that in the first hour there was a fast initial rate of increase in the fluorescence emission in the sample. However, in the second hour of immersion in water bath at 80 °C, this rate decreased and in the last hour of immersion, it nearly plateaus.

The most likely mechanism that can explain the release of molecules is the *retro*-Diels-Alder reaction (Scheme 4.2). In the characterization section of this chapter, this hypothesis will be discussed in more detail.
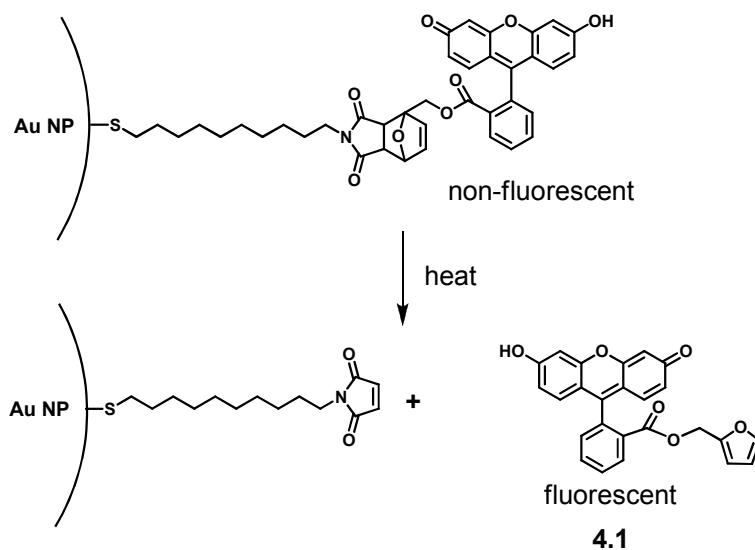
Scheme 4.2 Release of fluorescein furfuryl ester **4.1** from the surface of a gold NP by using heat to induce the *retro*-Diels-Alder reaction.

4.4.2 Photothermal Release of Molecules from Decorated Solid Spherical Gold NPs

Interaction of light via gold NPs SPR causes the photothermal effect, which results in localized heating over the NPs surfaces. Therefore, light can be used as a stimulus instead of external heat (i.e., water bath at 80 °C) to trigger the *retro*-Diels-Alder reaction. The novelty of this project comes from coupling the heat generated by the photothermal effect to the *retro*-Diels-Alder reaction.

The samples used in the photothermal release study were prepared the same way as those used in the thermal release study. In the first attempt, ambient light was used as a stimulus to trigger the release. However, no increase in the fluorescence emission was recorded even after 2 h. Thus, a more powerful light source was needed to cause the photothermal effect of enough magnitude to trigger the *retro*-Diels-Alder reaction. In previous publications where the

photothermal effect was used to cause cell death,[49] the primary source of light was a laser with wavelengths that overlap with the SPR absorption of the NPs.

4.4.3 Using Lasers as a Primary Light Source for the Photothermal Release

Laser is an acronym for Light Amplification by Stimulated Emission of Radiation. Laser beam output energy is measured in watts, which is the amount of energy (joule) of the emitted photons over time (second).[89] Using lasers as a light source provides adjustable output energy. Adjustable energy was desirable because one can pinpoint the threshold for the photothermal release by adjusting the energy of the laser output. Finding the threshold for the photothermal release of decorated NPs is important because the goal was to use the minimal energy to cause the photothermal release. Furthermore, there are two types of lasers that provide different operational modes of irradiation: i) continuous wave lasers; and ii) pulsed lasers. The continuous wave laser emits photons continuously while the pulsed laser emits photons in short time intervals. Depending on the types of pulsed laser, the pulse width can vary from a microsecond down to a femtosecond.[90] In our experiment, we used both types of lasers in an attempt to induce the photothermal effect. Initial experiments were carried out with a continuous wave laser due to the relatively easy access of this type of laser.

4.4.4 Continuous Wave Laser as a Primary Light Source for the Photothermal Release

In an attempt to release molecules from decorated solid spherical gold NPs, a continuous wave laser with a set emission wavelength of 532 nm, was

used as the light source. The wavelength of 532 nm was specifically chosen since it overlaps with the SPR absorption of the NPs. To find the threshold energy for the photothermal release, the power of the laser used to irradiate the sample was increased gradually from 1 W to 2.5 W. A noticeable increase in the fluorescence of the solution was observed by fluorescence spectroscopy (Figure 4.2A). During irradiation, the temperature of the solution was monitored and was shown to increase from 23 °C to 43 °C (Figure 4.2B). This change in temperature was measured using a platinum sensor thermometer with a resolution of 0.01 °C and an accuracy of ± 0.1 % below 200 °C (thermometer range: -50 to 400 °C). These results indicate that although the fluorescein moiety was released from the gold NPs, the release may be caused not only by the localized heating of the surface, but also by the increase in temperature of the aqueous solution upon irradiation. Increase in the temperature of the bulk solution suggested that the photothermal effect of NPs have an impact on their environment, which was contrary to the project goal. To achieve a more localized heating of the gold NPs, a pulse laser was applied as a light source.

(A)

(B)
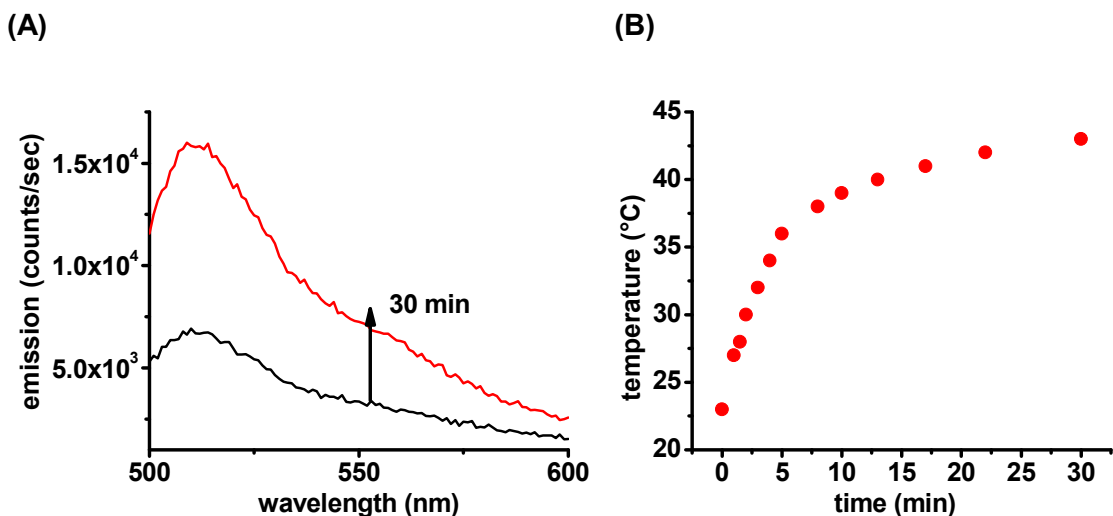
Figure 4.2 (A) Representative spectra showing changes in the fluorescence intensity (excitation at 490 nm) when an aqueous dispersion of solid spherical gold NPs decorated with the fluorescein Diels-Alder linker was irradiated with a continuous wave laser (λ = 532 nm, 2.5 W). (B) Increase in the temperature of the aqueous dispersion of decorated solid spherical gold NPs during irradiation with continuous wave laser (λ = 532 nm, 2.5 W).

4.4.5 Pulse Laser as a Primary Light Source for Photothermal Release

Unlike the continuous wave lasers, pulsed lasers emit short pulses of light with a set frequency. The pulse width and frequency of the pulses are dependent on parameters that are already programmed into the instrument. A pulsed laser is designed to accumulate the energy of the continuous wave and release that energy in pulses. Therefore, pulse laser is capable of providing much greater energy in a short period of time.[90] The combination of greater energy and short period of time should cause localized heating because of greater accumulation of energy in a short time. In addition, the energy of each pulse is tunable and can be set to a specific energy.

To trigger the release of fluorescein adducts from decorated solid spherical gold NPs, a pulsed laser with a pulse width of 3-6 ns, a frequency of 10 Hz and a wavelength of 532 nm was used. A shorter pulse width, such as the picosecond pulse laser, would have been more desirable but the nanosecond pulse laser was readily available. Therefore, the nanosecond laser was used to find the threshold of photothermal release from decorated solid spherical gold NPs.

To find the photothermal release threshold, different power outputs (10, 20, 40, 100 mW) of the laser were used (Figure 4.3A to D). At the beginning of the experiment four samples with identical concentrations were prepared from the stock solution of decorated gold NPs. Then, the background fluorescence of the sample was measured. The laser power was set to 10 mW and the sample was irradiated for a 15 s period, multiple times, and after each irradiation the fluorescence intensity was monitored (same procedure was used for the other 3 samples). For the first sample (as shown in Figure 4.3A) no change in the fluorescence intensity was observed after multiple irradiations. The result suggested that the magnitude of photothermal effect was not enough to trigger the *retro*-Diels-Alder reaction. The power output of the laser was increased to 20 mW and the second sample was irradiated. As shown in Figure 4.3B there was an increase in the fluorescence intensity of the sample. Furthermore, the laser output was increased to 40 mW and the third sample was irradiated at a 40 mW output. The fluorescence intensity, for the third sample, increased in greater magnitude (Figure 4.3C) compared to the second sample. The release observed

at 20 and 40 mW suggested that the threshold of photothermal release was between this ranges. Finally the fourth sample was irradiated at 100 mW (Figure 4.3D). The increase in the fluorescence intensity was even greater at 100 mW compared to 40 mW.
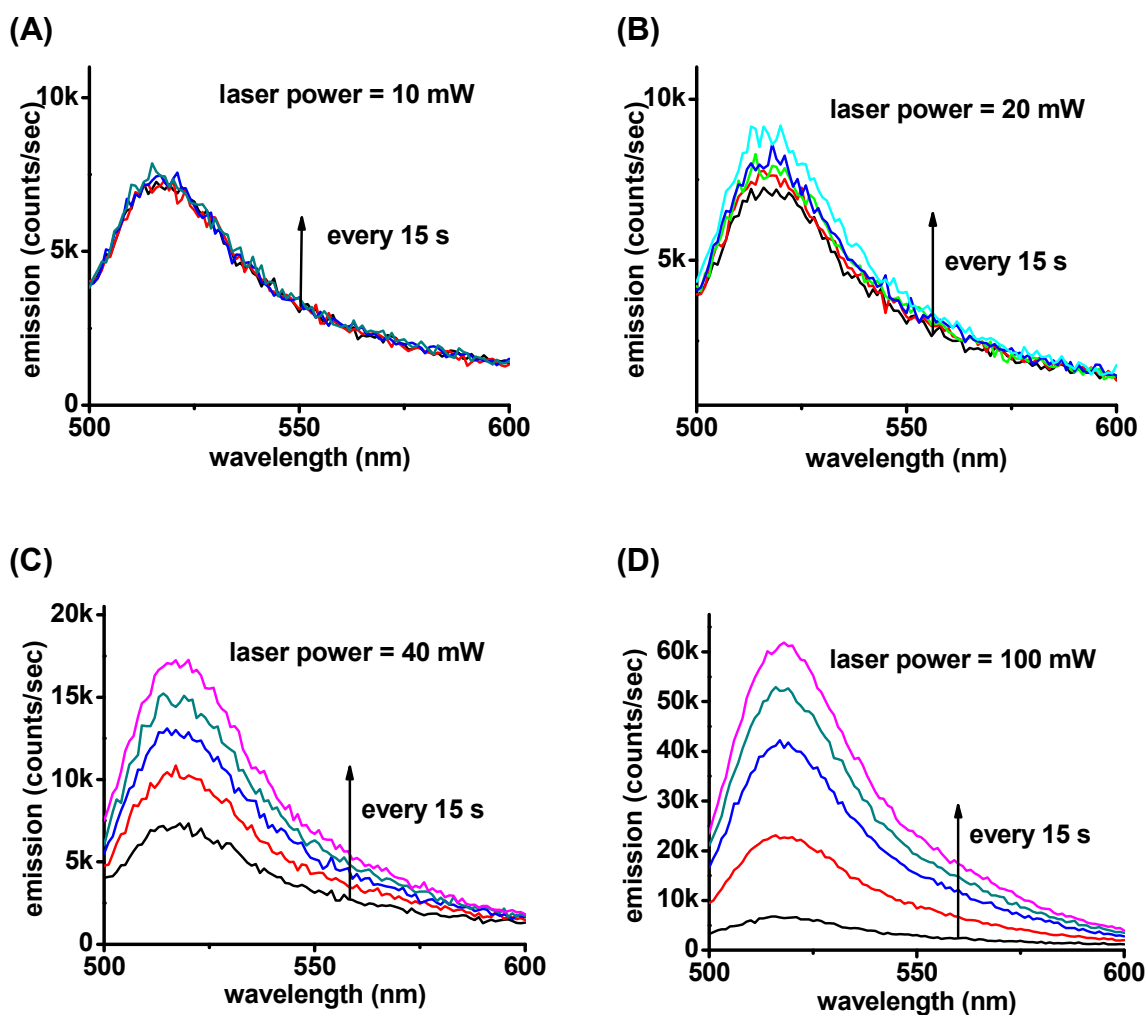
Figure 4.3 Representative spectra showing changes in the fluorescence intensity (excitation at 490 nm) when an aqueous dispersion of solid spherical gold NPs decorated with the fluorescein Diels-Alder linker was irradiated with a pulse laser (λ = 532 nm, 3-6 ns, 10 Hz) (A) at 10 mW power output, (B) at 20 mW power output, (C) at 40 mW power output, and (D) at 100 mW power output.

In Figure 4.4, the fluorescence spectrum for each data point was normalized with respect to the area of background fluorescence. Figure 4.4 shows that at the 10 and 20 mW power levels, the fluorescence intensity of the samples had insignificantly changed over multiple irradiations compared to times when higher power was used. The significant release was found to be at 40 ± 3 mW but the release process was slow at this power (Figure 4.4). A faster release was observed at 100 mW. Therefore, further pulsed laser studies, for decorated solid spherical gold NPs were conducted at 100 mW. Laser powers >100 mW released molecules at a greater rate (maximizing the fluorescence intensity in <1 min). The later process was undesirable because the fluorescence intensity reached a maximum with an inadequate number of data points for monitoring the release.
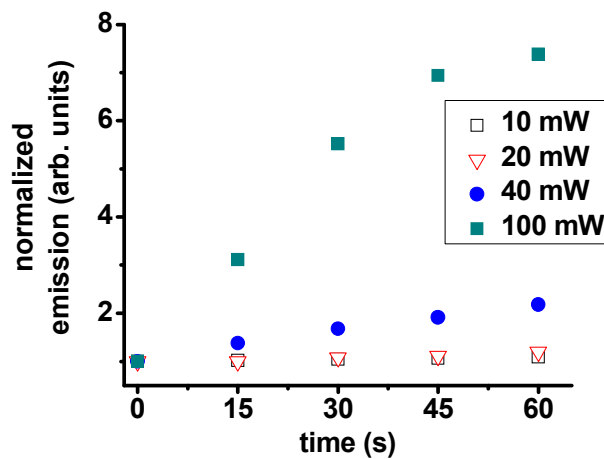
Figure 4.4 Normalized data for the photothermal release of decorated solid spherical gold NPs at different pulse laser powers (10, 20, 40, 100 mW) (pulse laser λ = 532 nm, 3-6 ns, 10 Hz). Each fluorescence spectrum (excitation 490 nm) was normalized by dividing the area of each spectrum at time (15, 30, 45, and 60 s) by area of background spectrum (area between 500-600 nm).

For the photothermal study, a pulse laser was used and an identical sample to the thermal study was prepared. The background fluorescence emission was measured. Then the sample was irradiated repeatedly at 30 s intervals and in between each interval a fluorescence measurement was obtained. After each radiation period, an increase in the sample's fluorescence intensity was observed (Figure 4.5A). This result was indicative of the release of fluorescein moieties from the gold surface. The data in Figure 4.5A were normalized by dividing the area under each spectrum (area between 500−600 nm) by the area under the background spectrum to produce Figure 4.5B. In Figure 4.5B, there was an initial fast rate of release in the first two minutes of irradiation, after which, the rate began to decrease over the next two minutes. The result suggested that most of the attached molecules were released because of the photothermal effect.
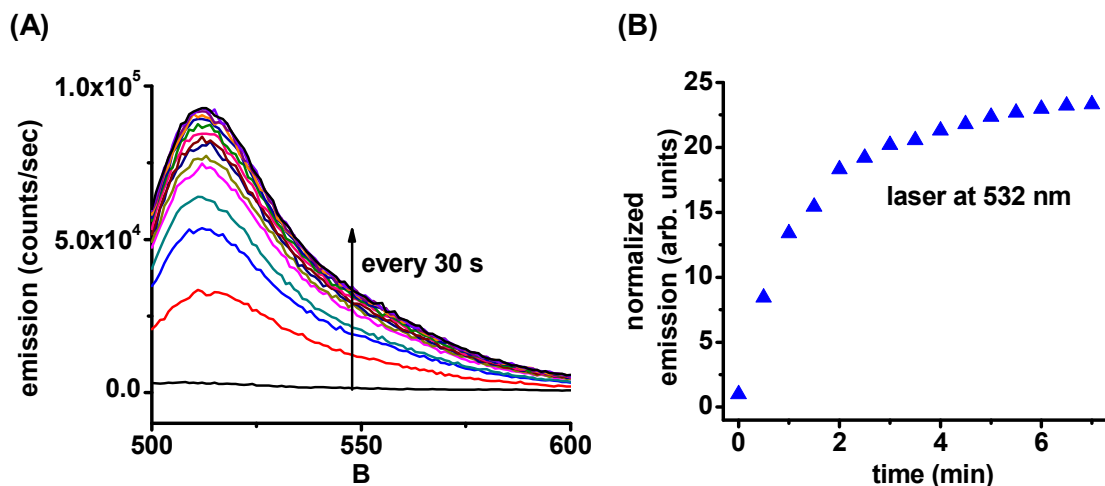
Figure 4.5 (A) Representative spectra showing changes in the fluorescence intensity (excitation at 490 nm) when an aqueous dispersion of solid spherical gold NPs decorated with the fluorescein Diels-Alder linker was irradiated with a pulse laser (pulse at λ = 532 nm, 3-6 ns, 10 Hz, 100 mW). (B) Increase in fluorescence intensity was observed when aqueous dispersions of solid spherical gold NPs decorated with the fluorescein Diels-Alder linkers were irradiated with laser (pulse laser λ = 532 nm) (excitation at 490 nm). The spectra are normalized by dividing the area of each spectrum by the background area between 500-600 nm.

During the photothermal release, the temperature of the solution was monitored and no significant change from 21.5 ± 0.5 °C were observed. In contrast to the results obtained with the continuous wave laser, the results obtained with the pulsed laser indicated that the photothermal release of fluorescein moiety could be due to localized heat at the gold NP surfaces.[91]

4.4.6 Monitoring for Thermal Release of Decorated Solid Spherical Gold NPs at 37 °C

The long-term goal of this project is to apply this method of photothermal release as a drug delivery mechanism. Therefore, an experiment was conducted

in a water bath at 37 °C, which is the average human body temperature. An aqueous dispersion of decorated solid spherical gold NPs was heated in a water bath at 37 °C for more than 200 min. The fluorescence intensity of the sample was recorded every 20 min (Figure 4.6A). The normalized data obtained from this experiment were plotted along with those obtained from the experiment using a thermal release at 80 °C (Figure 4.6B). Thermal treatment of the decorated gold NPs at 37 °C for over 200 min showed no sign of measurable increase in the fluorescence emission of the sample. Therefore, from a thermal stability point of view, the designed Diels-Alder adduct can be used *in vivo* studies since the *retro*-Diels-alder reaction does not take place to any appreciable degree at the human body temperature.
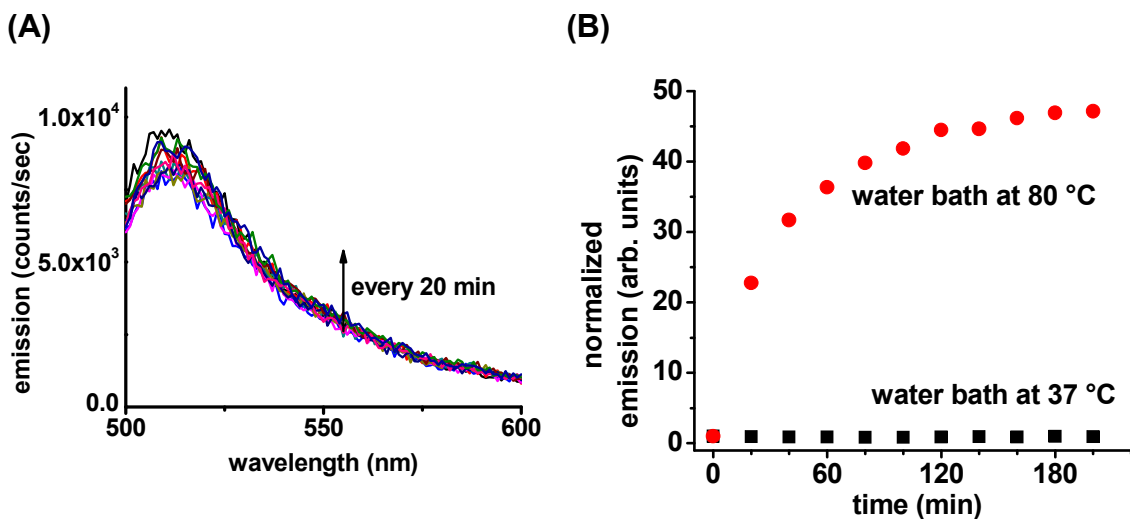
Figure 4.6 (A) Representative spectra showing changes in the fluorescence intensity (excitation at 490 nm) when an aqueous dispersion of decorated solid spherical gold NPs was heated in water bath at 37 °C. (B) Over lap of normalized fluorescence emission (excitation at 490 nm) data of decorated solid sphere gold NPs after water bath treatment at 80 °C and 37 °C.

4.5   Characterization of the Released Molecules

4.5.1   Plausible Release Mechanism of Fluorescein Moiety

The increase in fluorescence emission of the solution after the photothermal treatment is due to the detachment of the fluorescein moiety from the gold surfaces.[92] The dissociation of molecules could happen through several plausible pathways (Scheme 4.3). The first possible pathway is the *retro*-Diels-Alder reaction to generate compound **4.1**. The second pathway produces compound **4.2** by hydrolysis of the ester bond. The third pathway generates compound **4.3** by breakage of the Au−S bond. Finally, the fourth pathway produces compound **4.1** and **4.4** by *retro*-Diels-Alder reaction and by the breakage of the Au−S bond. To determine which pathway was followed during

the release, various techniques were applied to characterize the released molecules.
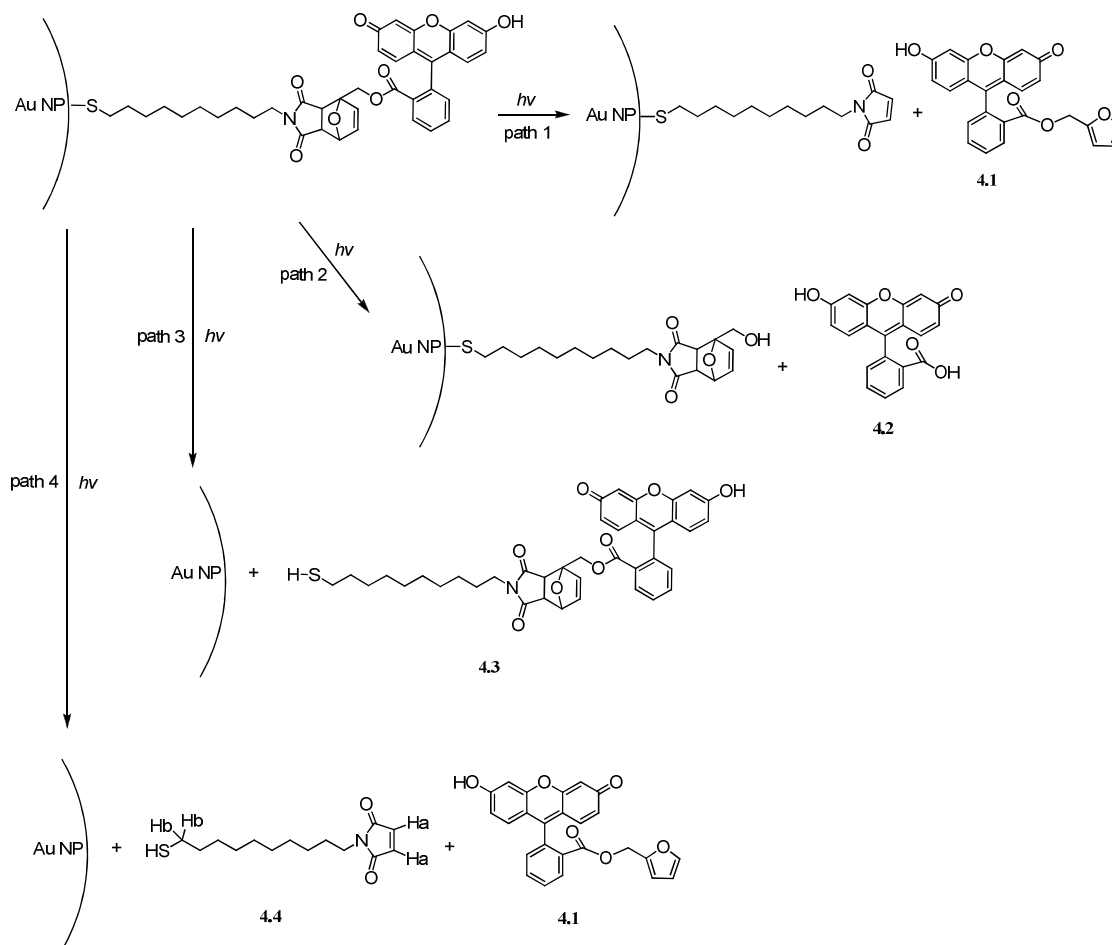
Scheme 4.3 Possible released molecules from gold NPs after photothermal treatment.

4.5.2 Characterization of Released Molecules by Nuclear Magnetic Resonance Spectroscopy

To characterize the released molecules after the photothermal release, nuclear magnetic resonance (NMR) spectroscopy was used. To reduce the peak corresponding to water in the ^{1}H NMR spectrum, solid spherical gold NPs were synthesized in D_2O. After synthesizing the NPs, the fluorescein Diels-Alder linker, previously dissolved in deuterated methanol, was added to the solution of solid

spherical gold NPs. The solution was incubated at 4 °C for 8 h and the decorated

NPs were purified by centrifugation and the subsequent removal of supernatant

followed by re-suspension in deuterated methanol (4 times at 10,000 rpm) in

order to remove the unbound fluorescein Diels-Alder linkers. The purified solution

of decorated solid spherical gold NPs was divided into two fractions. The first

fraction was pelleted by centrifugation and a ^{1}H NMR study was conducted on

the supernatant. The ^{1}H NMR spectrum of the first fraction showed no specific

peak between 6 and 8.5 ppm, where fluorescein's protons are expected to

appear (Figure 4.7B). The second fraction was irradiated with pulse laser (pulse

at λ = 532 nm, 3-6 ns, 10 Hz, 100 mW) for 7 min. After the irradiation the sample

was pelleted by centrifugation and ^{1}H NMR spectroscopic study was conducted

on the supernatant. The ^{1}H NMR spectrum of the irradiated fraction showed

multiple peaks between 6 and 8.5 ppm (Figure 4.7C). Comparing the ^{1}H NMR

spectrum of irradiated sample with ^{1}H NMR spectrum of compound **4.1** (Figure

4.7A) suggested that the released molecules from the NPs was compound **4.1**.
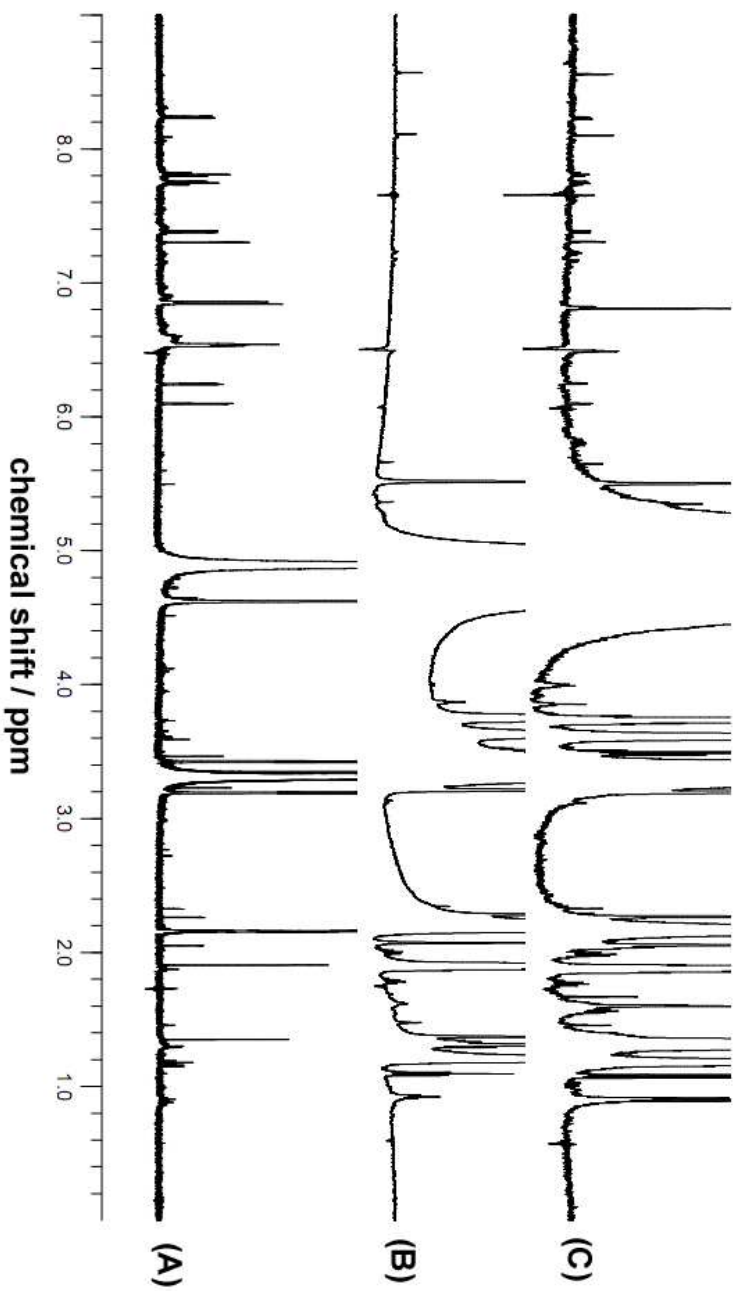
Figure 4.7 (A) ^{1}H NMR spectrum (600 MHz, deuterated methanol) of fluorescein furfuryl ester. (B) ^{1}H NMR spectrum (600 MHz, deuterated methanol) of supernatant of decorated solid spherical gold NPs before irradiation with pulse laser, and (C) supernatant from decorated solid spherical NPs after irradiation with pulse laser (pulse at λ = 532 nm, 3-6 ns, 10 Hz, 100 mW).

84

The results from the nuclear magnetic resonance of the released molecules after irradiation of the decorated NPs suggested that the release process was through path 1, 4, or a combination of these paths because only these paths could have produced compound **4.1**. Further, the spectrum of the released molecules was compared to the spectrum for the disulfide form of compound **4.4** (Figure 4.8A). In the disulfide form of compound **4.4** (Scheme 4.3) the chemical shift for H_b was at 2.7 ppm as shown in Figure 4.8A. (Note that for a similar alkylthiol the chemical shift for H_b would be 2.7 ± 0.2 ppm.) A Comparison of spectrum (A) in Figure 4.8 to spectrum (B), which is the spectrum of the released molecules, suggested that the release was through path 1. The absence of the H_b peak in Figure 4.8B was the evidence for such a claim. In contrary, the presence of H_a in Figure 4.8B suggested that the release was through a combination of path 1 and 4 (Scheme 4.3).
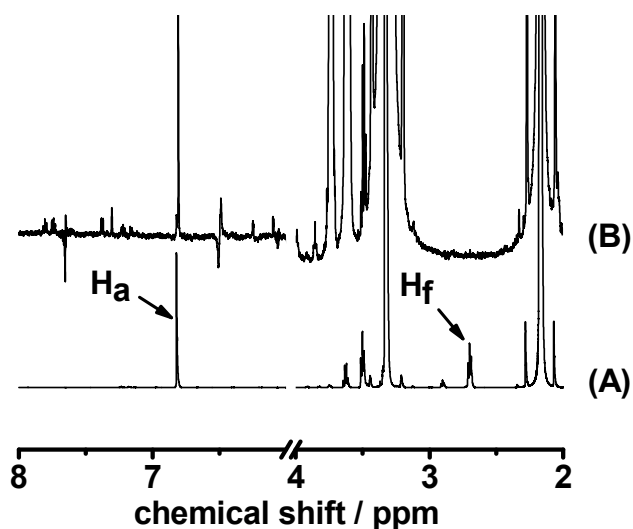
Figure 4.8 (A) ^{1}H NMR spectra (600 MHz, deuterated methanol) of compound **4.4**. (B) ^{1}H NMR spectra (600 MHz, deuterated methanol) Supernatant of decorated solid spherical NPs after pulse laser irradiation (pulse at λ = 532 nm, 3-6 ns, 10 Hz, 100 mW).

4.5.3 Characterization of Released Molecules by Mass Spectrometry

In addition to the nuclear magnetic resonance spectroscopy, mass spectrometry was used to characterize the released molecules from the decorated solid spherical gold NPs. To conduct this experiment, a solution of solid spherical gold NPs decorated with a fluorescein Diels-Alder linker was irradiated with the pulse laser (pulse at λ = 532 nm, 3-6 ns, 10 Hz, 100 mW) for 7 min. The sample was pelleted by centrifugation and the supernatant was analyzed by low resolution mass spectra. As shown in Figure 4.9, two major peaks were detected at 333.2 and 413.2 *m/z* that matched the molar mass of compound **4.2** and **4.1** (Scheme 4.3), respectively. Compound **4.3** has molar mass of 681.5 g/mol, which was not detected by the mass spectrum. In addition the molar mass of compound **4.4** (Scheme 4.3), which is 269.4 g/mol, was not observed. Therefore, the results from mass spectrometry suggest that the photothermal release of molecules from the decorated solid spherical gold NPs was the results of a *retro*-Diels-Alder reaction and hydrolysis of the ester. Therefore, mass spectrometry analysis suggested that the release mechanisms were through path 1 and 2.
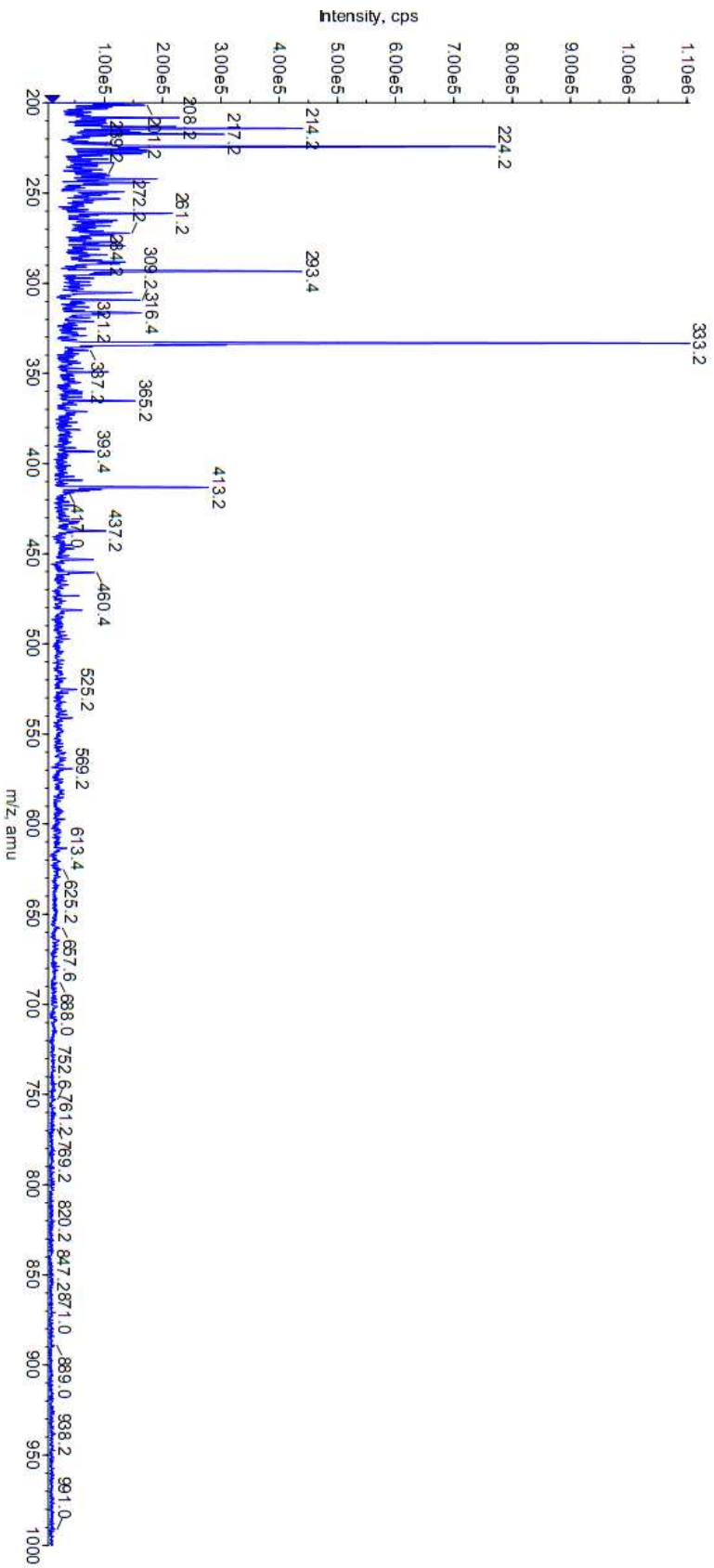
Figure 4.9 Mass spectrum analysis of the released molecules from solid spherical gold NPs after 7 min of pulse laser (pulse at λ = 532 nm, 3-6 ns, 10 Hz, 100 mW) irradiation.

87

4.5.3 Characterization of Released Molecules by Capillary Electrophoresis

4.5.4 Introduction to Capillary Electrophoresis

Capillary electrophoresis is a technique which separates species based on their charge to mass ratio.[93] The separations of ionic species take place in a moving conductive eluent (i.e., buffer) under the influence of an electric field.[93] A schematic of the separation technique is shown in Figure 4.10. The instruments main components are the following: the sample containing ionic species (sample injection), source vial (anode), destination vial (cathode), capillary field with buffer solution, and sample detector. To inject the sample, the capillary inlet was placed in the sample vial and by applying pressure, the sample was introduced into the capillary. After injection of the sample, the capillary inlet returns back to the source vial. The migration of the sample begins when one applies high voltage between the source vial and the destination vial. The applied voltage causes the electroosmotic flow in the capillary. Electroosmotic flow (EOF) is the movement of a layer of positive charges from the wall of the capillary towards the cathode while a high voltage is applied (Figure 4.10). As the positive layer moves toward the cathode, it drags the rest of the eluent with it, including anions. Another force acting in the capillary is called the electrophoretic mobility, which is motion of charged molecules in the fluid under the influence of an electric field. In the case of positively charged species, the migration is faster because the electrophoretic mobility and EOF are in the same direction. In the case of negatively charged species, the electrophoretic mobility is against the EOF; therefore, the migration is slower as shown in Figure 4.10 for the charge species.
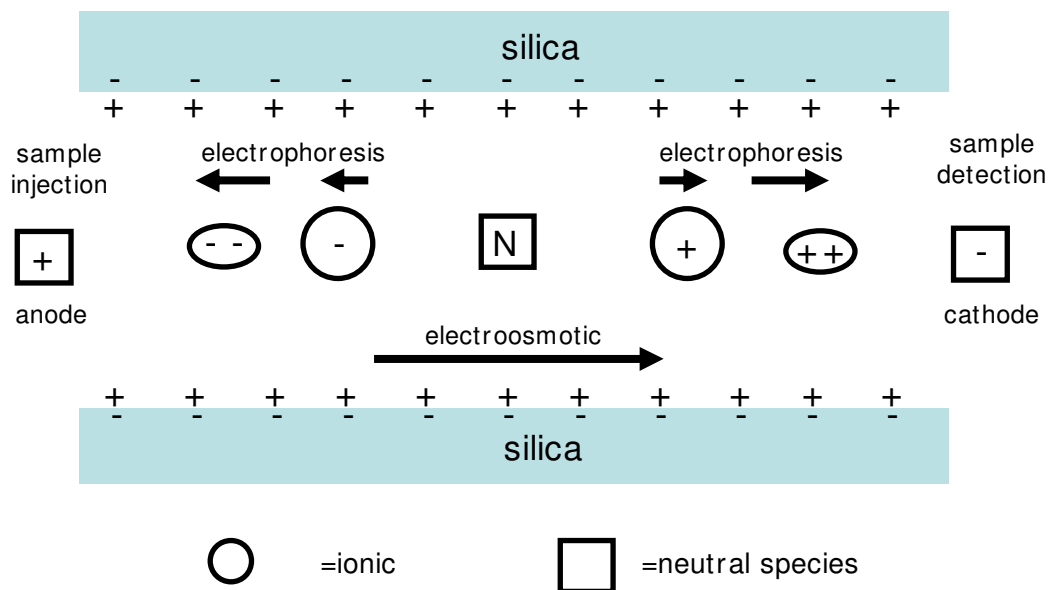
Figure 4.10 Diagram of the capillary electrophoresis system.

Furthermore, capillary electrophoresis can be modified to what is called micellar electrokinetic chromatography (MEKC) by adding of surfactants into the eluent.[94] When the surfactants are added in concentrations above the critical micelle concentration, micelles form in the buffer solution. During the separation, neutral molecules partition into micelles depending on their size and hydrophobicity. Neutral molecules that partition less or not at all into micelles, move with the same speed as the eluent. On the other hand, molecules that partition into the micelles more easily travel at a lower speed since micelles are highly negatively charged.[94] As a result, the MEKC method would allow for the separation of not just charged molecules, but also neutral molecules as well. Another benefit of this technique is a low detection limit of 10^{-18} M when coupled with a laser induced fluorescence detector.[95]

4.5.5 Separation of Released Molecules in Capillary Electrophoresis

Characterization based on capillary electrophoresis requires a set of standards to compare with the molecules released due to the photothermal effect of decorated gold NPs. From the three fluorescent compounds suggested to have released after the photothermal treatment of the decorated gold NPs (Scheme 4.3), compounds **4.1** and **4.2** were readily available and used as the standards. Compound **4.3** was not available, but the absence of this and other compounds will be determined by other means and will be explained later on in this chapter.

A mixture of compounds **4.1** and **4.2** was separated by capillary electrophoresis (Figure 4.11A). Then, an aliquot of the mixture was spiked with compound **4.1** and analyzed by capillary electrophoresis. An increase in the peak intensity at 5.3 min was clearly observable in electropherogram (Figure 4.11B). Therefore, the peak at 5.3 min was assigned to compound **4.1**. Compound **4.2** was added to another aliquot of the mixture, and the solution was run on the capillary electrophoresis (Figure 4.11C). The electropherogram indicated an increase in the peak intensity at 6.3 min. Therefore, the peak at 6.3 min was assigned to compound **4.2**. In the coming electropherograms, the migration times for compound **4.1** and **4.2** are slightly different for each run due to either a change in the capillary tube or using a new batch of eluent.
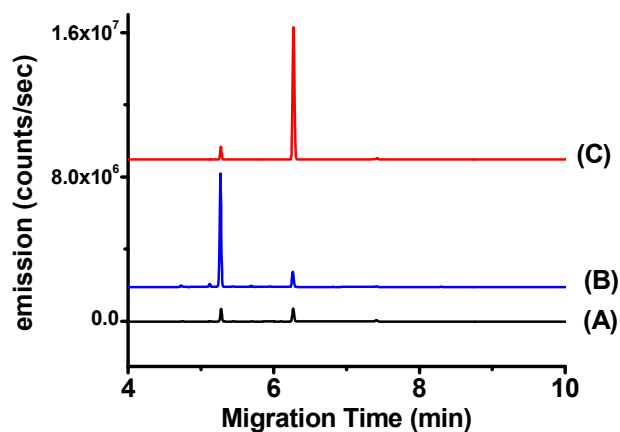
Figure 4.11 (A) Electropherograms (excitation at 488 nm) showing mixture of compounds **4.1** and **4.2** analyzed by capillary electrophoresis, (B) electropherogram of mixture A spiked by compound **4.1**, and (C) electropherogram of mixture A spiked by compound **4.2**.

4.5.6 Characterization of Thermally Released Molecules from Solid Spherical Gold NPs

A sample of an aqueous solution containing decorated solid spherical gold NPs, before the thermal treatment, was pelleted by centrifugation and the supernatant was analyzed by capillary electrophoresis. The capillary electrophoresis did not detect any peaks from the sample prior to thermal treatment. The result from the capillary electrophoresis suggested that prior to thermal treatment of the sample, the concentration of fluorescein moiety in the solution was negligible. The same sample was re-suspended and heated in a water bath at 80 °C for 1 h and was pelleted by centrifugation. The supernatant was analyzed by the capillary electrophoresis. Two peaks were detected at 5.9 and 7.1 min as shown in Figure 4.12A. To confirm that the detected peaks correspond to compounds **4.1** and **4.2**, the sample was spiked with both compounds **4.1** and **4.2** and was analyzed by capillary electrophoresis. As shown

in the electropherogram (Figure 4.12B), there was an increase in the intensity of both peaks, which concluded that the released molecules from the NPs are compounds **4.1** and **4.2**. This result indicates that the fluorescein adduct **4.1** was released through the *retro*-Diels-Alder reaction and the fluorescein adduct **4.2** was released through hydrolysis of the ester bond. No other peaks were detected after monitoring the capillary electrophoresis signal for a total of 20 min.
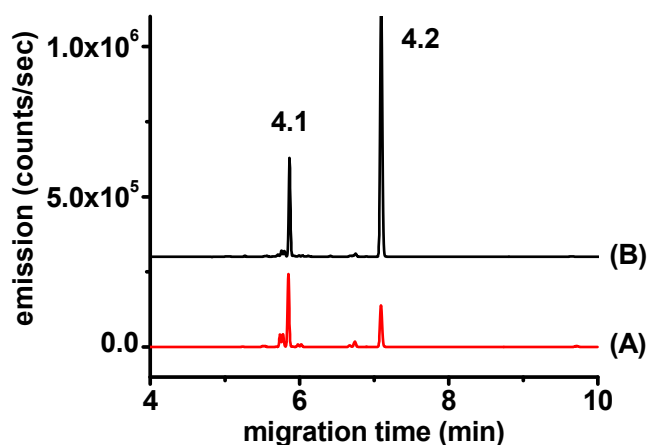
Figure 4.12 Electropherograms (excitation at 488 nm) showing (A) the formation of compounds through thermal release of decorated gold NPs, and (B) electropherograms of same sample after spiking it with compound **4.1** and **4.2**.

4.5.7 Characterization of Photothermally Released Molecules

A sample of an aqueous solution containing decorated solid spherical gold NPs was pelleted by centrifugation and the supernatant was analyzed by capillary electrophoresis. The capillary electrophoresis did not detect any peak from the sample prior to photothermal treatment. Then the sample was re-suspended and irradiated with the pulsed laser and pelleted by centrifugation. An aliquot of the supernatant was injected into the capillary electrophoresis

instrument. The analysis of the photothermal release detected peaks similar to the thermal study as shown in Figure 4.13A. Capillary electrophoresis detected two peaks at 5.9 and 7.1 min. To confirm the identity of these peaks, the sample was spiked with the standards (i.e., **4.1** and **4.2**) and analyzed by capillary electrophoresis. In Figure 4.13B the electropherogram indicated an increase in the fluorescence signal for both peaks. This observation confirmed that the photothermal release mainly took place through the *retro*-Diels-Alder reaction. After monitoring the capillary electrophoresis signal for a total of 20 min no other peaks were detected.
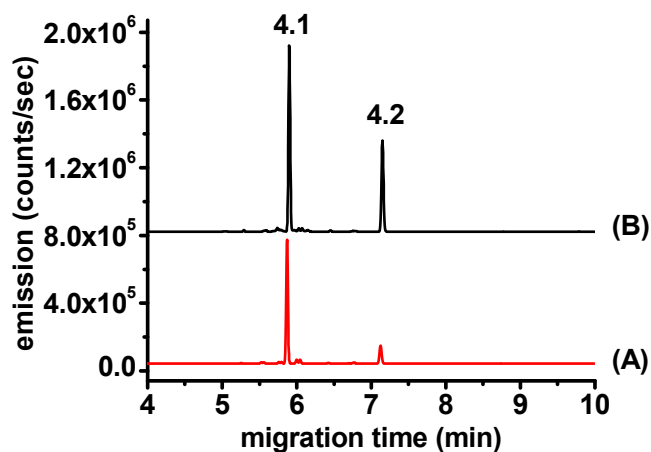
Figure 4.13 Electropherograms (excitation at 488 nm) showing (A) the formation of compounds through photothermal release of decorated solid spherical gold NPs, and (B) electropherograms of the same sample after spiking it with compounds **4.1** and **4.2**.

4.5.8 Quantification of the Released Molecules

The previous results confirmed that during the thermal and photothermal treatment of decorated gold NPs, compounds **4.1** and **4.2** were the released molecules from the NPs. However, it is possible that other molecules, such as

compound **4.3** (Scheme 4.3), were also released but were not detected due to their decomposition. One way to check for this was to compare the amount of fluorescence intensity detected by capillary electrophoresis and fluorometer after the photothermal effect. A fluorometer can detect any fluorescent molecules released from the decorated NPs. Thus, the fluorescence intensity of the sample can be measured by a fluorometer. Then the concentration of the sample can be determined by making a series of standard dilutions of compound **4.1**. Once the concentration of the sample is determined from the fluorometer, a similar experiment can be performed to determine the concentration of the sample from the capillary electrophoresis. If the concentration obtained from each instrument is similar then no other fluorescent molecules can be present in the sample except compound **4.1** and **4.2**.

Therefore, a series of standard dilutions of compound **4.1** were measured on both a fluorometer and capillary electrophoresis. Dilution curves are provided in Figure 4.14A and B, respectively.

(A)
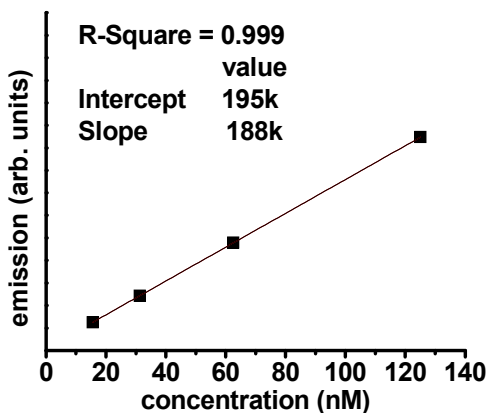
(B)
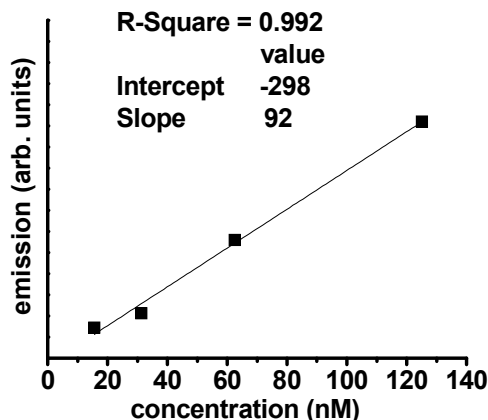
Figure 4.14 Series of standard dilutions of compound **4.1** on (A) fluorometer, and (B) capillary electrophoresis. Each data point is the summation of the integrated area for each corresponding fluorescence emission spectrum at the respective concentrations. The emission is integrated from 500 to 600 nm, and the excitation wavelength in (A) is 490 nm and in (B) is 488 nm.

Furthermore, the fluorescence emission of a sample after photothermal release was measured by both capillary electrophoresis and by a fluorometer. First, the concentration of the sample was determined based on the standard dilution curve obtained from the fluorometer (Figure 4.14A). From the equation obtained for the linear regression analysis in Figure 4.14A, the concentration of molecules released from the decorated gold NPs after 7 min of irradiation with pulse laser (pulse at λ = 532 nm, 3-6 ns, 10 Hz, 100 mW) was found to be 60 ± 3 nM (for further details see the experimental section, Figure 4.20). Then, the same sample was injected into the capillary electrophoresis and the concentration, with respect to the capillary electrophoresis linear regression analysis in Figure 4.14B, was found to be 63 ± 6 nM (for further details see the experimental section, Figure 4.21). In the capillary electrophoresis measurement, the intensity of each

peak was corrected with respect to measured deviations in the signal for the internal standard, which accounts for slight variations in the volume injected into the capillary electrophoresis.

Comparing the concentration of fluorescein moiety in the sample obtained by the fluorometer (60 $\pm$ 3 nM) and capillary electrophoresis (63 $\pm$ 6 nM), indicates that any fluorescent molecules that were detected by the fluorometer were also detected by capillary electrophoresis. Therefore, the only fluorescent molecules released from the NPs were most likely to be compounds **4.1** and **4.2**.

In summary, combining the results from nuclear magnetic resonance spectroscopy, mass spectrometry, and capillary electrophoresis, all suggest that path 1 (Scheme 4.3) was the most likely mechanism of the release. However, there was evidence that the other paths such as path 2 and 4 could have contributed to the released molecules.

4.6   Quantification of Released Molecules per NP

4.6.1   Estimated Number of Dye Molecules Released per Solid Spherical Gold NP

To measure the number of molecules released from a single solid spherical gold NP, two parameters are required: i) the concentration of NPs; and ii) the concentration of the released molecules. In the case of the released molecules, the concentration can be determined using their mass (or moles) dissolved in the solution. However, in the case of the NPs, this method does not apply because of the polydispersity of the gold NPs. The size uniformity of the solid spherical gold NPs is simply an approximation, therefore, the concentration

96

calculated using the mass of the NPs dissolved in the solution will also be an approximation.

4.6.2 Estimated Concentration of Decorated Gold NPs

The common method to determine the concentration of gold NPs in a solution involves measuring the concentration of gold atoms in the solution and dividing it by the number of gold atoms in one NP.[42] The concentration of gold atoms in the solution was measured using inductively coupled plasma mass spectrometry (ICP-MS). The results from the ICP-MS measurement indicated that the concentration of the decorated solid spherical gold NPs was 2.11 µg/mL.

(Note: the samples used to estimate the concentration of decorated gold NPs (section 4.6.2), to study the hydrolysis of the ester bond (section 4.6.4), and to quantify molecules released per gold NP due to thermal and photothermal effect (section 4.6.5) had identical concentrations of solid spherical gold NPs.)

In order to find the number of gold NPs in the solution, further calculations are required. The total volume of gold in the solution can be calculated from Equation (Eq.) 4.1, which is the total concentration of gold atoms in solution, obtained from the ICP-MS result, divided by the density of gold. The result from Eq. 4.1 provides the total volume of the gold per 1 mL of sample. The approximate size distribution of solid gold NPs was indicated in Chapter 2, the average diameter of solid gold NPs was determined to be 17.8 ± 0.9 nm for 100 NPs. Based on the approximate radius of 8.9 nm for a solid spherical gold NP, the volume of each sphere can be measured from Eq. 4.2. The number of

particles (Eq. 4.3) in 1 mL of the solution can be obtained by dividing the total volume of the gold in the solution (Eq. 4.1) by the volume of a single particle (Eq. 4.2).

Density of gold $= 19.3 g/cm^3$

Volume of gold NPs (per mL) = $\dfrac{2.11 \times 10^{-6} g}{19.3 g/cm^3} = 109 \pm 5 \times 10^{-9} cm^3$ **Eq. 4.1**

Volume of sphere: $4/3\pi r^3$

Volume of gold particles = $4/3 \times \pi \times (8.9 nm)^3 = 3.0 \pm 0.3 \times 10^{-24} m^3$ **Eq. 4.2**
$$= 3.0 \pm 0.3 \times 10^{-18} cm^3$$

Number of particles in 1 mL of water = $\dfrac{109 \times 10^{-9} cm^3}{3.0 \times 10^{-18} cm^3} = 36 \times 10^9$ **Eq. 4.3**

This result offers an approximation with an error margin of 5% relative to the ICP-MS results.[96] Including the error in the average size distribution of particles, which is 5%, the total number of NPs in 1 mL of water was found to be $36 \pm 4 \times 10^9$ (for further details see the experimental section, example derivation for error calculations).

4.6.3 Estimating the Concentration of Released Molecules from Gold NPs

To measure the number of molecules released per NP, all of the attached molecules must be released from the surface of the gold NPs in an irreversible fashion. One method to do this is the use of heat to induce the *retro*-Diels-Alder reaction. However, due to the Diels-Alder reactions equilibrium, some of the released molecules could undergo a Diels-Alder reaction and lose their fluorescence property due to re-attachment to the gold surfaces. Another method of release is hydrolysis of the ester bond, which has ~90% yield.[97] Hydrolysis of

the ester bond in the presence of a base and heat has been shown to effectively convert the ester bond to carboxylic acid and alcohol.[97]

4.6.4 Hydrolysis of the Ester Bond in Fluorescein Diels-Alder Linkers Attached to Gold NPs

Hydrolysis of an ester in the presence of a base or an acid as a catalyst will facilitate this reaction upon heating. A base catalyst is preferred for two reasons:

1. fluorescein is pH sensitive and has a higher fluorescence intensity at a higher pH, and

2. using acid as a catalyst lactonizes the fluorescein into a non-fluorescence compound (Scheme 4.4), which is undesirable.[98]
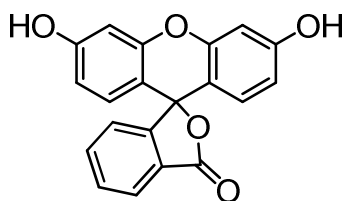
Scheme 4.4 Fluorescein in its lactone form.

Therefore, a base was used as a catalyst to hydrolyze the ester bond between the fluorescein and the NP (Scheme 4.5). More specifically potassium hydroxide was the chosen base. A sample of decorated solid spherical gold NPs was adjusted to pH 12.3 using an aqueous solution of 0.2 M KOH. The background fluorescence spectrum was taken before heating the sample to 80 °C. The fluorescence spectrum of the sample was taken in 20 min intervals. The

experiment was stopped when the fluorescence emission began to reach a maximum (Figure 4.15), indicating the completion of the hydrolysis.
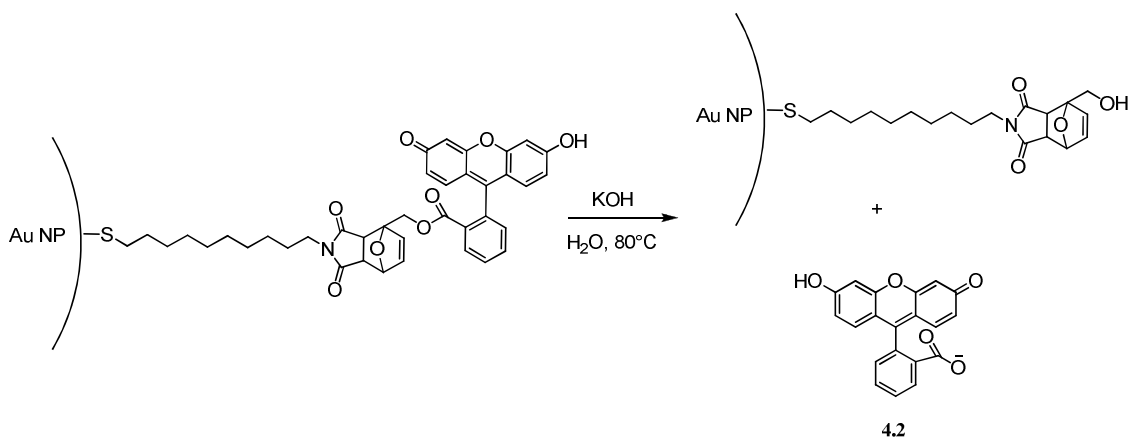
Scheme 4.5 Hydrolysis of an ester bond in the presence of base to cleave the fluorescein from the surface of a NP.
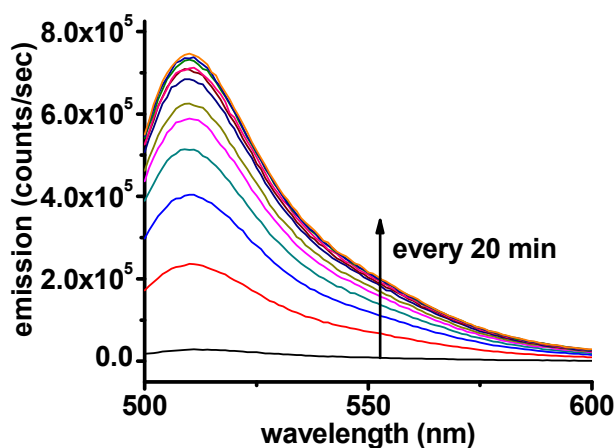
Figure 4.15 Representative spectra showing changes in the fluorescence intensity (excitation at 490 nm) when an aqueous dispersion of solid spherical gold NPs decorated with the fluorescein Diels-Alder linker was heated in a water bath at 80 °C under basic (pH 12.3) conditions.

In addition, to account for the pH dependent fluorescence of fluorescein, a series of standard solutions were prepared at pH 12.3. The concentration of fluorescein in the solution was measured by Eq. 4.4, which was obtained from a

linear regression fit of series of standards (for further details see the experimental section, Figure 4.22):

$$X = \frac{Y + 57681}{274954}$$ **Eq. 4.4**

where X is the concentration of fluorescein in nM and Y is the area under fluorescence emission spectrum. After completion of hydrolysis of the ester bond, Y was measured to be 29844361 by integrating the fluorescence spectrum between 500−600 nm (Figure 4.15, highest emission spectrum). Insertion of this number into the Eq. 4.4, gives the total concentration of fluorescein released from the gold NPs to be 108 ± 6 nM in a 1 mL sample. The number of molecules in a 1 mL sample can be calculated from equation Eq. 4.5:

Number of molecules in 1 mL= 108 (nM) x 0.001 (L) x N_A **Eq. 4.5**

where N_A is the Avogadro's number (6.022 x 10^{23} molecules/mole). The number of released molecules in 1 mL was found to be 6.6 ± 0.4 x 10^{13} and the number of molecules released per gold NP was calculated by dividing this number by the number of gold NPs (Eq. 4.6):

Number of molecules per NP= $\dfrac{6.6 \times 10^{13}}{36 \times 10^{9}} = 1829$ **Eq. 4.6**

Based on the calculations, the estimated number of molecules released per NP was 1800 ± 200. The molecules released from the hydrolysis of decorated NPs were characterized by the capillary electrophoresis. The presence of a single peak in the electropherogram is shown in Figure 4.16A. The observed peak was fluorescein, confirmed by spiking the sample with a solution

of fluorescein (Figure 4.16B). The completion of the reaction and characterization of fluorescein molecules by the capillary electrophoresis indicates that the hydrolysis of ester bond was successful.
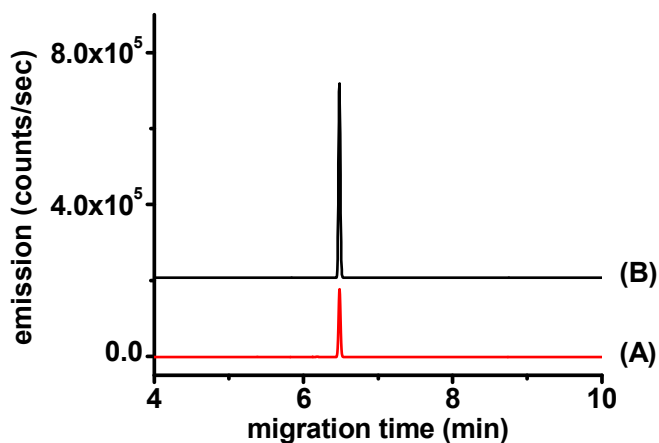
Figure 4.16 Electropherograms of the hydrolysis of decorated gold NPs after the completion of the reaction. (A) The electropherogram shows the release of fluorescein from gold NPs, and (B) Sample A spiked with fluorescein.

4.6.5 Number of Molecules Released per Gold NP Due to the Thermal and Photothermal Release

In the previous section, the total concentration of released molecules from the NPs and the approximate number of NPs in 1 mL were estimated. The number of particles in the solution was determined to be $36 \pm 4 \times 10^9$ particles/mL from the ICP-MS analysis. The concentration of fluorescein furfuryl ester **4.1** after 220 min of thermal treatment was found to be 43 ± 4 nM (for further details see the experimental section, Figure 4.23). The concentration of fluorescein furfuryl ester **4.1** after 7 min of pulse laser irradiation was found to be 21 ± 2 nM (for further details see the experimental section, Figure 4.24). Using

Eq. 4.7, the number of molecules released after 220 min of thermal treatment was found to be $2.6 \pm 0.2 \times 10^{13}$ molecules:

Number of molecules in 1 mL= 43 (nM) x 0.001 (L) x N_A **Eq. 4.7**

    The number of molecules released per NP after thermal treatment can be deduced from Eq. 4.8:

Number of molecules released per NP$=\dfrac{2.6 \times 10^{13}}{36 \times 10^{9}} = 722$ **Eq. 4.8**

    Using Eq. 4.9, the number of molecules released after 7 min of the photothermal effect was found to be $1.3 \pm 0.1 \times 10^{13}$ molecules:

Number of molecules in 1 mL= 21 (nM) x 0.001 (L) x N_A **Eq. 4.9**

    The number of molecules released per NP after laser irradiation can be deduced from Eq. 4.10:

Number of molecules released per NP$=\dfrac{1.3 \times 10^{13}}{36 \times 10^{9}} = 361$ **Eq. 4.10**

    The total number of molecules released from the decorated solid spherical gold NPs after 220 min of thermal treatment was 720 ± 90 and after 7 min of laser irradiation was 360 ± 50. Comparing the number of molecules released by the photothermal and thermal treatment to the total number of molecules on NPs (1800 molecules), the 7 min laser irradiation resulted in ~20% and 220 min of thermal treatment resulted in ~40% release of molecules from the NP surfaces. This low percentage of release relative to the thermally driven release in solution may be due to the anchoring of the molecules onto the gold surfaces, which

hinders their otherwise free movement. Specifically, during the photothermal effect the heat is transported away from the surfaces of NPs through the surface coating of molecules by molecular vibrations.[99] This direction dependent heat transfer in response to the 100 mW laser irradiation may not be as efficient as the thermal effect when the molecules are suspended freely in solution. Further studies are needed to address the reasons for the observed decreased release when the molecules are anchored to the surfaces of the gold NPs.

4.7   Release of Molecules from Silica/Gold Core-Shell NPs

4.7.1   Introduction

As mentioned at the beginning of this chapter, two nanostructures were prepared to demonstrate the photothermal release of molecules from gold surfaces. Earlier in the chapter, the photothermal release of molecules from solid spherical gold NPs was demonstrated. This section demonstrates the release of molecules using silica/gold core-shell NPs. Silica/gold core-shell NPs have SPR absorptions at 650−900 nm, which means that an 800 nm light source, rather than a 532 nm light source, can be used to trigger a photothermal effect.

Because of the similarity in concept of photothermal release between solid spherical gold NPs and silica/gold core-shell NPs, brevity is employed to reduce redundancy in the results obtained from the thermal and photothermal release from decorated silica/gold core-shell particles. In addition, the characterization and calculations for the concentration of the released molecules that were presented for solid spherical gold NPs are omitted for the silica/gold core-shell particles. The absence of capillary electrophoresis characterization and

concentration studies is caused by the irreproducibility in the synthesis of silica/gold core-shell particles with a maximum SPR absorption of 650 nm. Due to the inconsistency in the SPR of silica/gold core-shell NPs the production was halted and further study on decorated silica/gold core-shell NPs was not pursued.

4.7.2 Thermal and Photothermal Release of Molecules from Decorated Silica/Gold Core-Shell NPs

Silica/gold core-shell particles suspended in water, obtained from Dennis Hsiao, were decorated with the fluorescein Diels-Alder linkers and purified as previously mentioned in this chapter. A fluorescence spectrum of the sample was taken and the sample was placed in a 60 °C water bath. Fluorescence spectra of the heated sample was recorded every 30 min over a period of 3 h. An increase in the fluorescence intensity of the sample was observed over time (Figure 4.17A). Fluorescence emission is also plotted with respect to time (Figure 4.17B). Data from Figure 4.17B are normalized by dividing the area under each spectrum in Figure 4.17A (between 500−600 nm) at each point in time, by the area under the background spectrum. The increase in the fluorescence emission indicates the release of the fluorescein moiety from the gold surfaces. Comparing the thermal release from decorated silica/gold core-shell NPs with decorated solid spherical gold NPs, one can conclude that the released mechanism is identical and it should occur through a *retro*-Diels-Alder reaction and hydrolysis. This would be a reasonable conclusion without further characterization of the released molecules because the only factors that have changed are the size and surface chemistry of the NPs. Since the size and surface chemistry of the NPs are most

likely irrelevant in the release mechanism, the released molecules should be identical to the ones released from solid spherical gold NPs.

(A)

(B)
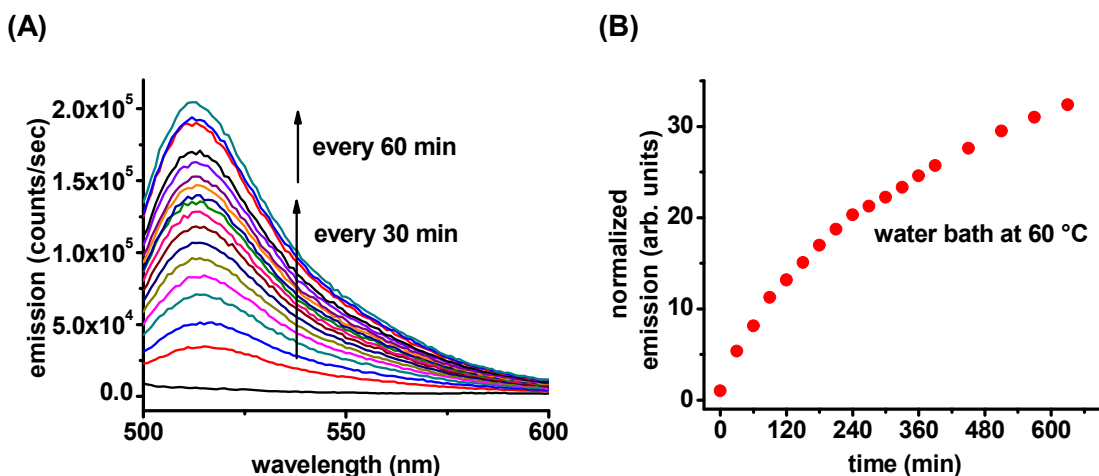
Figure 4.17 (A) Representative spectra showing changes in the fluorescence intensity (excitation at 490 nm) when an aqueous dispersion of 204 nm silica/gold core-shell NPs decorated with the fluorescein Diels-Alder linker is heated in a water bath at 60 °C. (B) Increase in fluorescence intensity with respect to time (excitation at 490 nm) when aqueous dispersions of silica/gold core-shell NPs decorated with the fluorescein Diels-Alder linkers were heated at 60 °C. The spectra are normalized by dividing the area of each spectrum by the background (area between 500-600 nm).

A sample identical to the one used in the thermal experiment was prepared to demonstrate the photothermal release from silica/gold core-shell NPs. Fluorescence spectrum for this sample was acquired before laser irradiation. The sample was irradiated with a pulsed NIR laser (800 nm, 100 fs, 1 kHz, 800 mW) for 2 min and then another fluorescence spectrum was taken. The irradiation was repeated several times for 2 min durations with a pulsed NIR laser (Figure 4.18A). Figure 4.18A indicates that there was an increase in the fluorescence intensity of the decorated silica/gold core-shell NPs, dispersed in an aqueous solution, after irradiation with the laser. A better representation that

shows this increase in the fluorescence intensity can be seen in Figure 4.18B where each spectrum is normalized with respect to the initial background fluorescence intensity. The increase in the fluorescence intensity during the laser irradiation suggests that the release of the fluorescein moiety from the gold surfaces resulted from the photothermal effect. This photothermal release from the silica/gold core-shell NPs confirms that multiple wavelengths can be used to release molecules from gold NPs. The advantage of using the silica/gold core-shell NPs is that they require longer wavelengths of light (λ = 800 nm). The use of NIR light would be useful in potential biological applications for these NPs because the NIR light has better penetration in biological tissues compared to visible light.
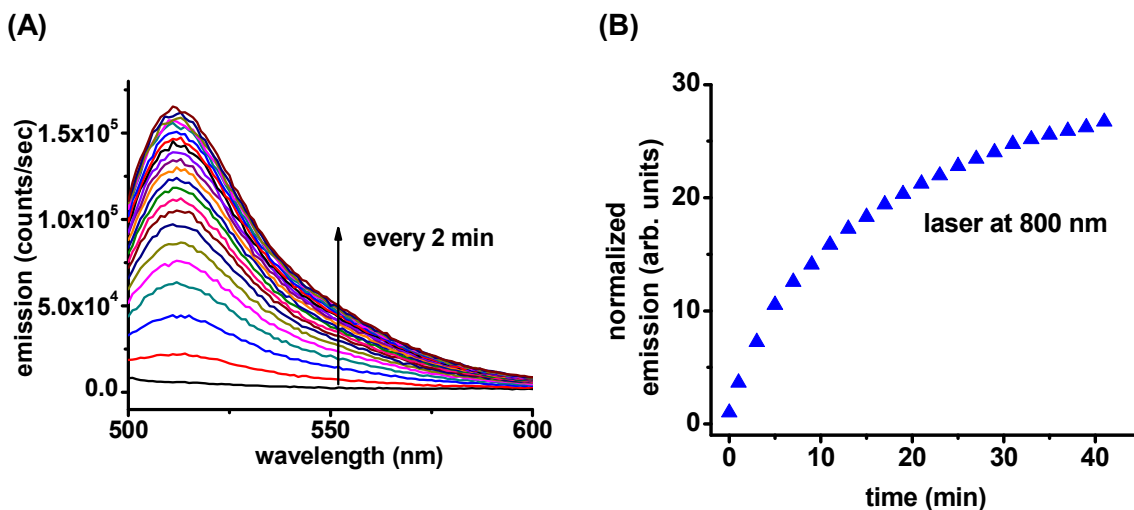
Figure 4.18 (A) Representative spectra showing changes in the fluorescence intensity when an aqueous dispersion of 204 nm silica/gold core-shell NPs decorated with the fluorescein Diels-Alder linker was irradiated with laser (λ = 800 nm, 100 fs, 1 kHz, and 800 mW). (B) Increase in fluorescence intensity with respect to time when aqueous dispersions of 204 nm silica/gold core-shell NPs decorated with the fluorescein Diels-Alder linkers were irradiated with laser (λ = 800 nm). The spectra are normalized by dividing the area of each spectrum by the background (area between 500-600 nm).

4.8   Conclusion

The novelty of the work presented in this chapter was the use of light as a stimulus to trigger a release of molecules from the surfaces of gold NPs. In summary, gold NPs were decorated with fluorescein Diels-Alder linkers. An aqueous solution of decorated solid spherical gold NPs showed an increase in fluorescence intensity when the sample was irradiated with a pulsed laser. Nuclear magnetic resonance spectroscopy, mass spectroscopy, and capillary electrophoresis analysis suggested that after 7 min of irradiation, the released molecules were fluorescein furfuryl ester. The released molecule was the product of a *retro*-Diels-Alder reaction from attached molecules to the gold NPs. For the first time, the experiments in this chapter utilized the photothermal effect to

release molecules from surfaces of gold NPs. The highlight of this result was the use of surface localized heat during the irradiation of gold NP to release molecules. In addition, similar photothermal release was demonstrated using silica/gold core-shell NPs decorated with fluorescein Diels-Alder linkers. The advantage of core-shell NPs were their NIR SPR absorption. The release from decorated core-shell particles using 800 nm wavelength pulsed laser confirmed that NIR can also be used to release molecules. As a result of the above mentioned experiments, multiple wavelengths were used to demonstrate the release of molecules from gold NPs.

4.9 Experimental Section

4.9.1 General Information

Unless otherwise stated, all chemicals were purchased from Sigma Aldrich and used without further purification. Water used for the synthesis and purification of NPs was from a Barnstead NANOpure Diamond water purification system (18 MΩ). Purifications of samples were performed using Fisher accuSpin 400 general purpose tabletop centrifuge. All the fluorescence measurements were taken with the samples in Fisherbrand quartz fluorescence cells (10 mm path length) using a Photon Technology International QuantaMaster spectrometer (data acquisition parameters set to an excitation of 490 ± 2 nm while monitoring emission from 500-600 ± 2 nm). Solid gold NPs concentrations were measured on a Perkin Elmer Elan 6000 inductively coupled plasma mass spectrometry. The samples preparation for ICP-MS: 0.05 mL of the sample was aliquoted into a 15 mL polypropylene tube and reacted with aqua regia. The digested solution was then made to final volume of 5 mL with distilled/de-ionized water. The samples analysis of ICP-MS: The sample was analyzed by conventional ICP-MS, at a dilution of x1. The element was fully quantified against a certified standard using single point calibration. The sample analysis and operation of the ICP-MS was done according to CANTEST in-house standard operation procedure. For further information on the ICP-MS results contact Wilson Chan at WChan@cantest.com sample number: AB-4-60 (1)

High resolution mass spectra for the compounds were obtained using an Agilent 6210 TOF LC/MS (ESI+). Irradiation of solid gold NPs was done using a CW laser operating at 532 nm (Coherent, Verdi) and a nanosecond Nd:YAG (neodymium-doped yttrium aluminium garnet, $Nd:Y_3Al_5O_{12}$) pulse laser from Continuum, model PL8000 (3-6 ns, 10Hz, 532 nm) with beam radius of 0.7 cm. Irradiation of silica/gold core-shell NPs with NIR light was accomplished using a CW laser operating at 532 nm (Coherent, Verdi) to pump a mode-locked Ti:Sapphire oscillator (Spectra Physics, Tsunami 3960a), which produced a pulsed train at 82 MHz, with a wavelength tunable from 750 to 850 nm and pulse duration of 65 fs. This light was then sent through a Ti:Sapphire chirped pulse regenerative amplifier (Positive Light, Spitfire) for amplification and the amplifier was pumped by a pulsed intracavity frequency-soluble, Q-switched Nd:YLF (neodymium-doped yttrium lithium fluoride, $Nd:YLiF_4$) laser (Positive Light, Merlin), which operated at 1 kHz with pulse duration of 100 fs, pulse energy of 1 mJ and wavelength of 800 nm and beam radius of 0.4 cm. Temperatures were monitored using an RTD Platinum Thermometer (VWR International, Pt-100Ω, NIST Traceable) with temperature range of -50 to 400 °C and resolution of 0.01 °C with accuracy of ±0.1% below 200 °C and resolution of 0.1 °C with accuracy of ±0.15% above 200 °C.. Aqueous solutions of gold particles were irradiated by laser as shown in Figure 4.19.
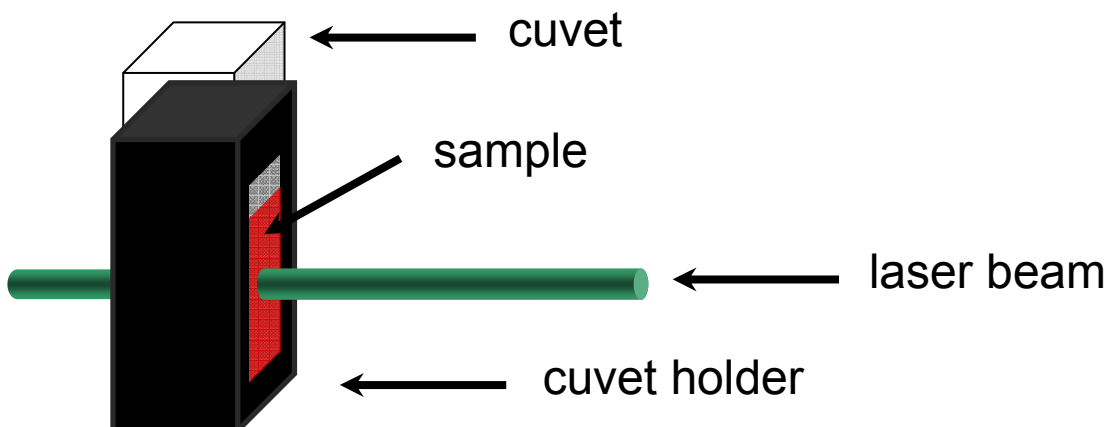
Figure 4.19 Quartz cuvet containing aqueous solution of gold NPs placed in the cuvet holder during the irradiation time.

4.9.2 Capillary Electrophoresis Apparatus and Procedures

Capillary Electrophoresis data were obtained on a Beckman-Coulter, PA800 equipped with a laser-induced fluorescence detector (Ar laser 488 nm). The optimal buffer composition was chosen to be 10 mM boric acid, pH 9.2, containing 50 mM sodium dodecylsulfate (SDS). The buffer was prepared by dissolving analytical grade boric acid in 18 MΩ water and adjusting the pH with 1.0N NaOH prior to the addition of SDS. The buffer was filtered through a 0.22 μm vacuum filtration device before use. The fused silica capillary was purchased from Beckman-Coulter and had an internal diameter of 75 μm, a total length of 60 cm, and the length from injection to detection was 50 cm. The capillary was conditioned prior to each sample injection by rinsing it for 2 min with 0.1 M NaOH followed by water (2 min) and then with a buffer for another 2 min with pressure of 20 psi for each. The samples were injected into the cathode end of the capillary using hydrodynamic pressure (0.5 psi) for 3 s and electropherograms

were acquired at a constant voltage of -30 kV at 22 °C. Eletropherograms were acquired and analyzed using System Gold Software (Beckman-Coulter) and displayed by plotting them with Origin 8.0.

4.9.3 Supporting Information for Calculations

The area was calculated by integrating each spectrum between 500−600 nm using OriginPro 8.

concentration = (area - 195000)/188000		
		error
emission area =	11503884	
concentration (nM) =	60	3
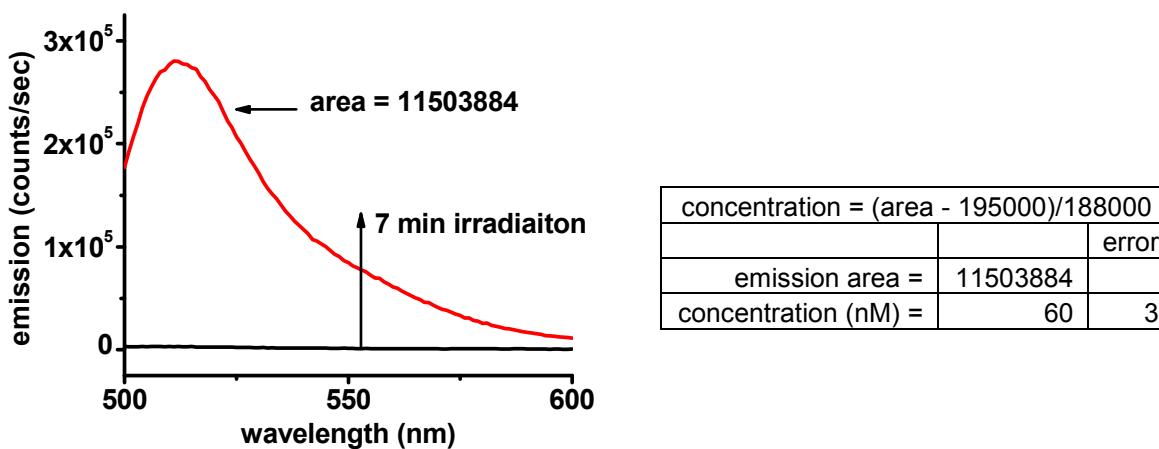
Figure 4.20 Representative spectra showing changes in the fluorescence intensity (excitation at 490 nm) when an aqueous dispersion of solid spherical gold NPs decorated with the fluorescein Diels-Alder linker was irradiated with pulse laser (pulse at λ = 532 nm, 3-6 ns, 10 Hz, 100 mW) for 7 min. Inset shows the calculation for the concentration of released molecules based on the integration of the spectrum and equation deducted from linear regression (Figure 4.14A).

concentration = (area + 298)/91		
		error
emission area (**4.1**) =	3679	
concentration (nM) =	43	4
emission area (**4.2**) =	1535	
concentration (nM) =	20	2
total (nM) =	63	6
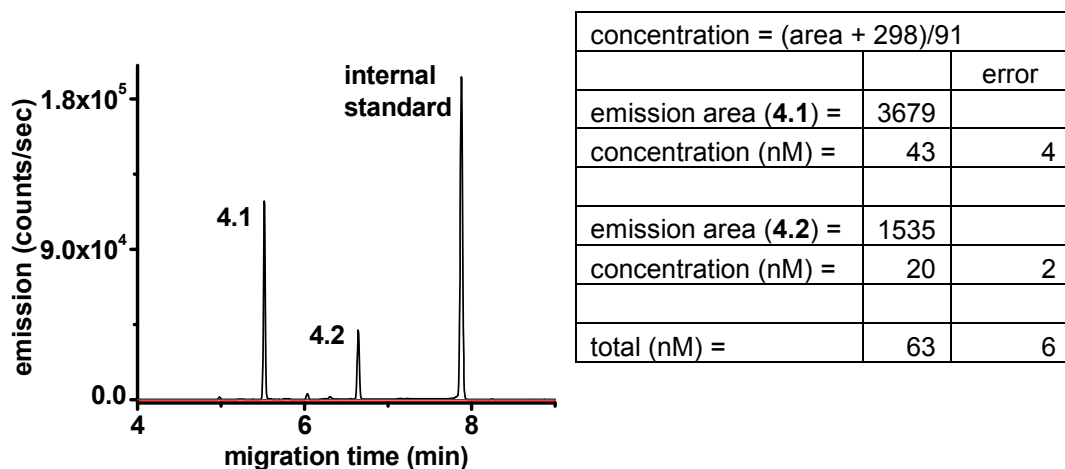
Figure 4.21 Electropherograms (excitation at 488 nm) showing the formation of compounds after laser irradiation of decorated solid spherical gold NPs. Inset shows the calculation for the concentration of released molecules based on the integration of the peaks **4.1**, **4.2** and equation deducted from linear regression (Figure 4.14B).
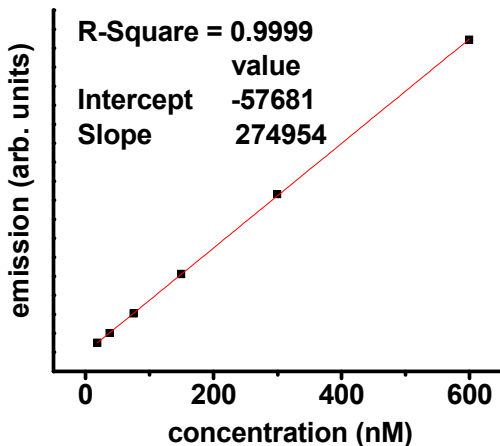
Figure 4.22 Series of standard dilutions of compound **4.2** at pH 12.3. Each data point is the summation of the integrated area for each corresponding fluorescence emission spectrum at the respective concentrations. The emission is integrated from 500 to 600 nm, and the excitation wavelength is 490 nm.
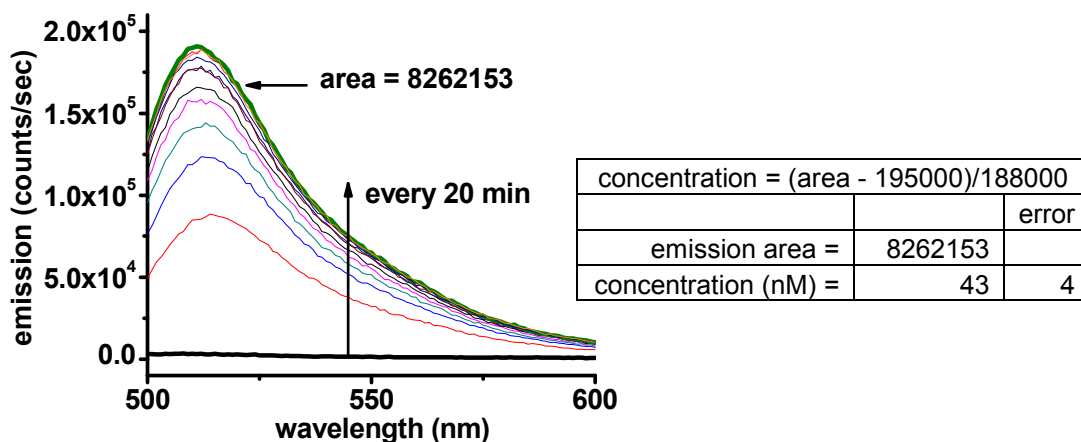
Figure 4.23 Representative spectra showing changes in the fluorescence intensity (excitation at 490 nm) when an aqueous dispersion of decorated solid spherical gold NPs with the fluorescein Diels-Alder linker was heated in a water bath at 80 °C for 220 min. Inset shows the calculation for the concentration of released molecules based on the integration of the spectrum and equation deducted from linear regression (Figure 4.14A).
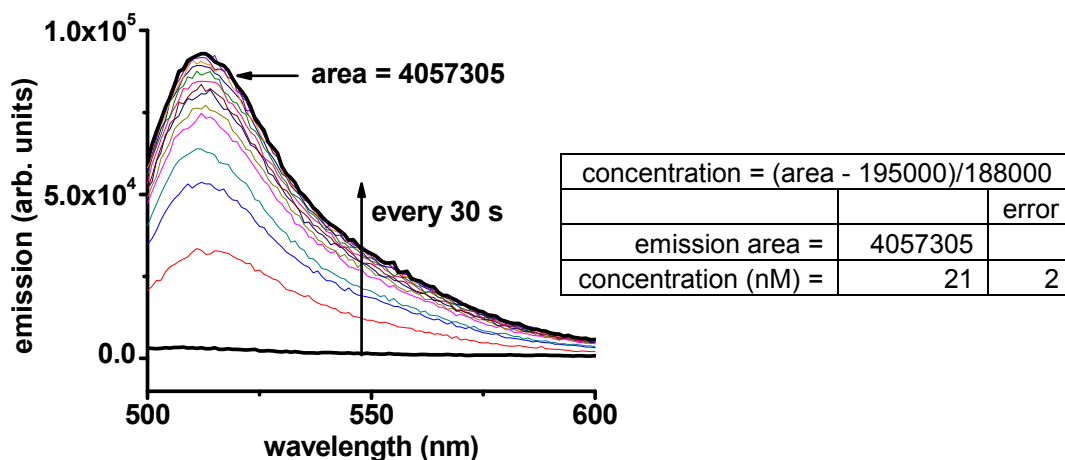
Figure 4.24 (A) Representative spectra showing changes in the fluorescence intensity (excitation at 490 nm) when an aqueous dispersion of solid spherical gold NPs decorated with the fluorescein Diels-Alder linker was irradiated with a pulse laser (pulse at λ = 532 nm, 3-6 ns, 10 Hz, 100 mW) for 7 min. Inset shows the calculation for the concentration of released molecules based on the integration of the highest spectrum and equation deducted from linear regression (Figure 4.14A).

Example derivation for error calculations:

Given: $p = x \pm y$ Error: $\delta p = \sqrt{(\delta x)^2 + (\delta y)^2}$

Given: $p = \dfrac{x \times y}{z}$ Error: $\delta p = |p| \sqrt{(\dfrac{\delta x}{x})^2 + (\dfrac{\delta y}{y})^2 + (\dfrac{\delta z}{z})^2}$

Example: Eq. 4.3

Number of particles in 1 mL of water = $\dfrac{109 \pm 5 \times 10^{-9}\, cm^3}{3.0 \pm 0.3 \times 10^{-18}\, cm^3} = 36 \times 10^9$

Error: $\delta p = |36 \times 10^9| \sqrt{(\dfrac{5}{109})^2 + (\dfrac{0.3}{3})^2} = 4 \times 10^9$

Therefore: $p \pm \delta p = 36 \pm 4 \times 10^9$

CHAPTER 5: CONCLUSIONS AND OUTLOOK

5.1 Conclusions

The lack of effective and efficient methods to deliver a therapeutic agent in the human body has created a need for a more advanced drug delivery systems. Nanomaterials, composed of organic, inorganic or hybrid materials with dimensions on the nanoscale, have the potential to fulfill this need by facilitating the delivery of drugs in a more effective way. Using nanomaterials in drug delivery systems can provide a route for the masking, delivering and releasing of drugs. Each step in the drug delivery systems (i.e., masking, delivering and releasing) provides a unique advantage for the process. The solubility and pharmacokinetics, which are some of the problems facing many drugs, can be solved by attaching the drug onto the surfaces of nanostructures or within the nanostructures. The systemic toxicity caused by many drugs, can be avoided by targeted delivery and release on demand of drug molecules using nanomaterials. Consequently, drug delivery systems have the capability to deliver therapeutic agents more efficiently and effectively than free administration of the therapeutic agent.[9]

Gold NPs are among many nanomaterials that have been studied as a platform for drug delivery systems. The nanometer dimensions of gold NPs give rise to some unique physical properties that make them attractive candidates as drug delivery system. These properties such as SPR and the photothermal effect

have, respectively, been shown to be useful for bio-sensing and cell abolition. Furthermore, surface decoration of gold NPs with thiolated molecules provides a platform for the attachment of therapeutic agents or bio-recognition molecules to the surfaces of the gold. Attachment of bio-recognition molecules to gold NPs are helpful for targeted delivery of gold NPs to specific biological tissues or organs. Combining the physical properties of gold NPs with their surface decoration, makes them an attractive platform for further studies as drug delivery systems.

Drug delivery systems consist of masking, delivering and releasing of a drug, the focus of this thesis was on the releasing step. Two types of gold NPs were synthesized to demonstrate such a release mechanism. The first type of NPs were solid spherical gold NPs with diameters of 18 nm and a SPR absorption centred at 520 nm. The second type were silica/gold core-shell NPs with diameters of 204 nm and SPR absorptions centred at 650 and 900 nm. The two nanostructures' independent SPR properties were used to demonstrate that triggering the release mechanism with light can be tuned across the visible and NIR region of the electromagnetic spectrum.

The interaction of light with gold NPs at their SPR frequency, which convert the photon energy to phonon vibrations, was used to trigger the release mechanism. The release mechanism was demonstrated by attachment of fluorescein Diels-Alder linkers to the gold NPs' surfaces. The fluorescein Diels-Alder linker had three components: i) the thiol group allows the molecular structure to be anchored to the gold surfaces through Au−S bonds; ii) the fluorescein segment was used to monitor the release of molecules by

fluorescence spectroscopy after the photothermal effect; and iii) a Diels-Alder adduct was incorporated between the thiol segment of the molecule and the fluorescein dye. By applying heat, the function of the Diels-Alder reaction is to undergo a reverse reaction and release the fluorescein moiety.

To exhibit the release mechanism, the gold NPs were decorated with fluorescein Diels-Alder linkers. Both thermal and photothermal treatment of each of the decorated gold NPs (i.e., solid spherical gold and silica/gold core-shell NPs) showed an increase in the fluorescein moieties in the aqueous solution. Further characterization of the released molecules from the solid spherical gold NPs with nuclear magnetic resonance spectroscopy, mass spectrometry, and capillary electrophoresis suggested that the released molecules were mainly fluorescein furfuryl esters. The results from the analysis indicated that the released molecule was the *retro*-Diels-Alder product. The quantification of decorated solid spherical gold NPs, considering some approximations, suggested that there are ~1800 molecules attached to each gold NP. A photothermal treatment of the decorated solid spherical gold NPs for 7 min released ~360 molecules from each NP, which is ~20% of the total surface load of molecules on the NPs. In addition, similar results were obtained from the decorated silica/gold core-shell NPs. The aqueous solution of core-shell NPs was decorated with fluorescein Diels-Alder linkers. The solution was irradiated with 800 nm pulsed laser and the fluorescence spectra of the sample showed a corresponding increase in emission intensity. Hence, the release of molecules from two types of NPs with two different wavelengths were demonstrated. For the

first time, the obtained results demonstrated the controlled release of molecules by harnessing the photothermal effect from gold NPs.

5.2   Outlook

The short-term goal of our project was to show light can be used to trigger the release of molecules from gold NPs. It is clear that the next steps are to demonstrate the photothermal release of fluorescein moiety *in vivo* and the bio-conjugation of gold NPs. Both of these studies are currently in progress.

Another on-going project is focused on the different shapes of gold nanomaterials which were not discussed in this thesis. As mentioned in Chapter 4, silica/gold core-shell NPs with consistent SPR properties are hard to reproduce. Therefore, other gold nanomaterials are being synthesized such as gold nanorods[57] and nanocages,[100] for use in future photothermal release studies. These nanomaterials have an advantage over solid spherical gold NPs because their SPR absorption is tunable in the NIR region of electromagnetic spectrum. For example, the SPR absorption of nanorods can be tuned by changing the radius and length of the rods which can be controlled by synthetic routes.[57] Gold nanorods could be a good substitute for silica/gold core-shell NPs for applications in drug delivery systems.

In addition to the on going research, there are challenges that should be addressed for the long-term goals of this project. The challenges can be categorized in two sections:

1. those concerning the photothermal release mechanism, and

2. those concerning the use of gold NPs in drug delivery systems.

One of the important challenges facing the release mechanism is the presence of maleimide moieties after photothermal release. As mentioned in Chapter 4, a few solutions (i.e., addition of a polymeric layer or the modification of the Diels-Alder adduct) need to be investigated further to solve this problem. Another issue to consider is the attachment of drug molecules to the gold NPs, which requires some modification to the drug molecule. This modification may have the undesirable results of inactivation or decreased effectiveness of the drug. In addition, the drug's modification could face further challenges from synthetic point of view. As results of these challenges, the number of drugs that could be used with our release mechanism is limited. Therefore, using gold NPs in drug delivery systems should not be perceived as the only system, but rather as one option that could work for delivery of some drug molecules. To specifically address the second category of challenges, the toxicity of gold NPs and their stability when decorated with drug molecules *in vivo* have to be studied in greater detail before any gold NPs can be used as drug delivery systems. Thus, there are challenges and needs accompanying this project, which need to be addressed in the future.

REFERENCES:

1. "National Science and Technology Council Committee on Technology. The National Nanotechnology Initiative: research and development leading to a revolution in technology and industry.Washington (DC)7 Office of Science and Technology Policy; 2005."

2. Shatkin, J. A. *Nanotechnology Health and Environmental Risks*; CRC Press, 2008, P.6.

3. Gasman, L. *Nanotechnology applications and markets*; Artech House, 2006.

4. Samad, A.; Sultana, Y.; Aqil, M. *Current Drug Delivery* **2007,** *4*, 297-305.

5. Farokhzad, O. C.; Cheng, J. J.; Teply, B. A.; Sherifi, I.; Jon, S.; Kantoff, P. W.; Richie, J. P.; Langer, R. *Proceedings of the National Academy of Sciences of the United States of America* **2006,** *103*, 6315-6320.

6. Lee, C. C.; Yoshida, M.; Frechet, J. M. J.; Dy, E. E.; Szoka, F. C. *Bioconjugate Chemistry* **2005,** *16*, 535-541.

7. Ooya, T.; Lee, J.; Park, K. *Bioconjugate Chemistry* **2004,** *15*, 1221-1229.

8. Gibson, J. D.; Khanal, B. P.; Zubarev, E. R. *Journal of the American Chemical Society* **2007,** *129*, 11653-11661.

9. Ghosh, P.; Han, G.; De, M.; Kim, C. K.; Rotello, V. M. *Advanced Drug Delivery Reviews* **2008,** *60*, 1307-1315.

10. Koo, O. M.; Rubinstein, I.; Onyuksel, H. *Nanomedicine: Nanotechnology, Biology and Medicine* **2005,** *1*, 193-212.

11. Smith, A. M.; Duan, H.; Mohs, A. M.; Nie, S. *Advanced Drug Delivery Reviews* **2008,** *60*, 1226-1240.

12. Hong, R.; Han, G.; Fernandez, J. M.; Kim, B.-j.; Forbes, N. S.; Rotello, V. M. *Journal of the American Chemical Society* **2006,** *128*, 1078-1079.

13. Kyriakides, T. R.; Cheung, C. Y.; Murthy, N.; Bornstein, P.; Stayton, P. S.; Hoffman, A. S. *Journal of Controlled Release* **2002,** *78*, 295-303.

14. Rosi, N. L.; Giljohann, D. A.; Thaxton, C. S.; Lytton-Jean, A. K. R.; Han, M. S.; Mirkin, C. A. *Science* **2006,** *312*, 1027-1030.

15. Gerasimov, O. V.; Boomer, J. A.; Qualls, M. M.; Thompson, D. H. *Advanced Drug Delivery Reviews* **1999,** *38*, 317-338.

16. Hrubý, M.; Konák, C.; Ulbrich, K. *Journal of Controlled Release* **2005,** *103*, 137.

17. Pascal Jonkheijm, D. W., Hendrik Schröder, Christof M. Niemeyer, Herbert Waldmann. *Angewandte Chemie International Edition* **2008,** *47*, 9618-9647.

18. Kelly, K. L.; Coronado, E.; Zhao, L. L.; Schatz, G. C. *The Journal of Physical Chemistry B* **2003,** *107*, 668-677.

19. Abbruzzese, C.; Fornari, P.; Massidda, R.; Vegliò, F.; Ubaldini, S. *Hydrometallurgy* **1995,** *39*, 265-276.

20. Ellen E. Connor, J. M., Anand Gole, Catherine J. Murphy, Michael D. Wyatt. *Small* **2005,** *1*, 325-327.

21. Rosi, N. L.; Mirkin, C. A. *Chemical Reviews* **2005,** *105*, 1547-1562.

22. Cheng, M. M.-C.; Cuda, G.; Bunimovich, Y. L.; Gaspari, M.; Heath, J. R.; Hill, H. D.; Mirkin, C. A.; Nijdam, A. J.; Terracciano, R.; Thundat, T.; Ferrari, M. *Current Opinion in Chemical Biology* **2006,** *10*, 11-19.

23. Giulio F. Paciotti, D. G. I. K., Lawrence Tamarkin. *Drug Development Research* **2006,** *67*, 47-54.

24. Kimling, J.; Maier, M.; Okenve, B.; Kotaidis, V.; Ballot, H.; Plech, A. *The Journal of Physical Chemistry B* **2006,** *110*, 15700-15707.

25. Zhou, J.; Ralston, J.; Sedev, R.; Beattie, D. A. *Journal of Colloid and Interface Science* **2009,** *331*, 251-262.

26. Link, S.; Burda, C.; Wang, Z. L.; El-Sayed, M. A. *The Journal of Chemical Physics* **1999,** *111*, 1255-1264.

27. Richardson, H. H.; Hickman, Z. N.; Govorov, A. O.; Thomas, A. C.; Zhang, W.; Kordesch, M. E. *Nano Letters* **2006,** *6*, 783-788.

28. Khlebtsov, B.; Zharov, V.; Melnikov, A.; Tuchin, V.; Khlebtsov, N. *Nanotechnology* **2006**, 5167-5179.

29. Huang, X.; Jain, P. K.; El-Sayed, I. H.; El-Sayed, M. A. *Photochemistry and Photobiology* **2009,** *82*, 412.

30. Jain, P. K.; Huang, X.; El-Sayed, I. H.; El-Sayed, M. A. *Accounts of Chemical Research* **2008,** *41*, 1578-1586.

31. He, C.; Becker, C. H. *Physical Review A* **1997,** *55*, 1300-1306.

32. Gang Han, C.-C. Y., Byoung-jin Kim, Rosemary S. Turingan, Neil S. Forbes, Craig T. Martin, Vincent M. Rotello. *Angewandte Chemie International Edition* **2006,** *45*, 3165-3169.

33. Ravanat, J.-L.; Douki, T.; Cadet, J. *Journal of Photochemistry and Photobiology B: Biology* **2001,** *63*, 88.

34. Lee, S. E.; Liu, G. L.; Kim, F.; Lee, L. P. *Nano Letters* **2009,** *9*, 562-570.

35.   Kwart, H.; King, K. *Chemical Reviews* **1968,** *68*, 415-447.

36.   Chung, Y.; Duerr, B. F.; McKelvey, T. A.; Nanjappan, P.; Czarnik, A. W. *The Journal of Organic Chemistry* **1989,** *54*, 1018.

37.   Bhattacharya, A.; Mahajan, R. L. *Physiological Measurement* **2003**, 769-783.

38.   El-Sayed, M. A. *Accounts of Chemical Research* **2004,** *37*, 326-333.

39.   Nehl, C. L.; Hafner, J. H. *Journal of Materials Chemistry* **2008,** *18*, 2415-2419.

40.   Yuanzhe Piao, A. B., Jaeyun Kim, Ulrich Wiesner, Taeghwan Hyeon. *Advanced Functional Materials* **2008,** *18*, 3745-3758.

41.   Jain, P. K.; Lee, K. S.; El-Sayed, I. H.; El-Sayed, M. A. *The Journal of Physical Chemistry B* **2006,** *110*, 7238-7248.

42.   Liu, X.; Atwater, M.; Wang, J.; Huo, Q. *Colloids and Surfaces B: Biointerfaces* **2007,** *58*, 3-7.

43.   Xiaohua Huang, W. Q., Ivan H. El-Sayed, Mostafa A. El-Sayed. *Lasers in Surgery and Medicine* **2007,** *39*, 747-753.

44.   Vlerken, L. E.; Amiji, M. M. *Expert Opinion on Drug Delivery* **2006,** *3*, 205-216.

45.   Wolfe, a. P. *Imaging Phonons: Acoustic Wave Propagation in Solids*; Cambridge University Press, 1998.

46.   Roper, D. K.; Ahn, W.; Hoepfner, M. *The Journal of Physical Chemistry C* **2007,** *111*, 3636-3641.

47.   Ahmadi, T. S.; Logunov, S. L.; El-Sayed, M. A. *The Journal of Physical Chemistry* **1996,** *100*, 8053-8056.

48.   Cahill, D. G.; Ford, W. K.; Goodson, K. E.; Mahan, G. D.; Majumdar, A.; Maris, H. J.; Merlin, R.; Phillpot, S. R. *Journal of Applied Physics* **2003,** *93*, 793-818.

49.   Hirsch, L. R.; Stafford, R. J.; Bankson, J. A.; Sershen, S. R.; Rivera, B.; Price, R. E.; Hazle, J. D.; Halas, N. J.; West, J. L. *Proceedings of the National Academy of Sciences of the United States of America* **2003,** *100*, 13549-13554.

50.   Kumar, S.; Gandhi, K. S.; Kumar, R. *Industrial & Engineering Chemistry Research* **2007,** *46*, 3128-3136.

51.   Reimer, L.; Kohl, H. *Transmission Electron Microscopy: Physics of Image Formation*; Springer; 5th ed. edition, 2008.

52.   Aslan, K.; Luhrs, C. C.; Perez-Luna, V. H. *The Journal of Physical Chemistry B* **2004,** *108*, 15631-15639.

53.   Jirasek, A.; Hilts, M.; Shaw, C.; Baxter, P. *Physics in Medicine and Biology* **2006,** *51*, 1891-1906.

54.   Batista, E. A.; Iwasita, T. *Langmuir* **2006,** *22*, 7912-7916.

55.   Tam, F.; Moran, C.; Halas, N. *The Journal of Physical Chemistry B* **2004,** *108*, 17290-17294.

56.   Stolik, S.; Delgado, J. A.; Pérez, A.; Anasagasti, L. *Journal of Photochemistry and Photobiology B: Biology* **2000,** *57*, 90.

57.   Pérez-Juste, J.; Pastoriza-Santos, I.; Liz-Marzán, L. M.; Mulvaney, P. *Coordination Chemistry Reviews* **2005,** *249*, 1870-1901.

58.   Daniel, M.-C.; Astruc, D. *Chemical Reviews* **2004,** *104*, 293-346.

59.   Huang; Chen, F.; Bennett, P. A.; Tao. *Journal of the American Chemical Society* **2007,** *129*, 13225-13231.

60.   Sellers, H.; Ulman, A.; Shnidman, Y.; Eilers, J. E. *Journal of the American Chemical Society* **2002,** *115*, 9389-9401.

61.   Loo, C.; Lowery, A.; Halas, N.; West, J.; Drezek, R. *Nano Letters* **2005,** *5*, 709-711.

62.   Zambetti, M.; Giacobone, A.; Terenziani, M.; Zucchinelli, P.; Demicheli, R.; Biasi, S.; Piotti, P.; Bartoli, C.; Valagussa, P.; Bonadonna, G. *Oncologist* **1997,** *2*, 223-227.

63.   Stöber, W.; Fink, A.; Bohn, E. *Journal of Colloid and Interface Science* **1968,** *26*, 62-69.

64.   Duff, D. G.; Baiker, A.; Edwards, P. P. *Langmuir* **1993,** *9*, 2301-2309.

65.   Westcott, S. L.; Oldenburg, S. J.; Lee, T. R.; Halas, N. J. *Langmuir* **1998,** *14*, 5396-5401.

66.   Pham, T.; Jackson, J. B.; Halas, N. J.; Lee, T. R. *Langmuir* **2002,** *18*, 4915-4920.

67.   Ogino, K.; Chen, J.-S.; Ober, C. K. *Chemistry of Materials* **1998,** *10*, 3833-3838.

68.   Xiaonong Chen, E. R. *Journal of Polymer Science Part A: Polymer Chemistry* **2000,** *38*, 4373-4384.

69.   Chen, X.; Wudl, F.; Mal, A. K.; Shen, H.; Nutt, S. R. *Macromolecules* **2003,** *36*, 1802-1807.

70.   Aubert, J. H. *Journal of Adhesion* **2003,** *79*, 609-616.

71.   Balthazor, T. M.; Gaede, B.; Korte, D. E.; Shieh, H. S. *The Journal of Organic Chemistry* **1984,** *49*, 4547-4549.

72.   Bartlett, P. D.; Wu, C. *The Journal of Organic Chemistry* **1984,** *49*, 1880-1886.

73.   Iris, L.; Cäcilia, M.-M.; Andreas, H. *Angewandte Chemie International Edition in English* **1995,** *34*, 1607-1609.

74. McElhanon, J. R.; Zifer, T.; Kline, S. R.; Wheeler, D. R.; Loy, D. A.; Jamison, G. M.; Long, T. M.; Rahimian, K.; Simmons, B. A. *Langmuir* **2005,** *21*, 3259-3266.

75. Jerome, A. B. *Angewandte Chemie International Edition* **2006,** *45*, 4724-4729.

76. Woodward, R. B.; Baer, H. *Journal of the American Chemical Society* **1944,** *66*, 645-649.

77. Buttner, M.; Belser, T.; Oelhafen, P. *The Journal of Physical Chemistry B* **2005,** *109*, 5464-5467.

78. Gosselin, P.; Bourdy, C.; Mille, S.; Perrotin, A. *The Journal of Organic Chemistry* **1999,** *64*, 9557-9565.

79. Qian, X.; Peng, X.-H.; Ansari, D. O.; Yin-Goen, Q.; Chen, G. Z.; Shin, D. M.; Yang, L.; Young, A. N.; Wang, M. D.; Nie, S. *Nature Biotechnology* **2008,** *26*, 83-90.

80. Torchilin, V. P. *Pharmaceutical Research* **2007,** *24*, 1-16.

81. Duncan, R. *Nature Reviews Cancer* **2006,** *6*, 688-701.

82. Eghtedari, M.; Liopo, A. V.; Copland, J. A.; Oraevsky, A. A.; Motamedi, M. *Nano Letters* **2009,** *9*, 287-291.

83. Huang, Y. C.; Ge, B.; Sen, D.; Yu, H.-Z. *Journal of the American Chemical Society* **2008,** *130*, 8023-8029.

84. Brannon, J. H.; Magde, D. *The Journal of Physical Chemistry* **1978,** *82*, 705-709.

85. Mayilo, S.; Ehlers, B.; Wunderlich, M.; Klar, T. A.; Josel, H.-P.; Heindl, D.; Nichtl, A.; Kürzinger, K.; Feldmann, J. *Analytica Chimica Acta* **2009,** *646*, 119-122.

86. Wulandari, P.; Nagahiro, T.; Michioka, K.; Tamada, K.; Ishibashi, K.-i.; Kimura, Y.; Niwano, M. *Chemistry Letters* **2008,** *37*, 888-889.

87. Ulman, A. *Chemical Reviews* **1996,** *96*, 1533-1554.

88. He, H.; Xie, C.; Ren, J. *Analytical Chemistry* **2008,** *80*, 5951-5957.

89. Silfvast, W. T. *Laser Fundamentals*, 2 ed.; Cambridge University Press, 2008.

90. Paschotta, R. *Encyclopedia of Laser Physics and Technology*; Wiley-VCH, 2008.

91. Pitsillides, C. M.; Joe, E. K.; Wei, X.; Anderson, R., R.; Lin, C. P. *Biophysical Journal* **2003,** *84*, 4023-4032.

92. Schneider, G.; Decher, G.; Nerambourg, N.; Praho, R.; Werts, M. H. V.; Blanchard-Desce, M. *Nano Letters* **2006,** *6*, 530-536.

93. Chankvetadze, B. *Chemical Society Review* **2004,** *33*, 337-347.

94. Cheicante, R. L.; Stuff, J. R.; Dupont Durst, H. *Journal of Chromatography A* **1995,** *711*, 347-352.

95. Skoog, D. A. H., F.J.; Crouch, S.R. *Principles of Instrumental Analysis*; Thomson Brooks/Cole: Belmont, 2007; Vol. 6.

96. Chen, H.; Dabek-Zlotorzynska, E.; Rasmussen, P. E.; Hassan, N.; Lanouette, M. *Talanta* **2008,** *74*, 1547-1555.

97. Khurana, J. M.; Chauhan, S.; Bansal, G. *Monatshefte fur Chemie* **2004,** *135*, 83-87.

98. Vodolazkaya, N. A.; Gurina, Y. A.; Salamanova, N. V.; McHedlov-Petrossyan, N. O. *Journal of Molecular Liquids* **2009,** *145*, 188-196.

99. Wang, Z.; Carter, J. A.; Lagutchev, A.; Koh, Y. K.; Seong, N.-H.; Cahill, D. G.; Dlott, D. D. *Science* **2007,** *317*, 787-790.

100. Lee, Y. T.; Im, S. H.; Wiley, B.; Xia, Y. *Chemical Physics Letters* **2005,** *411*, 479-483.